

The influence of specific mitochondrial polymorphisms on the α -synuclein-induced pathology in a mouse model of Parkinson's disease

Dissertation
zur Erlangung des akademischen Grades

doctor rerum naturalium
(Dr. rer. nat.)

genehmigt durch die Fakultät für Naturwissenschaften
der Otto-von-Guericke-Universität Magdeburg

von Dipl.-Biol. Christina Schwitlick (geb. Fröhlich)
geb. am 25.05.1987 in Neubrandenburg

Gutachter: Prof. Dr. Dr. Jens Pahnke
Prof. Dr. Claus Pietrzik

eingereicht am 20.02.2015
verteidigt am 13.07.2015

To my love, husband and best friend,

Lars

Contents	3
Summary	6
Abbreviations	7
1. Introduction	9
1.1 Neurodegenerative Diseases	9
1.2 Dementia.....	9
1.3 Parkinson’s Disease.....	10
1.3.1 Definition & Epidemiology.....	10
1.3.2 Pathophysiology.....	11
1.3.3 Genetics & Etiology	13
1.3.4 Therapy.....	15
1.4 Alpha-synuclein	16
1.4.1 Characteristics & Function.....	16
1.4.2 Genetics.....	18
1.4.3 Pathology & Toxicity.....	19
1.4.4 ABC transporter & PD	20
1.5 Mitochondria.....	21
1.5.1 Structure & Function.....	21
1.5.2 The electron transport chain	22
1.5.3 Mitochondrial alterations & PD	24
2. Aims of work	26
3. Material & Methods	27
3.1 Material	27
3.1.1 Antibodies.....	27
3.1.2 Chemicals	27
3.1.3 Equipment.....	28
3.1.4 Kits	29
3.1.5 Primer.....	29
3.1.6 Software.....	29
3.2 Methods.....	30
3.2.1 Mouse models & Husbandry	30
3.2.2 Genotyping.....	30
3.2.3 Behavioral tests	33
3.2.4 Treatment with Thiethylperazine.....	33

3.2.5	Tissue preparation	34
3.2.6	Biochemical analyzes	34
3.2.7	Respirometry.....	36
3.2.8	Immunohistochemistry.....	39
3.2.9	Statistics.....	40
4.	Results	42
4.1	Characterization of the tg-aSYN mouse model with respect to PD	42
4.1.1	Phenotypical appearance of tg-aSYN mice.....	42
4.1.2	Immunohistological analyzes of tg-aSYN mice.....	43
4.1.3	Behavioral study on tg-aSYN mice.....	46
4.2	Influence of specific mitochondrial polymorphism on aSYN pathology in tg-aSYN mice.....	49
4.2.1	Immunohistological analyzes of tg-aSYN-mtNOD mice.....	49
4.2.2	Determination of aSYN in tg-aSYN and tg-aSYN-mtNOD mice using ELISA.....	51
4.2.3	Influence of mitochondrial polymorphisms on the behavior of tg-aSYN mice ...	52
4.3	Respirometric measurements of isolated brain mitochondria.....	55
4.3.1	Complex I- dependent respiration.....	56
4.3.2	Complex II- dependent respiration	58
4.3.3	Complex III- dependent respiration.....	60
4.3.4	Complex IV- dependent respiration.....	61
4.3.5	Maximal respiration rate upon uncoupling with FCCP	62
4.3.6	Resting states.....	63
4.3.7	Respiratory Control Ratio	64
4.4	Relevance of ABC transporter -ABCC1- activity on the aSYN pathology of tg-aSYN mice.....	65
4.4.1	Consequences of the ABCC1 knock-out on the histology of the tg-aSYN mice....	65
4.4.2	Quantification of aSYN upon ABCC1 knock-out using ELISA.....	66
4.4.3	Influence of ABCC1 activation using thiethylperazine on neuron integrity and the immune response	66
4.4.4	ABCC1 activation – quantification of aSYN by ELISA.....	68
5.	Discussion	69
5.1	The tg-aSYN mice is a convenient model for synucleopathies.....	69
5.2	Beneficial effects of mitochondrial polymorphisms on aSYN pathology in tg-aSYN mice.....	74
5.3	Respirometric measurements revealed mtDNA specific differences in oxygen consumption of isolated brain mitochondria.....	76
5.4	ABCC1 activity is not crucial for aSYN transport in the brain of tg-aSYN mice.....	81

5.5	Conclusion.....	83
	References	85
	List of figures	100
	List of tables	101
	Acknowledgements/Danksagung	102
	Declaration/Eidesstattliche Erklärung.....	103
	List of publications	104

Summary

Parkinson's disease (PD) is one of the most common neurodegenerative disorders with motor deteriorations in the world. Clinical manifestation includes symptoms like movement deficiencies, tremor, rigidity, bradykinesia, postural instability, and also dementia. PD is characterized by a vast loss of dopaminergic neurons in the substantia nigra *pars compacta* and the morphological hallmark of Lewy bodies and Lewy neurites, protein deposits within brain neurons. Alpha-synuclein (aSYN), a major constituent of these inclusions is localized at presynaptic sites in brain neurons and plays physiologically distinct roles in the modulations of synaptic activity, neurotransmitter release and lipid metabolism. It is still not fully understood which trigger initiates the deposition of aSYN in the brain of patients with PD and other neurodegenerative diseases. Mitochondrial dysfunction accompanied by the production of reactive oxygen species is currently debated to cause the pathological alterations in the brain of PD patients.

In the present work, a transgenic aSYN mouse model with the human 'A30P' mutation (tg-aSYN) was characterized and compared to a newly generated transgenic mouse model with specific mitochondrial polymorphisms, the tg-aSYN-mtNOD mice. In order to examine the influence of mitochondrial function modification, biochemical and histological aspects as well as the behavioural profiles were determined and compared in both mouse models. Respirometric measurements of isolated mouse brain mitochondria were conducted in order to evaluate functional effects of these mitochondrial polymorphisms and to find differences in complex-dependent respiration when compared to the conventional tg-aSYN mouse model. The results reveal that these specific mitochondrial polymorphisms lead to an increased complex II-dependent respiration that is accompanied by an improvement of motor performances and cortical neuron number in old tg-aSYN-mtNOD mice. An increase in higher-molecular weight species of aSYN was furthermore found as well as an enhanced microglial response in the brain. Based on the premise of a negatively affected energy metabolism in tg-aSYN mice, an additional study was performed to investigate a hypothesized export of aSYN by the energy-dependent ABC transporter ABCC1. Therefore, an ABCC1 knock-out mouse model was generated and investigated with regard to intracerebral aSYN level and neuronal and microglial cortex area. Furthermore, tg-aSYN mice were treated with thiethylperazine to assess the effects of ABCC1 activation on the stated parameter. It was thereby found that aSYN is not transported by ABCC1 as no significant differences upon knock-out as well as activation were determined in tg-aSYN mice. In summary, this study was able to reveal beneficial effects of increased complex II-dependent respiration on the aSYN pathology in a PD mouse model and points to promising pharmaceutical application option for the treatment of α -synucleinopathies.

Abbreviations

%	percent	DMSO	dimethyl sulfoxide
°	degree	DNA	deoxyribonucleic acid
°C	degree Celsius	DTT	dithiothreitol
α-KG	alpha-ketoglutarate	E46K	glutamic acid to lysine change at amino acid 46 in α-synuclein transcript
A30P	alanine to proline change at amino acid 30 in α-synuclein transcript	EDTA	ethylenediaminetetraacetic acid
A53T	alanine to threonine change at amino acid 53 in α-synuclein transcript	EGTA	ethylene glycol tetraacetic acid
Aβ	Amyloid β	ELISA	Enzyme-linked immunosorbent assay
ABC	ATP-binding cassette	ETC	electron transport chain
AD	Alzheimer's disease	ETF	electron-transferring flavoprotein-ubichinone oxidoreductase
ADP	adenosine diphosphate	FAD	flavin adenine dinucleotide
AGC	mitochondrial aspartate/glutamate carrier	FMN+	flavin mononucleotide
ASAT	aspartate amino-transaminase	fr	fasciculus retroflexus
Aqua dest.	aqua destillata	G3P	glycerine-3-phosphate
aralar	mitochondrial aspartate/glutamate carrier	GABA	gamma-aminobutyric acid
aSYN	alpha synuclein	GFAP	glial fibrillary acid protein
ATP	adenosine triphosphate	Glu	glutamate
ATP13A2	Probable cation-transporting ATPase 13A2	GWAS	genome-wide association study
Atr	atractyloside	Hc	hippocampus
BBB	blood brain barrier	HD	Huntington's disease
BCB	blood cerebrospinal fluid barrier	HIF	hypoxia-inducible transcriptions factor
BIM	brain incubation medium	HRP	horseradish peroxidase
BLP	basolateral amygdaloid nucleus, posterior part	HT	hypothalamus
BMP	basomedial amygdaloid nucleus, posterior part	Iba1	ionized calcium binding adapter molecule 1
bp	base pairs	IL-6	Interleukin-6
BSA	bovine serum albumin	kDa	kilodalton
CA	cornu ammonis	kPa	kilopascal
COX	cytochrome c oxidase	LB	Lewy body
cp	cerebral peduncle	lmeC	linear mixed-effects models with censored responses
CSF	cerebrospinal fluid	LN	Lewy neurite
CSPα	cysteine string protein α	LRP-1	low density lipoprotein receptor-related protein 1
Ctrl	control	LRRK2	leucine-rich repeat kinase 2
d	days	LV	lateral ventricle
DG	dentate gyrus	M	molar
DLB	Dementia with Lewy bodies	Mal	malate
DLG	dorsal lateral geniculate nucleus	MAS	malate/aspartate shuttle

MDR1	multidrug resistance protein 1	SNARE	soluble NSF (N-ethylmaleimide-sensitive factor) attachment protein receptor
MOPS	3-(N-orpholino) propane-sulfonic acid		
MPP+	1-methyl-4-phenylpyridinium ion	SNCA	alpha synuclein-gene
MPT	medial pretecal nucleus	SNP	single nucleotide polymorphism
MPTP	1-methyl-4-phenyl-1,2,3,6-tetrahydropyridine	SNpc	Substantia nigra <i>pars compacta</i>
MRP1	multidrug resistance-associated protein 1	SUCC	succinate
MSA	multiple system atrophy	T	thalamus
MSE	buffer containing mannitol-sucrose-EGTA	TAE	tris-acetate-EDTA
mtDNA	mitochondrial DNA	Taq	<i>Thermus aquaticus</i>
n	number	Tg	transgenic
NAC	non-Amyloid β component	Thy1	thymocyte differentiation antigen 1
NAD+	nicotinamide adenine dinucleotide	TMB	3,3',5,5'-tetramethylbenzidine
ND	Neurodegenerative disease	TMPD	N,N,N',N'-tetramethyl-p-phenylenediamine
NeuN	anti-neuronal nuclei	TNF α	tumor necrosis factor α
nm	nanometer	tRNA	transfer ribonucleic acid
nmol	nanomole	UPS	ubiquitin proteasome system
PBS	phosphate-buffered saline	VD	Vascular dementia
PCR	polymerase chain reaction	w/v	weight/volume
PD	Parkinson's disease	ZID	zona incerta, dorsal part
PDGF	platelet-derived growth factor		
PFA	paraformaldehyde	units	according to SI
P-gp	P-glycoprotein 1		
PINK1	PTEN (Phosphatase and tensin homolog)-induced putative kinase 1		
PMCo	posteromedial cortical amygdaloid area		
PTP	permeability transition pore		
Pyr	pyruvate		
RCR	respiratory control ratio		
REML	restricted maximum likelihood		
RNA	ribonucleic acid		
rpm	rounds per minute		
RSD	retrosplenial dysgranular cortex		
SC	somatosensory cortex		
SDH	succinate dehydrogenase		
SEM	standard error of mean		
SN	Substantia nigra		
SNAP-25	synaptosomal-associated protein 25		

1. Introduction

1.1 Neurodegenerative Diseases

Neurodegeneration describes a pathological process in the brain of elderly which leads to a progressing loss of neurons in specific brain structures and consequently to a gradual worsening of several related functions until death occurs (Przedborski *et al.*, 2003). Neurodegenerative diseases (NDs) cover a large group of devastating neurological diseases with different manifestations and clinical outcome like dementia, atrophy and movement deterioration (Przedborski *et al.*, 2003). They are categorized according to the location of the neuronal dysfunction in the brain and/or their ability to trigger dementia. But commonly a definite diagnosis can only be made *post mortem* (Massano *et al.*, 2012). The most prominent NDs include Alzheimer's disease (AD), Parkinson's disease (PD) and vascular dementia (VD) but also multiple system atrophy (MSA), Huntington's disease (HD) and prion diseases belong to this group (Przedborski *et al.*, 2003). They all share as common hallmark the main risk factor age. As the human population grows older, especially in the Western society, incidence of NDs increases rapidly. Prognoses further underline the importance of research in this field (World Alzheimer Report 2010; World Population Prospects: *The 2012 Revision, Key Findings and Advance Tables*). Besides having an inherited defect (<1 %) and old age, only presumptions exist concerning the cause of the diseases. It is likely that most NDs are initiated multifactorial. Here, stroke, infection, trauma, diabetes as well as depression, alcohol abuse and/or high blood pressure are discussed and even social and environmental factors like low education, ethnicity and/or exposition to pesticides were taken into consideration (Landrigan *et al.*, 2005; Baltazar *et al.*, 2014; Olanow *et al.*, 1999). A widely discussed cause for NDs is mitochondrial dysfunction and the resulting production of reactive oxygen species (ROS) in cells which leads to damage and malfunction (Martin, 2010). A further characteristic of certain NDs is the excessive production and intra- or extracellular deposition of different peptides and proteins e.g. Amyloid β in AD or α -synuclein in PD causing dementia and other clinical manifestations. The reason for the disturbed balance in those systems is still unknown and thus a wide spread subject of research (Swart *et al.*, 2014).

1.2 Dementia

Dementia describes a clinical syndrome which can be caused by injuries or follows diseases of the brain (e.g. NDs) and leads to abnormal cognitive function in elderly. Although also younger people can suffer from this disease, the risk to develop dementia is highest from the age of 65 years and almost doubles every five years (World Alzheimer Report 2009). It affects several cognitive abilities like memory, orientation and learning, emotional and social behavior and also

motivation, each case proceeding individually. To diagnose dementia, apart from memory at least one other function has to be affected, for example motoric activity, speech development or object recognition. Furthermore, for diagnosis, cognitive decline is required to be not reversible by medication (The ICD-10 Classification of Mental and Behavioural Disorders). Most cases are caused directly by disturbed mechanisms in the brain and are denoted as primary dementia whereas few cases occur secondarily as a consequence of metabolic disease or wrong medication (Mahler *et al.*, 1987). Different stages underline the progressive nature of dementia. First, cases usually present with mild symptoms like confusion, spatial or temporal disorientation. In the second stage patients forget their familiar surroundings and develop problems with speech and communication. In the last stage of dementia, complete care is necessary as patients have problems in walking, handling and in coordination of time and place. They are not able to recognize close relatives and often become aggressive and apathetic (2008 Alzheimer's disease facts and figures). Further important symptoms which appear with dementia include depression, hallucination and often anxiety (Mahler *et al.*, 1987; de Araujo *et al.*, 2014). Strengthening the rising importance of dementia, the latest Manual of Mental Disorders (DSM-5) constitutes a new entity in which dementia and amnesic disorders together form the group of 'major neurocognitive disorder (NCD)' (Diagnostic and Statistical Manual of Mental Disorders, 2013). More than half of the world wide dementia cases are classified as AD (World Alzheimer Report 2009). In Germany dementia is located among the ten most occurring causes of death along with heart diseases, stroke and lung illnesses (statistisches Bundesamt, 2014). High numbers of incidence, 7.7 million new patients every year (Dementia, 2012) and high economic cost, £23 billion (€ 28.5 billion) per year as pointed out by the Alzheimer's Research Trust in the United Kingdom (Luengo-Fernandez, 2010) show the urgent demand for research on this field and especially new therapy options.

1.3 Parkinson's Disease

1.3.1 Definition & Epidemiology

Parkinson's disease (PD) is a common form of neurodegenerative diseases and is thought to affect approximately 1.8 % of all people aged 65 years or older (Mollenhauer, 2010). Furthermore, it is the prevalent 'synucleinopathy', which describes an array of progressing degenerative diseases that share the abnormal deposition of α -synuclein in form of inclusion bodies. Other diseases belonging to this group are for example MSA, Dementia with Lewy Bodies, Lewy Body variant of Alzheimer's disease and neurodegeneration with brain iron accumulation type 1 (Del Tredici, 2000).

PD was first described in 1817 by James Parkinson in his monograph "Assay on the Shaking Palsy" and was renamed after his first descriptor by Jean-Martin Charcot more than 50 years

later (Goetz, 2011). The disease is clinically characterized by cardinal symptoms leading to 'parkinsonism', a syndrome which can be found in any patient with striatal damage or striatal dopamine deficiency, although PD is by far the most common cause. Those symptoms include tremor at rest, rigidity, bradykinesia and postural instability, making PD the most common movement disorder (Dickson *et al.*, 2009b). The progressing character of PD leads to a worsening of symptoms until daily life is no longer to cope with. A variety of further symptoms occurs during disease development, including hypokinesia, akinesia, hypomimia, hypophonia and problems with swallowing and writing. The general passive and apathetic behavior is reinforced by an accompanying depression and dementia (Dauer *et al.*, 2003). These two non-motor manifestations indicate that PD is a multisystemic disorder of the central nervous system (Massano *et al.*, 2012).

1.3.2 Pathophysiology

Pathological findings in the brain reveal a tremendous loss of dopaminergic neurons in the substantia nigra *pars compacta* (SNpc), which is located in the mesencephalon (midbrain). The cell bodies of the dopaminergic neurons are located within the SNpc, whilst the axons project into the striatum, which consists of putamen and caudate. Here, mainly neurons innervating the putamen are affected by a marked loss; they are projected from the primary sensory and motor cortices. Those cells innervating the caudate, which receives inputs from frontal and parietal association areas, display only moderate damage (Dauer *et al.*, 2003). This nigrostriatal pathway is part of the basal ganglia circuitry, which is involved in movement control and production and allows the correct execution of voluntary motion (Obeso *et al.*, 2008). As a consequence of the neuronal loss in the SNpc the concentration of the neurotransmitter dopamine and its metabolites decrease markedly in the striatum. This concentration imbalance triggers a whole cascade of events in the basal ganglia circuitry. The subsequently decreased activation of GABAergic neurons in the striatum leads to a diminished inhibition of the glutamatergic neurons in the Nucleus subthalamicus as well as the GABAergic neurons of Substantia nigra *pars reticulata* and globus pallidus *pars interna*. As a consequence an increased neuronal activity in these both output nuclei results in excessive inhibition of the ventrolateral thalamus which is connected to cortical and subcortical motor areas (Figure 1) (Blandini *et al.*, 2000).

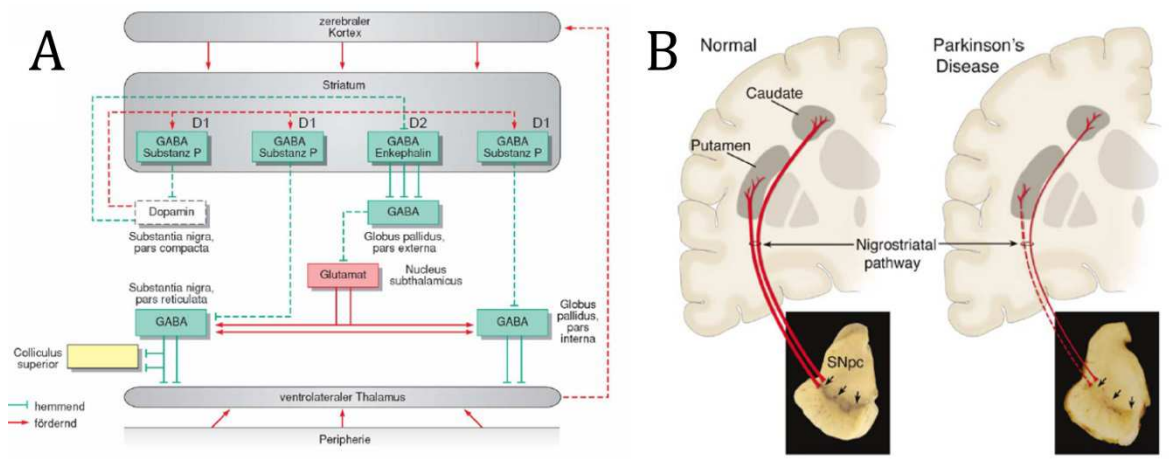


Figure 1: Nigrostriatal pathology in the PD brain.

A displays a schematic illustration of the basal ganglia circuitry ("Physiologie" 4. Edition 2004). B shows the difference in the nigrostriatal pathway between a normal and a PD brain (Dauer *et al.*, 2003).

The loss of neurons is greatest in the lateral ventral part of the SNpc (Fearnley *et al.*, 1991), where the death of neuromelanin containing cells leads to the characteristic pathological finding of depigmentation in this area (see Figure 1B). Interestingly, as it could be shown that the loss of neuron terminals in the striatum is more prominent than the loss of the dopaminergic neuron cell bodies in the SNpc, the idea of the "dying back" hypothesis emerged (Bernheimer *et al.*, 1973). This assumption starts from the premise that the main target of the degenerative process might be the neuron terminals rather than cell bodies as found in studies with MPTP (1-methyl-4-phenyl-1,2,3,6-tetra-hydropyridine)-treated mice which lack neuron loss in the SNpc if the axons and terminals in the striatum were protected (Wu *et al.*, 2003). The striatal cell loss is accompanied by an inflammatory reaction produced by activated microglia, as it was found in the SNpc of PD patients. The increased production of cytokines leads to neuron damage in these areas which can be prevented by early application of anti-inflammatory drugs (Schies, 2003). However, the role of microglia is discussed controversially for their part in neurodegenerative diseases (Russo *et al.*, 2014; Tansey *et al.*, 2010).

In addition to the dopaminergic cell loss also other neurotransmitter systems can be involved. Histological analyzes revealed neurodegeneration also in the serotonergic, noradrenergic and cholinergic system and in corresponding anatomical structures like locus coeruleus, nucleus basalis or raphe (Espay *et al.*, 2014).

The progress of PD can be subdivided into stages according to involved areas and the corresponding degree of degradation. Interestingly, in the first and second stage of the disease the SNpc remains normal and does not show any abnormality. In this time patients often complain about an impaired sense of smelling, sometimes years before the first motor symptoms emerge. Consistent with this finding, the first lesions occur in the anterior olfactory nucleus as well as in the olfactory bulb. After that, deteriorations in the lower brain stem appear

where the gain setting nuclei are located. In stage three and four the impairment of SNpc follows and in later stage five and six also thalamus and neocortical areas are included in the degenerative process. At this stages important structures of the limbic system display damages especially amygdala and hippocampus leading do cognitive deficits and dementia (for details see Table 1) (Braak *et al.*, 2003).

Table 1: Stages and affected brain structures in PD pathology
(adopted from (Braak *et al.*, 2003))

Stage	Affected brain structures
I	Medulla oblongata, dorsal IX/X motor nucleus, intermediate reticular zone
II	Caudal raphe nuclei, gigantocellular reticular nucleus, coeruleus-subcoeruleus complex
III	Midbrain, especially SNpc
IV	Prosencephalic lesions, temporal mesocortex (transentorhinal region), allocortex (CA2-plexus)
V	High order sensory association areas of neocortex and prefrontal neocortex
VI	First order sensory association areas of neocortex and premotor areas, mild changes in primary sensory areas and primary motor field possible

The diagnosis of PD is not only based on dopaminergic cell loss but requires also the presence of another pathological hallmark in the brain, Lewy bodies (LBs) and Lewy neurites (LNs) (Massano *et al.*, 2012). LBs are cytoplasmic protein aggregates, which are located in the cell soma of specific neurons. They comprise of α -synuclein (aSYN), ubiquitin, synphilin, parkin, and neurofilaments and build a nearly insoluble aggregate. LBs are not unique to PD but can be found in other synucleinopathies, too. They show a highly organized structure with a dense hyaline core and a surrounding halo and have a diameter of approximately 15 μ m (Dickson *et al.*, 2009b). Within the cell they occupy most of the cell body and inevitably lead to its death. The most affected anatomical structure is first of all the SNpc but in severe cases also amygdala and cortex bear LBs (Braak *et al.*, 2003). According to current research, the deposition of LBs is causative for the massive loss of dopaminergic neurons in the SNpc. LNs are probably pre-stage to LBs as they come in a thread-like shape and are mostly located in axons where they impair the metabolism of the cell (Dickson *et al.*, 2009a). As aSYN is the major constituent of these formations, much attention in the field of research has been devoted to this protein. It will be further described in an own section (see 1.4).

1.3.3 Genetics & Etiology

Idiopathic PD, which accounts for 90 % of all cases worldwide, occurs due to unknown mechanisms and develops sporadically on the basis of old age. In contrast, familial PD emerges

from genetic predisposition i.e. mutations in specific genes. These rare cases (< 10 %) provide the basis for most of the research done today. Until now 28 specific chromosomal loci have been linked to PD. Even though some loci still lack confirmation, six have been identified in which mutations directly lead to monogenic PD in either autosomal-dominant or autosomal-recessive manner (Klein *et al.*, 2012; Bertram *et al.*, 2005).

Among them, mutations in *SNCA* (*PARK1/PARK4*, synuclein, alpha [non A4 component of amyloid precursor]) lead to early-onset PD developing at an age of 50 years or earlier. The disease progresses rapidly with a severe phenotype and dementia as a usual syndrome (Bonifati, 2014). This rare locus hosts only three known mutations as well as duplication and triplication of the coding region. The mutations were found in few families worldwide. The most prominent is A53T (Alanine to Threonine in exon 4) followed by A30P (Alanine to Proline in exon 3) and E46K (glutamic acid to lysine in exon 3) which were each present in only one family so far (Zarranz *et al.*, 2004; Kruger *et al.*, 1998; Singleton *et al.*, 2013). A possible mechanism through which mutations in this gene cause PD is thought to be a gain of toxicity due to shift in conformation of α -synuclein to form stable β -sheets known to be more prone to aggregation (for further details see 1.4.2) (Brucule *et al.*, 2009).

Beside those genes leading to monogenic forms of PD (*SNCA*, *LRRK2*, *Parkin*, *PINK1*, *DJ-1* and *ATP13A2*) there are some further loci which are considered to be at least causative for PD. As mentioned before, some of the loci are not certain or lack confirmation or they are linked to PD but the gene remains to be identified, other lead to parkinsonism as part of some different disease. But based on GWAS (genome-wide association study) and other studies, it was possible to not only identify additional genes (e.g. *MAPT*, *NAT2*, *GAK*) but also length- and SNP (single nucleotide polymorphism) variants in *SNCA* and *LRRK2* leading to monogenic PD (Klein *et al.*, 2012).

However, genetic predisposition is not the only known risk factor beside age. Etiological factors in PD include also bacterial and viral infections, plant derived toxins, polluted water, industrial chemicals and other rural and environmental influences (Priyadarshi *et al.*, 2001). Here especially insecticides and herbicides as environmental toxins play an important role. Most importantly, MPTP, a byproduct of the synthesis of a heroine-like drug, caused a stir among researchers as it was found to induce irreversible parkinsonism in humans of all ages and thus, was the first identified dopaminergic neurotoxin, confirmed by using rhesus monkeys (Langston *et al.*, 1983; Burns *et al.*, 1983). Interestingly, its derivate MPP⁺ (1-methyl-4-phenylpyridinium ion), which is produced in astrocytes via monooxidase type B, was shown to inhibit complex I of the mitochondrial electron transport chain in dopaminergic neurons (Nicklas *et al.*, 1985; Singer *et al.*, 1987). Several other similar substances have been found, for example Paraquat, a herbicide which is structurally similar to MPTP or rotenone, a plant derived household insecticide which functions like MPTP as a mitochondrial poison (Betarbet *et al.*, 2000; Maturana

et al., 2014). As a consequence of disturbed mitochondrial function oxidative stress emerges in the form of ROS and may lead to cell death. Consequently, inhibition can prevent MPTP-induced parkinsonism (Przedborski *et al.*, 1992; Przedborski *et al.*, 1996). Mitochondrial dysfunction as cause of PD is a well-accepted hypothesis among researchers and is therefore further described in section 1.5. Altogether, these findings gave interesting insights into the mechanisms leading to PD. However, a causative role of those toxins for idiopathic PD seems unlikely as MPTP induced parkinsonism is not progressive and does not lead to Lewy body pathology or other pathologies in the brain (Schapira *et al.*, 2011; Jenner, 2003).

1.3.4 Therapy

Until today there is no cure for PD. Thus, symptomatic therapy is applied, since 1969 most commonly by administration of L-dopa, the precursor for the biosynthesis of various neurotransmitters such as dopamine. As a consequence, the dopamine level increases in the remaining dopaminergic neurons in the SNpc and striatum, compensating the loss of neurons in these areas and leading to a reduction of various symptoms (Cotzias *et al.*, 1969). Similar results are achieved by enzyme replacement therapy, in which genes encoding important enzyme for biosynthesis of dopamine become transferred into neurons of the striatum. Gene therapy, a novel method, provides genetic modifications of cells via viral or non-viral methods and leads also to an improvement of disease symptoms and to a decrease of side effects. An increase or reduction in gene expression can be achieved depending on the functional impairment (Bjorklund *et al.*, 2010; Coune *et al.*, 2012). The providing of the tyrosine hydroxylase gene, an enzyme in the biosynthesis of L-dopa, leads to a long term production of the enzyme and consequently dopamine (Kaplitt *et al.*, 1994). Another well-examined factor essential for therapy in PD is the growth factor GDNF (glial cell line-derived neurotrophic factor). It was shown that GDNF enhances the survival of dopaminergic neurons and increases axonal sprouting (Rosenblad *et al.*, 1998; Connor *et al.*, 2001). Promising results were gathered using a lentiviral vector delivering GDNF into specific areas of the brain. In a non-human primate model of PD it was possible to inhibit degeneration of cells and improve motoric function (Kordower *et al.*, 2000).

Moreover, deep brain stimulation is currently a well examined method to provide regaining of dopamine signaling via stimulation of the subthalamic nucleus. It furthermore leads to a reduction of drug intake and side effects (Benabid *et al.*, 2009).

However, the benefits of increasing the availability of dopamine are limited, since the chronic intake of L-dopa leads to severe side effects such as dyskinesia and dosage has to be increased regularly (Coune *et al.*, 2012). But even the successful gene therapy may only give benefits for a certain time frame or might only treat some symptoms. It was found that often even if motor deficits or other symptoms may be improved by therapy, the quality of life improves not.

Patients often suffer from social isolation and communication problems (Mylene *et al.*, 2013). To find best therapy options and a possible cure it is necessary to understand the metabolic basics that underlie the pathophysiology of PD and to prevent onset of the disease at the stage when neurons are still alive.

1.4 Alpha-synuclein

1.4.1 Characteristics & Function

Alpha synuclein (α SYN) is a 140 amino acid protein, which was assumed to be located to presynaptic sites in neurons of the brain and was therefore denoted synuclein (Iwai *et al.*, 1995). The first description was made based on isolated α SYN from the electrical organ of *Torpedo californica* (Maroteaux *et al.*, 1988). Today it is considered to be homolog to the human γ -synuclein (Maroteaux *et al.*, 1991). Besides α - and γ -synuclein, the family of synucleins includes also β -synuclein, which all share the same amino-terminal sequence but differ in the carboxy-terminal part (Tofaris *et al.*, 2005). Human α SYN is a protein of about 14 kDa and was first isolated due to its NAC fragment (non-Amyloid β component), which was found to be involved in Amyloid β pathogenesis in Alzheimer's disease (Ma *et al.*, 2003). It represents 1 % of all cytosolic proteins in the brain (Iwai *et al.*, 1995). Structurally, the protein can be divided into the N-terminal, the central- and the C-terminal region (see Figure 2). In the N-terminal part (amino acid 1-60) the three familial PD mutations can be found as well as amino acid repeats with the conserved KTKEGV motif. Furthermore, it hosts apolipoprotein lipid-binding motifs which support the forming of α -helical structures when binding to membranes. The central region (amino acid 61-95) is hydrophobic and comprises the NAC fragment, which is highly prone to aggregation. The last part (amino acid 96-140) is the C-terminal region. It contains many proline residues, which disrupt the secondary structure and make this part unstructured (Bellucci *et al.*, 2012).

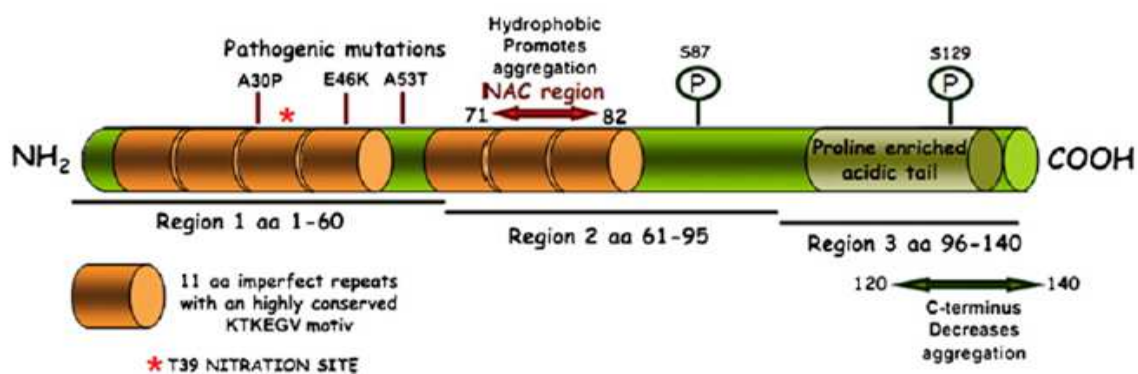


Figure 2: α -synuclein transcript with mutations respectively phosphorylation and nitration sites (Bellucci *et al.*, 2012).

α SYN is defined as a 'natively unfolded' protein as it does not form a secondary structure in aqueous solutions (Weinreb *et al.*, 1996). However, Bartels *et al.* (2011) found a folded tetramer of 58 kDa when using non-denaturing condition for the isolation from various different cell lines. They propose that destabilization of this tetramer leads to the abnormal aggregation potential of α SYN in PD. On the other hand, this topic was discussed controversially by Burre *et al.* (2013), who found α SYN as an unstructured monomer. Even if unstructured, preferences to obtain α -helices were observed, mainly in the N-terminal region of α SYN when binding to lipids, whereas the formation of fibrils is accompanied by β -sheet structures. The aggregation rate of α SYN furthermore can be promoted by factors such as low pH, the presence of Cu^{2+} or mutations (McClendon *et al.*, 2009; Montes *et al.*, 2014).

Three different splicing variant of α SYN in humans could be identified so far, including aSYN 126, aSYN 112 and aSYN 98 with different functional properties. While aSYN 126 was found to have protective effects in the aging brain, the other splicing variants promote aggregation of aSYN (Beyer *et al.*, 2009).

The function of α SYN is still not fully known. Very early, increased expression of the protein was found in a specific neuron population during the process of song learning in songbirds and thus, was hypothesized to relate to synaptic plasticity (Bellucci *et al.*, 2012). Today it is thought that the protein is implicated in the maintenance of synaptic membranes as well as the control of the expression, distribution and activity of specific proteins in the synapse. Furthermore, neurotransmitter release might be regulated by α SYN via control of synaptic activity. It was found that α SYN knock-out mice display an increased dopamine release, indicating a regulative function of the protein in the synapse (Abeliovich *et al.*, 2000). α SYN may also facilitate the neurotransmitter release by increasing the formation of SNARE (soluble NSF attachment protein receptor) complexes, as it binds to synaptobrevin-2 (VAMP2, vesicle associated membrane protein 2) (Burre *et al.*, 2010). Even if contradictory results exist with respect to its implication in neurotransmitter release, there are promising results indicating an important role for α SYN in this metabolism (Cabin *et al.*, 2002; Chandra *et al.*, 2004). A connection between aSYN and SNARE complexes was found in 2005. Chandra *et al.* were able to show that the deletion of CSP α (cysteine string protein α) in mice leads to a severe neurodegeneration phenotype (Chandra *et al.*, 2005). CSP α is known to serve as a chaperone in a complex together with other proteins and is able for example to refold denatured luciferase (Tobaben *et al.*, 2001) respectively prevents the aggregation of SNAP-25 (synaptosomal-associated protein 25), an important protein of the SNARE complex. The deletion of CSP α inhibits a proper SNARE complex assembly and increases ubiquitination and degradation of SNAP-25. Interestingly, an overexpression of α SYN was able to rescue the SNARE complex formation and the loss of SNAP-25, thus preventing neurodegeneration (Chandra *et al.*, 2005). The findings were confirmed by Burre *et al.* (2010), who found a linear relationship between SNARE complex assembly and α SYN level. Consistent

with that, α SYN is situated in equilibrium of free and membrane- respectively vesicle-bound states (Bisaglia *et al.*, 2006).

Additionally, the association of α SYN with the negatively charged membrane led to the assumption that it plays a role in modulating membrane lipids and its organization (Madine *et al.*, 2006; Kamp *et al.*, 2006) and is therefore involved in the cerebral lipid homeostasis (Kim *et al.*, 2012). It was furthermore observed that the mass of cerebral cholesterol, cholesteryl esters and triacylglycerols increased upon a deletion of α SYN in mice (Barcelo-Coblijn *et al.*, 2007). The binding of α SYN to lipids enabled the protein to form α -helical structures and to fibrillate (Lee *et al.*, 2003; Zhu *et al.*, 2003).

These recent results, discussed in various reviews (Stefanis, 2012; Bellucci *et al.*, 2012; Lee *et al.*, 2006), give only little insight into what is known of α SYN and its function today. Thus even if the exact role of α SYN remains still not fully understood, certain interesting mechanisms through which α SYN may function in the cell were already described.

1.4.2 Genetics

As mentioned before (1.3.3), missense mutations in the gene encoding α SYN (*SNCA*), as well as duplication or triplication, have been found to cause rare forms of familial PD. Depending on the mutation, the clinical and pathological manifestation can be completely different. The most common mutations are A53T, A30P and E46K which all lead to altered aggregation of α SYN (Lazaro *et al.*, 2014; Li *et al.*, 2001).

The interaction of α SYN with negatively charged liposomes is increased with the E46K mutated protein leading to an enhanced filament assembly (Choi *et al.*, 2004). However, it displays less fibril formation *in vitro* compared to wildtype protein (Fredenburg *et al.*, 2007). In contrast to that, the A53T mutation more rapidly leads to fibril formation *in vitro* than A30P mutated or wildtype α SYN (Conway *et al.*, 2000). Whereas A30P mutated α SYN shows a less abundant interaction with lipids of vesicles and membranes (Jo *et al.*, 2002; Stockl *et al.*, 2008), the formation of fibrils was slower compared to wildtype, especially at low concentrations (Li *et al.*, 2001), but oligomerization was faster in comparison (Krasnoslobodtsev *et al.*, 2013). However, a reduced formation of inclusions was confirmed when compared to E46K mutated α SYN (Lazaro *et al.*, 2014). The A30P (and A53T) mutation reduces the hydrophobicity of the protein (Li *et al.*, 2001). The interactions of the N-terminus are altered with these mutations and lead to interactions with the C-terminal end (Krasnoslobodtsev *et al.*, 2013). Additionally, the tendency to form α -helices in the N-terminal region was lower whereas it was enhanced in the case of β -sheets, possibly leading to altered aggregation as observed by Fourier transform infrared spectroscopy and Small angle X-ray scattering measurements (Li *et al.*, 2001; Li *et al.*, 2002). Interestingly, even though the α -helical structure formation was decreased due to the A30P mutation, no changes in β -sheet organization could be found in the α SYN protein structure

performing annealing molecular dynamics simulations (Balesh, 2011). Remarkably, Burre *et al.* (2012) have recently shown that the A30P mutation is unique among the α SYN mutations, as it solely leads to decreased synaptic targeting and diminished SNARE complex stability *in vitro*, proposing that the alanine may be crucial for α -helix formation.

Even though these mutations and the resulting PD cases are rare, they are highly important for the understanding of the pathophysiology of PD and, thus, for the research in this field, as they enable the modeling of the sporadic disease.

1.4.3 Pathology & Toxicity

The deposition of α SYN inside neurons leads to degeneration of those and to the symptoms occurring in several disease of the synucleopathy group. Beside genetic mutations, which account for only less than 10 % of all cases, posttranslational modifications have been in focus of research. Several interesting observations have been made concerning alterations occurring in wildtype aSYN (Bellucci *et al.*, 2012).

The main reason for aSYN to gain toxicity is thought to be the building of insoluble aggregates. Natively unfolded aSYN monomers start to form β -sheet rich oligomers, the protofibrils. These further form specific structures leading to more stable amyloid-like fibrils, which aggregate as Lewy bodies (Moore *et al.*, 2005).

Several posttranslational modifications are known today to alter the biophysical properties of the protein. The most prominent is the phosphorylation of serine at position 129 by casein kinase 1 and 2 (Okochi *et al.*, 2000) or G-protein-coupled kinases (Pronin *et al.*, 2000). As a consequence of the modification at the C-terminal site, fibrillation is promoted (Fujiwara *et al.*, 2002). Especially different modifications at the C-terminal part were found to alter the propensity of aSYN to aggregate, underlined by the finding that C-terminally truncated aSYN tends to form pathological accumulations *in vivo* and *in vitro* (Ulusoy *et al.*, 2010; Tofaris *et al.*, 2006).

Tyrosine nitration is another posttranslational modification known to occur in aSYN, leading to increased fibril formation. The nitration of tyrosine at position 39 located in the N-terminal part was found not only to promote aggregation but also to prevent the binding of aSYN to lipid vesicles, hence interfering with its physiological function. Furthermore, nitration slows down the process of proteasomal degradation (Giasson *et al.*, 2000; Hodara *et al.*, 2004).

Even the binding to lipids contains some difficulties, as the exposure to polyunsaturated fatty acids was shown to cause multimer/oligomer formation *in vitro* and *in vivo* (Perrin *et al.*, 2001; Sharon *et al.*, 2003). However, this topic is discussed controversially due to conflicting findings (Schapira *et al.*, 1990; Trostchansky *et al.*, 2006).

Recently, the role of protein degradation and clearance mechanisms in the pathogenesis of neurodegenerative diseases gained increasing attention. As the correlation between protein

deposition and magnitude of disease failed until now, the hypothesis emerged that soluble monomeric respectively oligomeric peptides are toxic species and aggregated protein is, in fact, a protective mechanism (Kopito, 2000; Pahnke *et al.*, 2009).

As the cell dynamically synthesizes and degrades proteins in order to ensure equilibrium, a defective degradation system would likely lead to tremendous impacts on the cell physiology. One degradation mechanism to dispose misfolded or damaged proteins is the ubiquitin proteasome system (UPS), which degrades proteins that are covalently bound to ubiquitin. Parts of the UPS as well as ubiquitinated proteins have been found in LBs, suggesting an impairment of the UPS in the pathophysiology of PD, which might be potentiated by the further accumulation of aSYN (Schlossmacher *et al.*, 2002; Emmanouilidou *et al.*, 2010). The finding that nearly all aSYN aggregated in LBs is phosphorylated at Serine-129 further supported the theory, because it was previously reported that Serine-129-phosphorylated aSYN can directly be degraded by the UPS without former ubiquitination (Machiya *et al.*, 2010). Interestingly, it could also be revealed that an exposure to environmental toxins such as rotenone and MPTP (as described before in 1.3.3) led to an impairment of the UPS *in vitro* and *in vivo* (Zeng *et al.*, 2006; Wang *et al.*, 2006). Furthermore, the finding of a very early onset variant of PD caused by *parkin* mutations, a gene coding E3 ubiquitin ligase, and the notion that no LB formation can be found in those cases underlined the concept of protein deposition being a protective mechanism of the cell to attenuate the toxicity of soluble protein.

Another way of degradation implicated in PD includes the lysosomes via micro- and macroautophagy. Using macroautophagy the cell is able to degrade a complete component of the cytosol including aggregated protein depositions, which may lead to failure in case of overload. Furthermore, the sequestered proteins might become a “source of reactive oxygen species inside” (Cook *et al.*, 2012).

It has long been thought that aSYN, as intracellular protein, cannot be found in the cerebrospinal fluid (CSF). However, convincing counterevidence was brought by Borghi *et al.* (2000); El-Agnaf *et al.* (2003), who proved the presence of aSYN in the CSF and plasma of PD patients as well as healthy controls. One possible explanation pointed out by the authors is the aSYN efflux from the brain since it was similarly discovered for A β in a mouse model of AD. Here, the transport via ABC transporter was found to be involved (Kortekaas *et al.*, 2005; Krohn *et al.*, 2011).

1.4.4 ABC transporter & PD

In recent years, a special transport system came into focus of neurodegeneration research, the ABC transporter (ATP-binding cassette transporter). Until today, 49 human ABC transporters were described subdivided into seven families (A to G) and distributed in different tissues, e.g. liver, lung, and blood-brain-barrier (BBB) as well as choroid plexus (reviewed in (Pahnke *et al.*,

2014). This large group of integral membrane proteins uses the energy of ATP to facilitate the influx of nutrients into the brain and the efflux of toxic compounds from the brain via the BBB/blood-cerebrospinal fluid (CSF)-barrier (BCB) by an active transport mechanism (Miller, 2015). Their localization in the membrane of epithelial cells of the BBB respectively the BCB enables them to be a functional barrier to protect against hazardous substances from the blood stream/CSF (Begley, 2004).

It was successfully proved that ABC transporters are crucial in the prevention and treatment of several diseases, particularly multidrug resistance in cancer and recently the proteopathies in the brain (Pahnke *et al.*, 2013). Especially in mouse models of Alzheimer's disease (AD) (Vogelgesang *et al.*, 2004; Cirrito *et al.*, 2005; Lam *et al.*, 2001), but also in PD patients (Bartels *et al.*, 2008b; Bartels *et al.*, 2009), several studies could show the contribution of ABC transporters, especially ABCB1 (P-glycoprotein, P-gp), on the clearance of toxic peptides from the brain (Kortekaas *et al.*, 2005). Even though, a diminished ABCB1 function was never confirmed in early stages of PD, it was in healthy elderly controls, therefore it probably doesn't play a causative role in PD pathogenesis (Bartels *et al.*, 2008a).

ABCA5 is an ABC transporter known to transport mainly lipids, e.g. sphingomyelin, and was recently found to be elevated in the brains of PD patients (Kim *et al.*, 2012) and associated with a reduced risk for developing PD revealed by GWAS (Simon-Sanchez *et al.*, 2009).

Interestingly, another ABC transporter of this family was reported to be implicated in the transport of aSYN, ABCA8. In the context of MSA, ABCA8 expression was reported to be upregulated with a concomitantly increased expression of aSYN in the affected regions of the brain (Bleasel *et al.*, 2013).

Only just, the ABCC1 transporter (Multidrug resistance-associated protein 1, MRP1) revealed promising results by reducing the A β burden in the diseased brain of an AD-mouse model upon pharmacologically increased activity and further supported the comprehension of the importance of this system. Interestingly, the knock-out of ABCC1 and the following decrease of the export function of only 11 % led to a 4-fold increased A β load (Krohn *et al.*, 2011). However, the possible impact of ABCC1 on the pathogenesis of PD was never studied so far and its further investigation is of utmost interest.

1.5 Mitochondria

1.5.1 Structure & Function

Mitochondria are 1-4 μ m sized cell organelles, which can be found in any eukaryotic cell except for erythrocytes (Kennady *et al.*, 2004; Cimen, 2008). Due to their main function of producing adenosine triphosphate (ATP) via oxidative phosphorylation, they are also denoted as "powerhouse of the cell" (Perier *et al.*, 2012).

Several cellular functions like muscle contractions, generation of ion gradients and synthesis of molecules highly depend on supply of ATP provided by mitochondria. Beside ATP production also other pathways are located within the matrix for example hem biosynthesis and urea cycle. Furthermore, Ca^{2+} homeostasis and apoptosis are both facilitated by opening of the permeability transition pore (PTP), either reversibly or irreversibly. By uncoupling of the oxidative phosphorylation mitochondria can also produce heat (Leonard *et al.*, 2000; Bonda *et al.*, 2010). Their characteristic structure, comprising of outer and inner membrane, the inter membrane space and the matrix, is adjusted to their physiological role. The outer membrane is permeable for small molecules (< 6 kDa) which can enter via porines (Zalman *et al.*, 1980; Gellerich *et al.*, 2000) and voltage dependent anion channels (Blachly-Dyson *et al.*, 1993), but otherwise displays a concentration gradient (Gellerich *et al.*, 1994). Additionally, larger molecules can enter using translocases of the outer membrane. The inner membrane builds several convolutions looming into the matrix (cristae), leading to an enhanced membrane surface necessary to provide the needed energy supply. Here, the complexes of the electron transport chain are situated as well as the PTP. The inner membrane itself is impermeable, especially for ions, thus metabolites can only pass via specific transport molecules (Bohnert *et al.*, 2012; Mannella, 2006). The matrix within the inner membrane contains RNA- and DNA polymerases, tRNAs and the mitochondrial genome (mtDNA) as well as several enzymes which are necessary for the citrate cycle, oxidation of pyruvate and fatty acids, and other biochemical processes (Alberts B., 2002).

The human mitochondrial genome is a double stranded circular plasmid containing 37 genes which code only for part of the mitochondrial proteins, while the rest is imported from the cytosol of the cell. Only 13 of these genes are necessary for complexes of the respiratory chain. Every mitochondrion hosts 2 to 10 copies of its own DNA. In contrast to the nuclear genome the mitochondrial genome is inherited only maternally via mitochondria in the ovum. Thus, gene defects and related diseases can only be passed on by the mother (Schon *et al.*, 2012).

1.5.2 The electron transport chain

The most prominent function of mitochondria is the production of energy in form of ATP (adenosine triphosphate) by oxidative phosphorylation. This is ensured by using the energy of the reduction of oxygen to water to produce ATP from ADP (adenosine diphosphate). The reaction is realized in steps which take place in the complexes of the electron transport chain (ETC, respiratory chain).

Briefly, preceding this process is the glycolysis in which glucose is degraded to pyruvate in the cytosol of the cell; this step includes the production of NADH from NAD^+ (nicotinamide adenine dinucleotide). Pyruvate is transported into the mitochondrial matrix where it is converted into acetyl-CoA via oxidative decarboxylation, which becomes further oxidized during the citrate

cycle. Additionally, the citrate cycle leads to the production of NADH and FADH from NAD⁺ respectively FAD (flavin adenine dinucleotide) which are used to transfer electrons that emerged during the cycle to the complexes of the ETC (see Figure 3) ("Biochemie: Eine Einführung für Mediziner und Naturwissenschaftler" 2004).

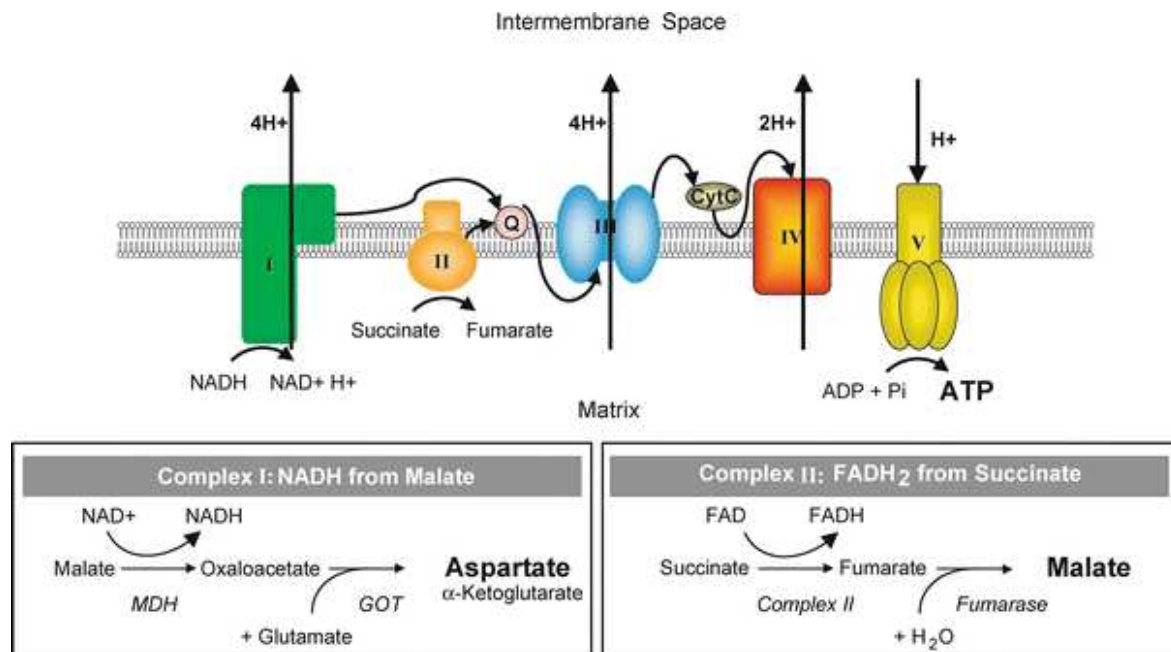


Figure 3: Schematic illustration of the ETC and additionally reactions catalyzed by complex I and II (Cuperus *et al.*, 2010).

The ETC comprises of four complexes (I–IV) and the ATP-synthase. Complex I (NADH-dehydrogenase-ubiquinone oxidoreductase) starts transferring two electrons from NADH from the citrate cycle to FMN⁺ (flavin mononucleotide) under the production of FMNH₂ and NAD⁺. NADH which is made during glycolysis is transported into the matrix via glycerol-3-phosphate shuttle using glycerol-3-phosphate, which oxidizes to dihydroxyacetone phosphate, and to deliver two electrons and protons to FAD. The shuttle requires Ca²⁺ for activation (McKenna *et al.*, 2006). Those two electrons, shifted to FMN by NADH, are further transferred to ubiquinone via iron-sulfur clusters. Subsequently, four protons are transported from the matrix into the inter membrane space. Complex II (Succinate dehydrogenase-ubiquinone oxidoreductase, SDH) is not involved in the transport of protons across the membrane but also donates electrons to reduce ubiquinone (coenzyme Q). This reduction is achieved through the dehydration of succinate to fumarate and the adjoining reduction of FAD to FADH. The reduced ubiquinone passes its electrons to cytochrome c via complex III (ubiquinone-cytochrome c oxidoreductase) and is thereby oxidized again, while cytochrome c becomes reduced. Meanwhile, four protons are transported across the membrane. In complex IV (cytochrome c oxidase), the oxidation of cytochrome affiliates and O₂ is reduced to H₂O, leading to proton crossing through the membrane once more. The so-built proton gradient is simultaneously used by the ATP-synthase

(ATPase) to generate ATP from ADP and phosphate. The ADP/ATP translocase then transfers ATP into the matrix in exchange of ADP (Cecchini, 2003).

As the oxygen consumption is tightly coupled to the ATP production, it is possible to divide the respiration into different functional states, as done by Chance et al. in 1955 (see Table 2). In this classification, state 4 displays a resting state, in which no ADP is phosphorylated due to insufficient supply, following no ATP is produced and respiration proportionately low, unless the inner membrane is uncoupled respectively damaged. State 3 refers to the maximal possible respiration reached when the cell is sufficiently supplied with substrate, oxygen and ADP and the limitation is only given by the enzymatic reaction of the single complexes of the ETC (Chance *et al.*, 1955).

Table 2: Classification of functional states of mitochondrial respiration
(adopted from (Chance *et al.*, 1955))

state	ADP level	substrate level	Limiting substance
1	low	low	ADP
2	high	~0	Substrate
3	high	high	respiratory chain
4	low	high	ADP
5	high	high	oxygen [<0]

1.5.3 Mitochondrial alterations & PD

The link between mitochondrial alterations and neurodegenerative diseases has been made on the basis of several indicators that were found to be involved in one or several diseases, such as structural alterations, diminished ATP production, increased ROS, mutations in the mitochondrial genome, deficiency in complexes of the ETC as well as impairments in mitochondrial motility and Ca^{2+} homeostasis (Perier *et al.*, 2012).

The association of mitochondrial dysfunction with the pathogenesis of PD has been in focus of research since it was observed, that complex I-deficiency due to exposure to MPTP, first unintentionally by drug addicts and later experimentally in nonhuman primates and mice, leads to dopaminergic neuron loss in the SNpc and the development of parkinsonism (Dauer *et al.*, 2003). The identification of further complex I inhibitors like rotenone and other pesticides confirmed these findings (Betarbet *et al.*, 2000; Hong *et al.*, 2014; Richardson *et al.*, 2009).

Complex I deficiency was also discovered in brains of patients with sporadic PD (Schapira *et al.*, 1990) and could be bypassed in mice by probably increasing an complex II-depending mechanism (Tieu *et al.*, 2003) or by using an alternative electron carrier (methylene blue) in rats (Wen *et al.*, 2008).

One of the consequences of a reduced complex I activity is an insufficient supply with ATP as it was found in the brain of mice (Dias *et al.*, 2013). However, a depletion of complex I activity as

severe as needed to cause a reduced ATP level couldn't be found in PD patients and is therefore not likely to cause sporadic PD (Perier *et al.*, 2012), it might still support disease progression.

Inherited PD can be initiated by mutations in the mitochondrial genome (mtDNA). For example, mutations in the mtDNA polymerase γ lead to parkinsonism (Luoma *et al.*, 2004). However, mutations in the mtDNA are thought to occur during life with increasing age as part of normal aging (Lin *et al.*, 2006). By creating a mouse model with mutated, proof-reading deficient mtDNA polymerase, Trifunovic *et al.* were able to show that mutations in the mtDNA led to decreased life span of mice according to an early onset of various ageing-related phenotypes (Trifunovic *et al.*, 2004). Further evidence for the link between mitochondria alteration and PD was recently presented by Rhinn *et al.*, who describe a shift in the preferred accumulation site of aSYN from synaptic terminals towards mitochondria initiated by a specific transcript variant of α SYN, referred to as α SynL (Rhinn *et al.*, 2012).

One of the most discussed incidences, in connection with mitochondrial alterations, is the increased production of reactive oxygen species (ROS). ROS emerges endogenously during oxidative phosphorylation when molecular oxygen is reduced to superoxide anion (O_2^-) instead of converted into water in the mitochondria. This happens when the oxidative phosphorylation is inhibited or excessive calorie consumption took place. Normally, ROS is neutralized by antioxidants, such as glutathione and carotenoids, as well as enzymes like superoxide dismutase (Szeto, 2006). Otherwise, it induces profound damage of important biological molecules like DNA, lipids and proteins as observed in brain tissue of PD patients (Dauer *et al.*, 2003).

Complex I deficiency was found to increase ROS production, likely because of the diminished electron transfer and the resulting failure in the conversion of oxygen to water (Ramsay *et al.*, 1987) and in turn, ROS harms complex I subunits, as was observed in the frontal cortex of PD patients (Keeney *et al.*, 2006) Additionally, glutathione depletion was found in the SNpc, too (Gu *et al.*, 1998).

Furthermore, *DJ-1* (PARK7) mutations have been found to lead to increased ROS production, thereby causing autosomal-recessive PD (Andres-Mateos *et al.*, 2007) and to be prevented by an overexpression of *PINK1* (PTEN (Phosphatase and tensin homolog)-induced putative kinase 1) and *Parkin* as determined in cell culture (Irrcher *et al.*, 2010). Interestingly, an overexpression of *PINK1*, in which mutations also cause autosomal-recessive forms of PD, can prevent the binding of aSYN to mitochondrial membrane and consequently the inhibition of mitochondrial fusion (Kamp *et al.*, 2010).

Importantly, neurons are particularly vulnerable to mitochondrial alterations due to their high dependence on energy and Ca^{2+} homeostasis, favoring an involvement of mitochondrial dysfunction in the pathogenesis of PD. However, it remains to be evaluated if these display an initial or secondary effect to PD pathogenesis and in which way several indicators, mentioned in the beginning, interact.

2. Aims of work

The present work was accomplished to investigate the influence of mitochondrial polymorphisms on the PD pathogenesis in mice and to contribute understanding to the relevance of energy-dependent mechanisms in the context of PD.

For this purpose, the well-known PD mouse model, tg-aSYN, was to be characterized to assess its histological, biochemical and behavioral profile in young and old age. Based on the results, the intention was to determine the effects of specific mitochondrial polymorphisms on this mouse model. Therefore, a newly generated mouse, tg-aSYN-mtNOD, was to be examined with respect to following questions.

1. Do the mitochondrial polymorphisms lead to changes in histological, biochemical or behavioral characteristics of the mouse model such as:
 - a. aSYN coverage as well as neuronal and microglial area in the cortex,
 - b. intracerebral aSYN level,
 - c. movement deteriorations and spatial orientation?
2. Does the investigation of functional effects of the changed mitochondrial genome and its polymorphisms by respirometry point to differences in complex-dependent respiration between the background strains of the mouse models, tg-aSYN and tg-aSYN-mtNOD?

A follow-up study based on the promising results was appointed to verify a transport of aSYN via the ABC transporter ABCC1 using two strategies.

1. Does an ABCC1 knock-out mouse model display differences in intracerebral aSYN level and/or neuronal and microglial area in the cortex?
2. Is the pharmacological activation of ABCC1 able to counteract the aSYN burden and neuronal decline present in the brain of tg-aSYN mice?

In order to determine the influence of ABCC1 on the PD pathogenesis, a new mouse model was generated, the ABCC1 knock-out mouse, tg-aSYN-ABCC1^{-/-}.

3. Material & Methods

3.1 Material

3.1.1 Antibodies

	clone	Company
Anti-human α -Synulcein	5G4	aj roboscreen
Glial Fibrillary Acid protein (GFAP)	polyclonal	DAKO
Ionized calcium binding adapter molecule 1 (Iba1)	polyclonal	WAKO
Anti-Neuronal Nuclei (NeuN)	A60	Chemicon (Millipore)

3.1.2 Chemicals

	Company
2-Mercaptoethanol	Carl Roth GmbH
3-(N-morpholino)propanesulfonic acid (MOPS)	Sigma-Aldrich
α -Ketoglutarate	Sigma-Aldrich
Acetic acid	Carl Roth
Adenosine diphosphate (ADP)	Sigma-Aldrich
Agarose	Biozym Diagnostik GmbH
Antimycin A	Sigma-Aldrich
Ascorbate	Sigma-Aldrich
Atractyloside	Sigma-Aldrich
Azide	Sigma-Aldrich
Bovine serum albumin (BSA)	SERVA Electrophoresis GmbH
Calcium chloride (CaCl ₂)	Merck KGaA
Carbonyl cyanide-4-(trifluoromethoxy)-Phenylhydrazone (FCCP)	Sigma-Aldrich
citrate	
D-Glucose	Sigma
Digitonin	Sigma-Aldrich
Dimethyl sulfoxide (DMSO)	Merck KGaA
Dithiothreitol (DTT)	Sigma-Aldrich
Ethanol 96 %	Carl Roth GmbH
Ethidium bromide	Carl Roth GmbH
Ethylenediaminetetraacetic acid (EDTA)	Merck KGaA
Ethylene glycol tetraacetic acid (EGTA)	Sigma-Aldrich
Glutamate	Sigma-Aldrich
Glycero-3-phosphate	Sigma-Aldrich
Guanidinhydrochloride	Carl Roth GmbH
HCl	Carl Roth GmbH
Heparin	Sigma-Aldrich
Igepal CA630	Fluka Biochemika
KCl	Carl Roth GmbH

KH ₂ PO ₄	Merck KGaA
Malate	Sigma-Aldrich
Mannitol	Sigma-Aldrich
Methanol	VWR
Milk powder	Carl Roth GmbH
MgCl ₂ *(6H ₂ O)	Carl Roth GmbH
Nagarse	Sigma-Aldrich
NaCl	Carl Roth GmbH
Na ₂ CO ₃	Carl Roth GmbH
NaH ₃	Carl Roth GmbH
NaHCO ₃	Carl Roth GmbH
Na ₂ HPO ₄	Sigma-Aldrich
Paraffin Paraplast	Leica Biosystems /Menarini
PBS (10x)	Sigma-Aldrich
Paraformaldehyde (PFA)	Carl Roth GmbH
Proteinase K	Carl Roth GmbH
PVDF membrane	Carl Roth GmbH
Pyruvate	Sigma-Aldrich
RNAlater	Applied Biosystems
Rotenone	Sigma-Aldrich
Succinate	Sigma-Aldrich
Sucrose	Merck KGaA
TEMED	Carl Roth GmbH
N,N,N',N'-tetramethyl-p-phenylenediamine (TMPD)	Merck KGaA
Thiethylperazine (Torecan®)	Novartis
Tris	Carl Roth GmbH
Tris-HCl	Carl Roth GmbH
Tween 20	Merck
Xylene	Carl Roth GmbH

3.1.3 Equipment

	Company
BOND-MAX Autostainer	Leica Microsystems GmbH/Menarini
Centrifuge Universal 320R	Hettich
Precellys® 1.4mm zirconium oxide beads	Saphire bioscience
Chip cuvette	Analytic Jena AG
Electrophoresis power supply EV 231	Consort bvba
Embedding system Leica EG 1160	Leica Biosystems
Feeding needle	Fine Science Tools
Freezer -20 °C	gorenje
Freezer -80 °C	Kryotec
Glass homogenizer	WHEATON
Histokinette STP 120	Mikrom
Homogenisator SpeedMill PLUS	analytic jena

Microtome RM 2155	Leica Biosystems
Mirax Midi	Zeiss
OROBOROS oxygraph-2k	Oroboros Instruments
Pannoramic MIDI	3DHistech
Paradigm™ detection platform	Beckman-Coulter/Molecular Devices
Pole (Pole test)	custom made
Rotarod	Ugo basile
Scale Santorius	Santorius
Scandrop	Analytic Jena AG
Sunrise™	Tecan Group Ltd
Syringes	Hamilton Messtechnik GmbH
Thermocycler	Biometra
Thermoshaker	EuroElone
UVsolo TS Imaging System	Biometra GmbH
Vortexer LMS VTX-3000L	LMS

3.1.4 Kits

	Company
Bicinchoninic Acid Kit	Sigma-Aldrich
Bond-Max™ Bond Polymer Refine Detection-Kit (DAB R30)	Leica
Complete Mini protease inhibitor cocktail	Roche Diagnostics
GeneRuler 100 bp	Fermentas
Human α -Synuclein Mono ELISA kit	ajRoboscreen
Taq PCR Master Mix Kit	Qiagen

3.1.5 Primer

	Sequence
<i>Human SNCA</i> fwd	5'-TGTAGGCTCCAAAACCAAGG-3'
<i>Human SNCA</i> rev	5'-TGTCAGGATCCACAGGCATA-3'
<i>MRP1</i> wild type fwd	5'-AAGACAAGGGCTTGGGATGC-3'
<i>MRP1</i> rev	5'-CCATCTCTGAGATCTTGCCG-3'
<i>MRP1</i> knock-out fwd	5'-GGAGCAAAGCTGCTATTGGC-3'

3.1.6 Software

	Company
Pannoramic Viewer	3DHISTECH Ltd
BZ Analyzer	Keyence
Prism 6	GraphPad Software Inc.
JMP 9	SAS institute
R 3.0.2	R Development Core Team
Axio Vision	Zeiss

3.2 Methods

3.2.1 Mouse models & Husbandry

All mice used for the accomplishment of this study were housed in climate-controlled environment on a 12 h light/dark cycle with free access to rodent food (SNIFF, Germany) and water. All experiments were conducted in accordance to the European Union and the state law of the government of Saxony-Anhalt and approved by the local animal ethics committee. C57BL/6J mice were purchased from Jackson Laboratory (Bar Harbor, ME, USA) and provide the genomic background of the used transgenic mouse strains. They serve as control (Ctrl) throughout the entire work.

Tg-aSYN mice were obtained from and described earlier by Kahle *et al.* (2001) and carry the human transgene aSYN with 'A30P' mutation, which is expressed under the neuron specific Thy1 (thymocyte differentiation antigen 1) promoter (Kahle *et al.*, 2001), ensuring a robust expression of human aSYN with 'A30P' mutation.

To generate the mtDNA conplastic strain tg-aSYN-mtNOD, an inbred mouse strain (NOD/LtJ) purchased from Jackson Laboratory which has been sequenced previously was used (Yu *et al.*, 2009). Female NOD/LtJ mice were mated with male C57BL/6J mice and backcrossed for more than ten generations to ensure mice to have the genomic DNA of C57BL/6J mice and the mitochondrial DNA of NOD/LtJ mice. Afterwards, male aSYN (A30P)-B6 mice became crossed to females of the conplastic strain to generate tg-aSYN-mtNOD mice.

For the respirometry experiments, mice without any protein overexpression but with specific genomic and mitochondrial background i.e. C57BL/6J respectively mtNOD mice were used.

The generation of the tg-aSYN-ABCC1^{-/-} mice was realized by crossing previously described tg-aSYN mice with FVB.129P2-Abcc1^{atm1Bor N12} (Abcc1^{-/-}) mice (Taconic Farm Inc., Denmark) for at least 9 generations to ensure a pure C57BL/6J background.

3.2.2 Genotyping

In order to control breeding conditions and to ensure the expected human aSYN overexpression respectively successful knock-out of ABCC1 in every single mouse, genotyping was essential. Here, the presence of the human transgene respectively the knock-out of the transporter in the murine genome was confirmed by polymerase chain reaction (PCR).

3.2.2.1 Mouse tail preparation

Once the mice reached an age of 20 days, part of their mouse tail was captured, snap-frozen and denatured over night at 55°C using lysis buffer. Digestion of tissue was provided by addition of proteinase K (Carl Roth) leading to the release of DNA. The enzyme was then inactivated at 95°C for 30 minutes and the mixture was centrifuged for 10 minutes with 14000 rpm prior to PCR.

Table 3: Composition of Lysis buffer

	Concentration
Tris pH 9	10 mM
KCl	1 M
Igepal CA-630	0.4 % (v/v)
Tween 20	0.4 % (v/v)
Aqua dest.	to bring to volume

3.2.2.2 Polymerase chain reaction (PCR)

PCR is a commonly used method to amplify certain genes *in vitro* for different purposes. In this work PCR was used to confirm a specific genome status in mice. Human aSYN overexpression respectively ABCC1 knock-out was proved using a PCR kit (Taq PCR Master Mix Kit, Qiagen) and specific primers (see 3.1.5). A master mix was prepared as follows:

Table 4: Pipette scheme PCR Master Mix for the detection of human aSYN

	concentration [pmol/ μ L]	Volume [μ L]
H ₂ O		5.06
Taq Master mix (PCR kit)		5.5
primer <i>SNCA</i> fwd	0.2	0.22
primer <i>SNCA</i> rev	0.2	0.22
Master mix total		11
DNA		1
final		12

Table 5: Pipette scheme PCR Master Mix for the detection of ABCC1

	concentration [pmol/ μ L]	Volume [μ L]
H ₂ O		4.71
Taq Master mix (PCR kit)		5.5
primer <i>MRP1</i> wild type fwd	1	0.44
primer <i>MRP1</i> rev	0.55	0.24
primer <i>MRP1</i> knock-out fwd	0.25	0.11
Master mix total		11
DNA		1
final		12

The reactions were developed in a thermocycler under following conditions:

Table 6: Cycler protocol for the amplification of human aSYN

step	temperature	time	cycle number
initial denaturation	95°C	5 min	
denaturation	95°C	45 sec	35x
annealing	58°C	60 sec	
elongation	72°C	60 sec	
final elongation	72°C	5 min	
	4°C	∞	

Table 7: Cycler protocol for the amplification of ABCC1

step	temperature	time	cycle number
initial denaturation	95°C	5 min	
denaturation	95°C	45 sec	35x
annealing	62°C	60 sec	
elongation	72°C	90 sec	
final elongation	72°C	5 min	
	4°C	∞	

3.2.2.3 Agarose gel electrophoresis

PCR products were loaded on a 2 % agarose gel prepared with TAE buffer containing 3 µL ethidium bromide/100 µL. A pre-stained protein ladder was used to estimate the size of fragments. If transgenes were present, a band at ~250 bp became visible for aSYN and at 900 bp for wildtype- ABCC1 respectively at 600 bp if ABCC1 was knocked-out. Heterozygous ABCC1 knock-out mice display bands at either size. The gel was documented (UVsolo TS Imaging System, Biometra GmbH).

Table 8: Composition of TAE (Tris-Acetate-EDTA) buffer

	Concentration
Tris	2 M
Acetic acid	1 M
EDTA	50 mM
	pH 8.4
Aqua dest.	to bring to volume

3.2.3 Behavioral tests

To control the development of the mice, each mouse was weighed before behavioral tested.

3.2.3.1 Rotarod

Rotarod is a widely used method to conduct testing of coordination and motor function. The rotarod (Ugo basile, Italy) consists of a rotating rod (\varnothing 3cm) with a rough surface which is divided into 5 parts and thus allows testing five mice in parallel. Mice falling off the rod automatically trigger a switch which stops time measurement.

First, mice were trained on the rod. They had to walk at a constant speed of 4 rpm for one minute without falling. If passed, they were given a recovery time of at least 30 minutes and afterwards performed three consecutive trials with accelerating speed (4-32 rpm) for 4 minutes and with inter-trial intervals of at least 30 minutes for recovery. The time after which each mouse fell off the rod was documented whereas those passing 4 minutes without falling were removed and 240 seconds set as maximum duration. The time of the first passive rotation, that is rotation without actively walking but gripping on the rod, was also documented. The protocol was adopted and adjusted to meet own requirements (Tabuse *et al.*, 2010; Freitag *et al.*, 2003; Morris *et al.*, 2011).

3.2.3.2 Pole test

The Pole test is a common method to evaluate movement disorders in mice that are based on basal ganglia function, such as bradykinesia (Ogawa *et al.*, 1985). The experiments were carried out according to several existing protocols with minor adaptations (Sedelis *et al.*, 2001; Fernagut *et al.*, 2003; Fleming *et al.*, 2004; Matsuura *et al.*, 1997). A wooden pole (50 cm height, 0.8 cm diameter) with a rough surface was placed into the home cage of the tested mouse. Cage mates were removed during the time. The time measurement was started as soon as the mouse was place head upwards near the top of the pole. Two time points were determined: First, when they performed a turn of 180° (head facing downwards); second, when the mice reached the floor with all four limbs. On the first day, each mouse was habituated and trained three times on the pole with a recovery time of at least 10 minutes in between. On the second day they had to perform five consecutive trials with inter-trial intervals of at least 10 minutes. Data of mice which slipped or fell off the pole were not taken into account.

3.2.4 Treatment with Thiethylperazine

The treatment of tg-aSYN and tg-aSYN-ABCC1^{-/-} mice with thiethylperazine (Torecan®, Novartis) was conducted by oral gavage using a feeding needle (20 gauge). Thus, a standardized volume of thiethylperazine could be administered into the esophagus of each mouse in a fast and painless manner. Mice were treated daily from Monday till Friday, starting at an age of 50 days

until reaching 100 days of age. The weekend was set as recovery time. The application dose for this study was 15 mg/kg body weight thiethylperazine (human dosage) or a similar volume of water as control.

3.2.5 Tissue preparation

Mice were sacrificed by cervical dislocation and perfused transcardially with ice cold PBS (phosphate-buffered saline) (pH 7.4). One brain hemisphere was transferred into 4 % paraformaldehyde (for immunohistochemical analyses) or into ice cold MSE-A (for isolation of mitochondria, 3.2.6.3) while the second hemisphere was snap-frozen in liquid nitrogen and stored at -80°C.

Table 9: Composition of PBS (pH 7.4)

	Concentration
NaCl	137 mM
KCl	2.6 mM
Na ₂ HPO ₄	10 mM
KH ₂ PO ₄	1.8 mM
Aqua dest.	to bring to volume

3.2.6 Biochemical analyzes

3.2.6.1 Total protein quantification via spectrophotometry

The protein content in samples was determined by spectrophotometric measurements (Scandrop, Analytic Jena AG, Germany). Therefore, 4 µL sample was applied onto a chip cuvette and the absorption of light with the wave length of 280 nm was measured and normalized to 320 nm. The concentration was calculated automatically according to the Beer-Lambert law.

3.2.6.2 Enzyme-linked immunosorbent assay (ELISA)

To biochemically analyze the amount of monomeric and higher molecular forms of aSYN, ELISA measurements were performed. Therefore, snap-frozen mouse brains were dosed with 500 µL *RNAlater* (Applied Biosystems) and thawed gently on ice for at least one hour. The brain was afterwards homogenized with four ceramic beads for 30 seconds using a homogenizer (Homogenisator SpeedMill PLUS, analytic jena). After a short centrifugation step, a part of the homogenized brain and one ceramic bead were transferred into 20 volumes (w/v) carbonate buffer and homogenized again for 20 seconds. This solution was centrifuged for 45 minutes at 14000 rpm and 4°C. The supernatant was captured and denoted carbonate fraction. This fraction presents the soluble monomeric aSYN species. The remaining pellet was further used and mixed with 8 volumes (w/v) 5 M guanidine hydrochloride buffer, calculated from the initial tissue weight. The solution was allowed to mix gently at room temperature for 3 hours before

centrifuged again for 45 minutes at 14000 rpm and 4°C. The supernatant was collected as guanidine fraction, containing aggregates and higher molecular aSYN forms. The fractions were stored at -20°C until further usage. ELISA was performed according to the manufacturer's instruction using samples diluted 1:30,000 in dilution buffer (MONO kit, ajRoboscreen, Germany). The bound HRP-coupled antibody complex was visualized by TMB/H₂O₂ staining and absorption measurement using a PARADIGM spectrophotometer (Beckman-Coulter/Molecular Devices, Germany).

The optical densities of the standards were plotted against the aSYN concentration using the five-parameter logistic equation standard curve. The aSYN concentration of unknown samples was interpolated from this curve.

Table 10: Composition of Carbonate buffer (pH 11.5)

	Concentration
Na ₂ CO ₃	100 mM
NaCl	50 mM
Aqua bidest.	to bring to volume
protease inhibitor cocktail	add freshly (1 pill/10 mL)

Table 11: Composition of Guanidine buffer (pH 8)

	Concentration
Guanidine/HCl	5 M
Tris/HCl	50 mM
Aqua bidest.	to bring to volume

3.2.6.3 Isolation of mitochondria

The isolation of mitochondria was performed as described by Gellerich et al. (Gellerich *et al.*, 2008) following a modified protocol of Clark and Nicklas (Clark *et al.*, 1970). The execution of this method and the following respiratory measurement were done as part of a master thesis project (Zschiebsch, 2012, Master thesis).

The freshly prepared and in MSE-A buffer transferred mouse brain hemispheres (without cerebellum) were roughly hacked and homogenized accurately in 5mL MSE-A buffer containing 0.05 % nagarse using glass homogenizer. The MSE-A buffer is used to provide a specific chemical milieu for the mitochondria, as it contains not only EGTA (ethylene glycol tetraacetic acid) but also DTT (Dithiothreitol), which protects thiol groups against inactivation. The homogenates were further diluted with 20 mL MSE-A and centrifuged at 4000 rpm for 4 minutes at 4°C. The supernatant was filtered through a filter cloth and centrifuged again at 10500 rpm and 4°C for 10 minutes. The remaining pellet, containing the mitochondria, was filtered again and thus separated from cell debris. Afterwards, it was resuspended in 5 mL MSE-A containing 0.02 % digitonin in order to break up membranes and release the mitochondria. The solution was

centrifuged in 20 mL MSE-A at 10500 rpm and 4°C for additional 10 minutes. The pellet was resuspended in 100 μ L MSE-B and stored at 4°C.

Table 12: Composition of MSE-A (pH 7.4)

	Concentration
Mannitol	225 mM
Sucrose	75 mM
MOPS	20 mM
EGTA	1 mM
DTT	0.5 mM
Aqua dest.	to bring to volume

Table 13: Composition of MSE-B (pH 7.4)

	Concentration
Mannitol	225 mM
Sucrose	75 mM
MOPS	20 mM
EGTA	0.1 mM
DTT	0.5 mM
Aqua dest.	to bring to volume

3.2.6.4 Total protein concentration quantification via BCA

Protein concentration was determined using the Bicinchoninic Acid Kit (Sigma-Aldrich Chemie GmbH, Steinheim, Germany) and the SunriseTM Reader (Tecan Group Ltd., Männedorf, Switzerland). The protocol was performed according to manufacturer's instructions. The samples and standards were diluted in 10 mM PBS (phosphate buffered saline) and PBS served as blank value as well. Dilutions of 1:50 and 1:100, respectively, were used for mitochondrial protein samples, which were measured in duplicates.

3.2.7 Respirometry

Respirometry is a method used to analyze the functionality of mitochondria and to identify changes in single respiratory chain complexes. The whole experiment was conducted using OROBOROS oxygraph-2k (Oroboros Instruments, Innsbruck, Austria) equipped with Clark-type oxygen electrodes. To study different rates of respiration depending on specific substrates addition and the corresponding differences in complex-dependent oxygen consumption, mitochondria (0.06 mg protein/mL) were added to the measurement chamber containing BIM-1000 (brain incubation medium). This medium enriched with 11 nM Ca^{2+} was heated to 30°C. The oxygen concentration in air-saturated medium was considered to be 200 nmol O_2 /mL at 95 kPa.

For the accomplishment of this study four different experimental approaches were chosen, each comprising a specific sequential order of substrate addition leading to the imitation of certain physiological conditions in the cell (see Table 14) (based on (Trumbeckaite *et al.*, 2001; Gellerich *et al.*, 2002; Gellerich *et al.*, 2008; Gellerich *et al.*, 2012; Krebiehl *et al.*, 2010)).

Table 14: Order of substrate addition according to the four experimental protocols

Protocol I “COX I”	Protocol II “COX II”	Protocol III “ATPase”	Protocol IV “CI/II/III”
BIM-1000		BIM-0	
2 mM malate	2 mM malate	2 mM malate	2 mM malate
10 mM glutamate	10 mM α -ketoglutarate	10 mM pyruvate	10 mM glutamate
0.06 mg/ mL mitochondria			
2 mM ADP	2 mM ADP	100 μ M ADP	100 μ M ADP
200 μ M Ca^{2+}	200 μ M Ca^{2+}	2 mM ADP	2 mM ADP
100 μ M Ca^{2+}	100 μ M Ca^{2+}	10 mM glutamate	10 mM pyruvate
10 mM pyruvate	10 mM pyruvate	10 mM succinate	10 mM succinate
1.5 μ M rotenone	1.5 μ M rotenone	4x 25 nM FCCP	1.5 μ M rotenone
10 mM glycerol-3-phosphate	10 mM glycerol-3-phosphate		125 μ M atractyloside
10 mM succinate	10 mM succinate		
5 μ M antimycin A	5 μ M antimycin A		
2 mM ascorbate	2 mM ascorbate		
500 μ M TMPD	500 μ M TMPD		
5 mM azide	5 mM azide		

To start with protocol I (and II), mitochondria were incubated in BIM-1000 in the presence of 10 mM glutamate and 2 mM malate. The addition of 2 mM ADP (adenosine diphosphate) led to the maximal possible respiration reachable with these substrates, denoted as state $3_{\text{glu/mal}}$. This state was further stimulated by two subsequent Ca^{2+} additions, simulating the activation of mitochondrial substrate supply by extramitochondrial Ca^{2+} (Gellerich *et al.*, 2012). The addition of 10 mM pyruvate culminated in the maximal complex I dependent respiration, state $3_{\text{compl.I}}$. The next step included the addition of 1.5 μ M rotenone, a well-known complex I inhibitor, to completely repress complex I dependent respiration. After that, the addition of 10 mM glycerol-3-phosphate adjusted the respiration to state 3_{G3P} and the following succinate adding led to the maximal complex II dependent respiration, state 3_{succ} . To fully inhibit complex III dependent respiration and with that also complex II, antimycin A was given to the measurement. Now, ascorbate/TMPD (N,N,N',N'-tetramethyl-p-phenylenediamine) allows the measuring of the maximal respiration emerging from the oxidation of reduced cytochrome c by cytochrome c oxidase (complex IV). After the addition of azide, an inhibitor of cytochrome c oxidase, the respiration rate could be corrected by subtracting this value.

Protocol II starts from a different premise but follows the same procedure thereafter. The approach begins with the addition of 10 mM α -ketoglutarate instead of glutamate.

Protocol III and IV were performed in BIM-0, without EGTA, which means a larger endogenous Ca^{2+} content. This leads to the complete activation of Ca^{2+} stimulated substrate supply. Protocol III starts with 10 mM pyruvate and 2 mM malate, followed by the addition of small amounts of ADP to adjust a partial activation of respiration, which drops after a short while again to a state referred to as state 4. The subsequent supply of 2 mM ADP leads to the reaching of state $3_{\text{pyr/mal}}$, whereas the addition of 10 mM glutamate adjusts the maximal complex I respiration rate, state $3_{\text{compl.I}}$. Again, added succinate culminates in state $3_{\text{compl.III}}$. To exclude the possibility of a dysfunctional ATPase and a resulting limitation of the oxidative phosphorylation, FCCP was added gradually to uncouple the oxidative phosphorylation.

The last protocol starts with 10 mM glutamate and 2 mM malate and the sequential adding of ADP leading to state 4 and state $3_{\text{glu/mal}}$, as described before. 10 mM pyruvate adjusts the state $3_{\text{compl.I}}$ again. The supply of succinate allowed the determination of state $3_{\text{compl.III}}$ and rotenone inhibits, as seen before, the complex I dependent respiration and allows so the examination of state 3_{succ} . Finally, 125 μM atractyloside allows the registration of state 4_{atr} , in which no ADP is available as this glycoside prevents the transport of ADP.

Furthermore, several ratios and special properties were analyzed from the resulting data. The oxygen consumption was calculated from the time derivative of oxygen concentration (DATGRAPH Analysis software, OROBOROS INSTRUMENTS, Innsbruck, Austria). Data are given in $\text{nmol O}_2/\text{min}/\text{mg}$ mitochondrial protein.

Table 15: Composition of BIM-1000 (pH 7.4)

	Concentration
Mannitol	120 mM
MOPS	40 mM
KH_2PO_4	5 mM
KCl	60 mM
MgCl_2	5 mM
EGTA	1 mM
Aqua dest.	to bring to volume

Table 16: Composition of BIM-0 (pH 7.4)

	Concentration
Mannitol	120 mM
MOPS	40 mM
KH_2PO_4	5 mM
KCl	60 mM
MgCl_2	5 mM
Aqua dest.	to bring to volume

Table 17: substrates and their solvents used for respirometry

substrate	solvents
α -ketoglutarate	Tris-HCl (500 mM)
adenosine diphosphate	ultra-pure water
ascorbate	ultra-pure water
antimycin A	ethanol
atractyloside	DMSO
azide	ultra-pure water
calcium chloride	ultra-pure water
FCCP (Carbonyl cyanide-4-(trifluoromethoxy)phenylhydrazone)	ethanol
glutamate	Tris-HCl (500 mM)
glycerol-3-phosphate	BIM-1000
malate	Tris-HCl (500 mM)
pyruvate	Tris-HCl (500 mM)
rotenone	ethanol
succinate	Tris-HCl (500 mM)
TMPD (N,N,N',N'-tetramethyl-p-phenylenediamine)	ultra-pure water

3.2.8 Immunohistochemistry

For immunohistochemical analyzes, 72 hour paraformaldehyde-fixed brain hemispheres were paraffin-embedded and de-hydrated according to the following scheme:

Table 18: Dehydration protocol for paraformaldehyde-fixed brain hemispheres

reagent	time [min]
Formalin 4 % buffered	5
Ethanol 70 %	180
Ethanol 80 %	60
Ethanol 80 %	120
Ethanol 90 %	60
Ethanol 90 %	60
Ethanol abs.	120
Ethanol abs.	120
Xylene	120
Xylene	120
Paraffin 60°C	240
Paraffin 60°C	240

Afterwards, the tissue was cut into 4 μ m thick coronal sections using a microtome (Leica Biosystems). The following de-paraffinization and re-hydration, as well as immunostaining procedure was performed with the BOND-MAX Autostainer (Leica Microsystems

GmbH/Menarini). In order to block endogenous peroxidases and to retrieve epitopes, the sections were pretreated, for 5min with citrate, EDTA buffer pH 8.5 or enzymatically according to the manufacturer's instructions of the used antibodies (see 3.1.1). The antibodies were incubated for 30 min with the following dilutions: aSYN clone 5G4 (1:6000), NeuN (1:500), Iba1 (1:1000) and GFAP (1:500) and were detected with BOND-MAX Bond Polymer Refine Detection kit (DAB R30). Additionally, these sections were counterstained with hematoxylin leading to a strong blue staining of the cell nucleus. The slides with four sections each were digitalized by Mirax Midi automated slide scanner with a resolution of 230 nm (Scheffler *et al.*, 2011). To capture microscopic images for further analysis, the panoramic viewer (3DHISTECH Ltd., Hungary) and BZ Analyzer (Keyence, Germany) were used.

3.2.8.1 Semi-quantitative Analysis of Immunohistochemistry

To examine possible differences in microglia response and distribution as well as quantity of neurons, the partial area covered by Iba1-positive cells or the amount of NeuN-positive cells, respectively, in the cortex of all mouse strains was determined by using the Hybrid cell count function of the BZ Analyzer (Keyence, Germany). Four images were taken using the same magnification from four different slices of the same animal brain. The ratio of stained cell area to unstained cortex area was calculated and the mean value was used for the evaluation.

3.2.9 Statistics

Statistical analyses of the ELISA, Immunohistochemistry and Respirometry data were performed using GraphPad™ prism 6 and one-way ANOVA followed by Sidak's multiple comparison test respectively Kruskal-Wallis test followed by Dunn's multiple comparison test if normal distribution was not given. Significance was reached when $p \leq 0.05$.

Statistical analyzes of behavioral test were performed by the Institute for Mathematical Stochastic using JMP 9 (SAS institute, Heidelberg, Germany).

To evaluate the rate of censoring in the rotarod data set, one-way ANOVA followed by Bonferroni's multiple comparison test was used. Variance stabilizing transformation of data (arcsine-square root transformation) did not change the outcome of statistical analysis in this case; therefore the raw data was used instead. Significance was reached if $p < 0.05$.

The Quantile-Quantile plot of the rotarod data shows that these are distributed normally until reaching the censoring cut-off time point. Additional analyses were performed using R 3.0.2 (R Development Core Team, www.r-project.org) and the package 'lme4'. This function fits a 'Linear Mixed-Effects Models with Censored Responses' as is provided by this data set. Analyzes was performed for the time frame of 9 to 41 weeks and for mid-age time points (25-33 weeks). No single time points were analyzed. Significance was reached if $p < 0.05$.

The 'pole test' data set was non-parametrically transformed to mean ranks to ensure a better adjustment to normal distribution and fitted to a linear mixed model with fixed effects for genotype and random effects for animals. Statistical analyzes were performed using the REML (restricted maximum likelihood) approach and additional two-sided t-test with adjusted degrees of freedom to determine differences only for the data of main interest, collected between 25 and 33 weeks of age and between 37 and 41 weeks of age, respectively. No single time points were analyzed. Here again, significance was reached if $p < 0.05$.

4. Results

4.1 Characterization of the tg-aSYN mouse model with respect to PD

Before starting the comparison of tg-aSYN and tg-aSYN-mtNOD mice it was important to characterize the PD mouse model concerning its histological, biochemical and behavioral profile. The following analyzes were conducted using heterozygous tg-aSYN mice at an age of 50 to 300 days, C57BL/6J mice served as control.

4.1.1 Phenotypical appearance of tg-aSYN mice

The first observation of tg-aSYN and control mice did not reveal any obvious differences in phenotype and behavior. A previous study, which was part of a master thesis project, described that only a very small proportion of tg-aSYN displayed severe abnormalities in motor behavior, including weakness in the limbs and following gait instabilities as well as rigor in the hind limbs and paralysis. However, eye defects were detected in a large proportion of both mouse models, tg-aSYN and control mice, which were twofold higher in tg-aSYN mice. These findings were made using heterozygous and homozygous mice at an average age of approximately 300 days (Gröger, 2012, Master thesis). Thus, differences were expected not earlier than 300 d of age in tg-aSYN mice. Consistent with that, the examination of mice from 50 d to 300 d of age revealed no differences in phenotype or in development and weight.

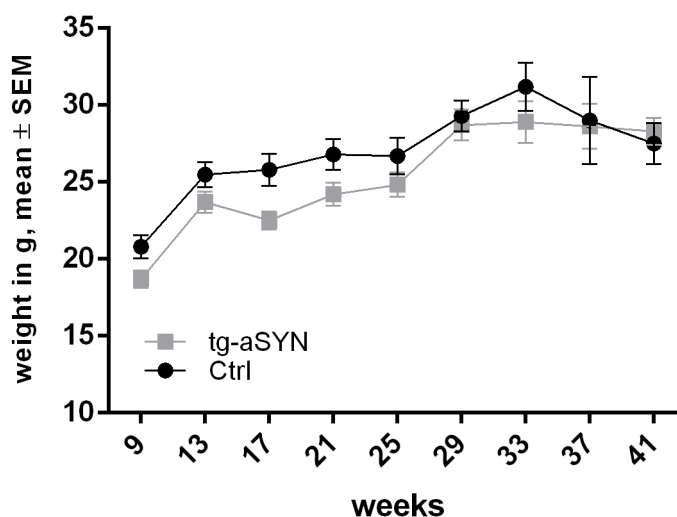


Figure 4: Weight of tg-aSYN and C57BL/6J mice from 9 to 41 weeks of age.

Beside a tendency to less weight of tg-aSYN mice in the first 4 month of age, mice developed equally in both models. Data is presented as means \pm SEM ($n \geq 5$).

4.1.2 Immunohistological analyzes of tg-aSYN mice

The immunostained coronal paraffin-embedded brain sections of tg-aSYN mice revealed an intensive signal in various anatomical structures of the brain. Here especially cortex, thalamus, hippocampus, basolateral amygdala, geniculate nucleus and zona incerta were stained most intensively. Hypothalamus, medial amygdala, dentate gyrus and other structures displayed only mild immunoreactivity. No Lewy body or Lewy neurite pathology was observed in the whole brain.

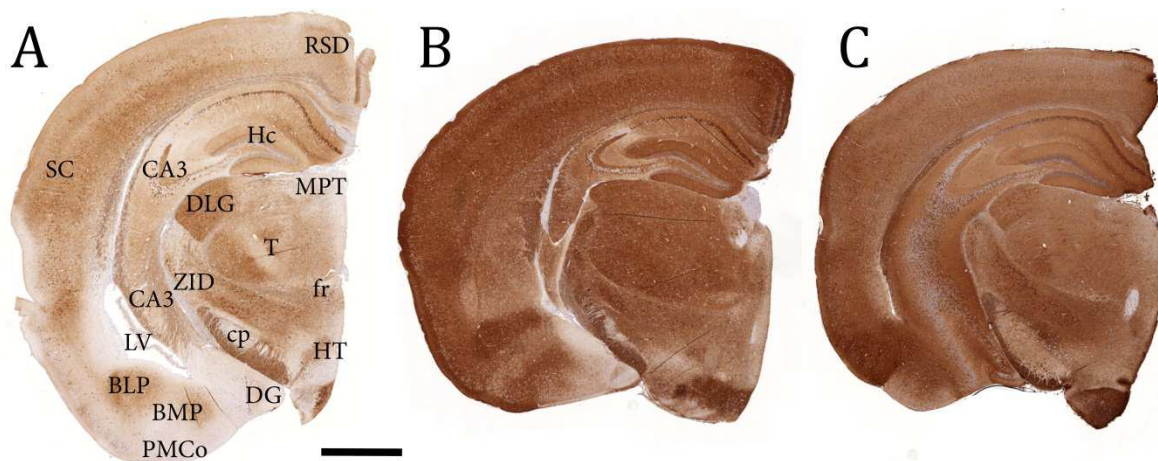


Figure 5: aSYN-immunoreactivity of 50 d old and 300 d old tg-aSYN mice.

Sections were immunostained using an anti-human-aSYN antibody, clone 5G4, and were counterstained for nuclei with hematoxylin. Localization of anatomical structures is shown in (A). Intense immunolabelling was detected in the neuropil of the cortex, hippocampus, thalamus, basolateral amygdala, geniculate nucleus and zona incerta, whereas staining of hypothalamus, mediale amygdala and dentate gyrus was less intense. No distinct differences were observed between young (B) and old tg-aSYN mice (C). RSD, retrosplenial dysgranular cortex; Hc, hippocampus; MPT, medial prefrontal nucleus; SC, somatosensory cortex; CA, cornu ammonis; DLG, dorsal lateral geniculate nucleus; T, thalamus; ZID, zona incerta, dorsal part; fr, fasciculus retroflexus; cp, cerebral peduncle; LV, lateral ventricle; BLP, basolateral amygdaloid nucleus, posterior part; BMP, basomedial amygdaloid nucleus, posterior part; DG, dentate gyrus; HT, hypothalamus; PMCo, posteromedial cortical amygdaloid area; Scale bar = 1000 μ m.

The comparison between young and old mice (50 d vs. 300 d) showed no distinct differences in signal intensity or alterations in anatomical structures stained. As a quantitative analysis was not possible due to the diffuse staining pattern, a visual estimation was made using enlarged images of cortex and hippocampus. (see Figure 6). The examination of the hippocampus revealed no obvious changes between the time points. However, it was possible to display that the CA2 region lacked aSYN expression in contrast to the moderate expression pattern in the CA1 and CA3 region. The enlarged cortex sections (see Figure 6 A,B) showed a vigorous labeling of neurons especially in the layer V and layer II/III whereas other layer only exhibited moderate expression.

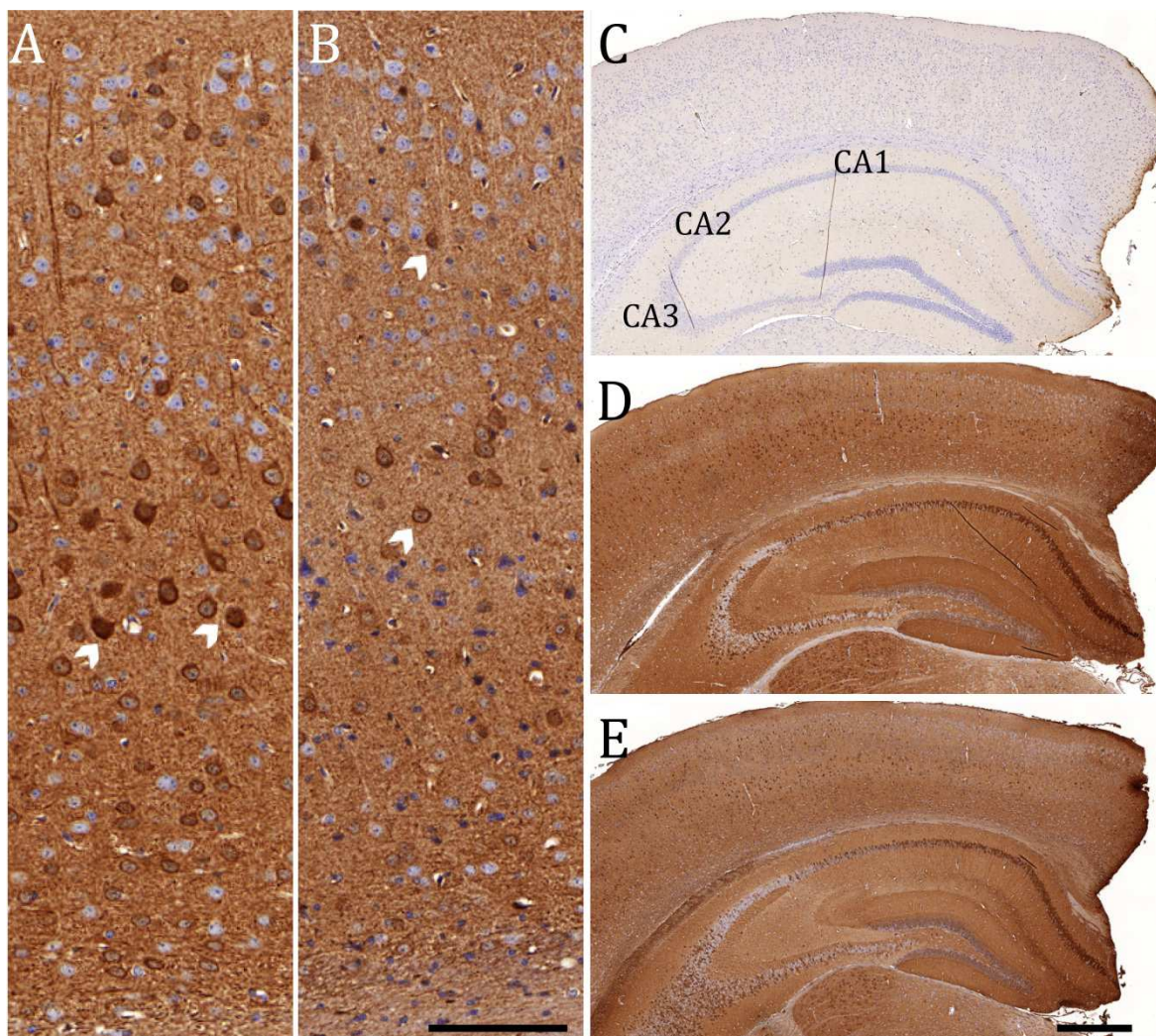


Figure 6: Load of human aSYN in cortex and hippocampus of young and old tg-aSYN mice.

The enlarged Cortex sections (A,B) revealed no obvious difference between 50 d (A) and 300 d (B) old tg-aSYN mice. Although fewer stained neurons in the cortex of 300 d old mice (B) indicated a less progressed degeneration process in younger mice (A). Arrows point to intensive stained neuron soma. The most vigorous staining was observed in layer V and II/III of the cortex (A,B). The pyramidal cells of the hippocampus displayed the most intensive staining in the CA1 and CA3 region whereas the CA2 region spared any labeling and was aSYN-negative (D,E). No staining was detectable in Ctrl mice (C). CA, cornu ammonis; Scale bar = 100 μ m in A-B; 500 μ m in C-E.

Immune response and neuronal integrity in the cortices of tg-aSYN mice compared with control mice were investigated, since neurodegeneration in PD is accompanied by a marked cell loss and most often with a high number of activated microglia and astrocytes (Mosley *et al.*, 2012). Microglia were immunostained against Iba1, neurons against NeuN and astrocytes against GFAP. A difference was solely detected in the intensity of neuronal staining. 300 days old mice showed a less pronounced NeuN immunoreactivity compared to young ones (see Figure 7 A-B). Iba1- and GFAP staining revealed no differences (see Figure 7 C-F).

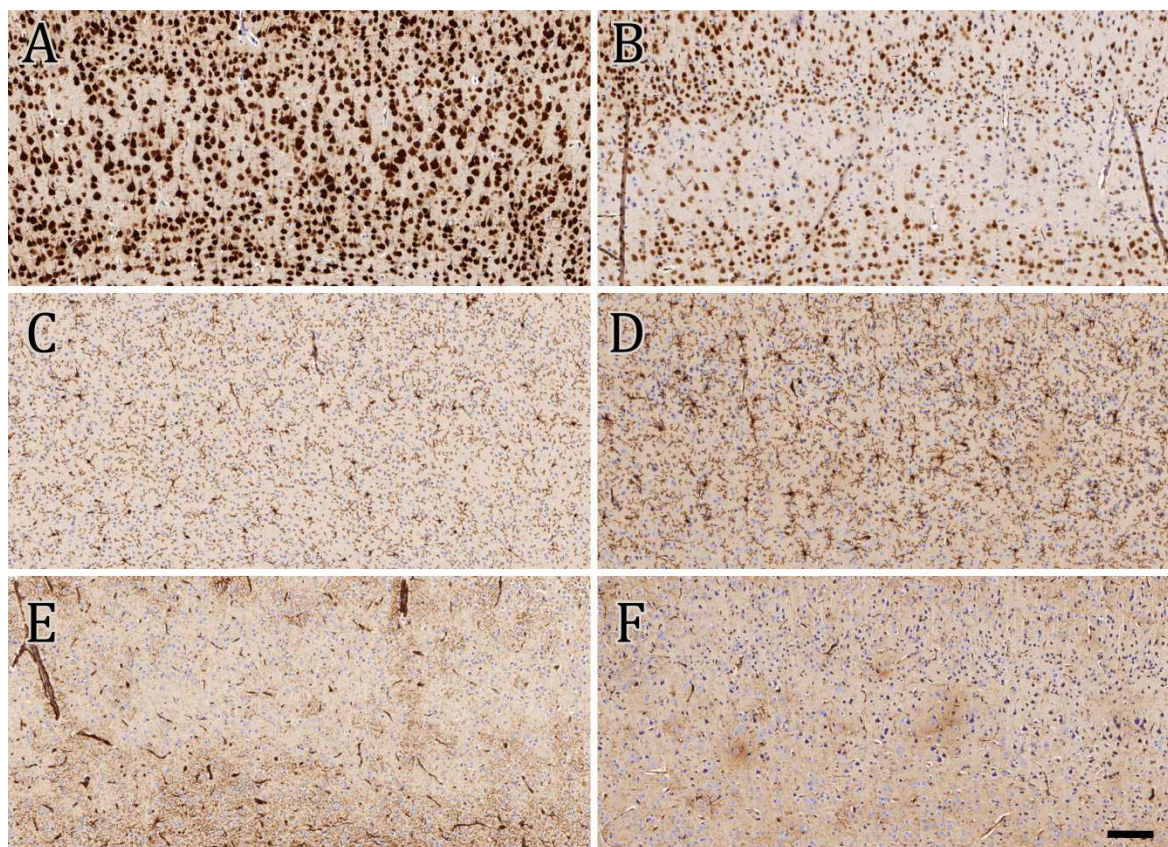


Figure 7: Immunohistochemical analyses of young and old tg-aSYN mice.

The panel shows paraffin-embedded sections of the cortex, immunostained using anti-NeuN (A,B), anti-Iba-1 (C,D) or anti-GFAP (E,F). The first columns display young tg-aSYN (A,C,E), the second columns old tg-aSYN mice (B,D,F). Young tg-aSYN mice (A) showed a more intensive NeuN-staining compared to old ones (B). Iba-1 staining showed a slightly stronger microglial activity in old transgenic mice (D) compared with young mice (C), whereas there were hardly any changes visible for GFAP staining (E,F). Scale bar = 100 μ m (A-F).

The notion of a more pronounced NeuN immunoreactivity in old tg-aSYN mice was confirmed by semi-quantitative analysis of the ratio of area covered by NeuN positive cells to cortex area (see Figure 8A). Young animals showed no differences in the quantity of neurons between both genotypes. However, old tg-aSYN mice displayed a significantly lower NeuN immunoreactivity than old control mice leading to about 35 % less cortex area covered by neurons ($p=0.0248$; see Figure 8A). The quantification of microglial area, revealed no difference (see Figure 8B).

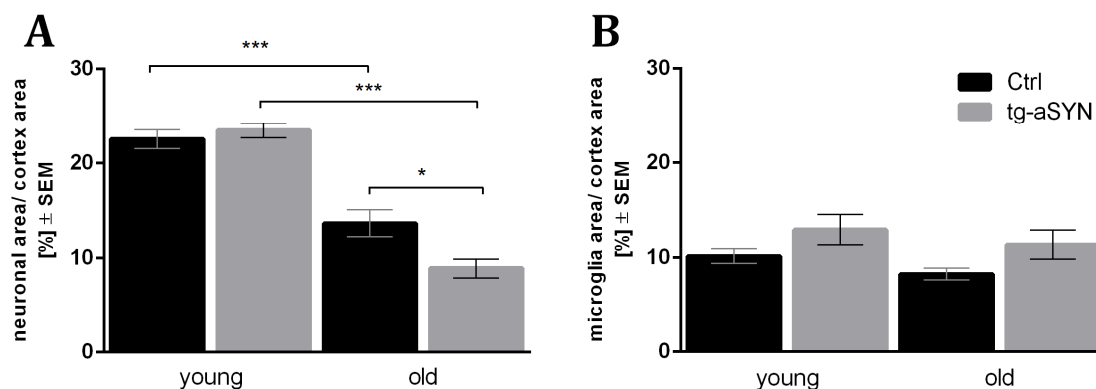


Figure 8: Semi-quantitative analysis of immunohistochemistry.

Analysis revealed a significant difference in neuron integrity between young and old mice and especially between old tg-aSYN and Ctrl mice (A). Examination of microglial response showed no difference between both mouse models (B). Data is presented as means \pm SEM ($n \geq 5$), * $p \leq 0.05$; ** $p \leq 0.01$; *** $p \leq 0.001$ (one-way ANOVA followed by Sidak's multiple comparison test)

4.1.3 Behavioral study on tg-aSYN mice

As PD is a progressive motor disorder, behavioral tests are the gold standard for estimating severity of the disease. Here the rotarod test and the pole test were used to assess different types of motor parameter.

4.1.3.1 Rotarod

A preliminary study was performed for the purposes of a master thesis and the results were used to set up the rotarod test. Prior to the present work it was found that tg-aSYN mice, determined from an age of 300 d, showed no significant differences compared to control mice until 450 days of age. After, there was a rapid decline in transgenic and control mice. A difference between young and old tg-aSYN mice was visible from 300 d of age (Gröger, 2012, Master thesis).

To assess the course of behavior alterations starting from earlier time points, a new study was performed, using male heterozygous tg-aSYN and C57BL/6J (control) mice beginning from 9 weeks of age and finished by the age of 41 weeks, with special focus on the mid-age time points (25-33 weeks).

In order to minimize the usage of laboratory animals, mice were tested longitudinally. Previous tests showed that learning effects between the time points can be neglected. Nonetheless, these circumstances were considered in the statistical analysis.

The first evaluation of the rotarod data set was conducted with respect to the percentage of censoring (see Figure 9). The cut-off-time in this study was set to 240 seconds and more mice as expected were able to stay on the rod for the duration of this period.

Interestingly, no significant differences were found in the amount of censored data between tg-aSYN (34 %) and control mice (23 %) at mid-age time points, i.e. 25-33 weeks (see Figure 9).

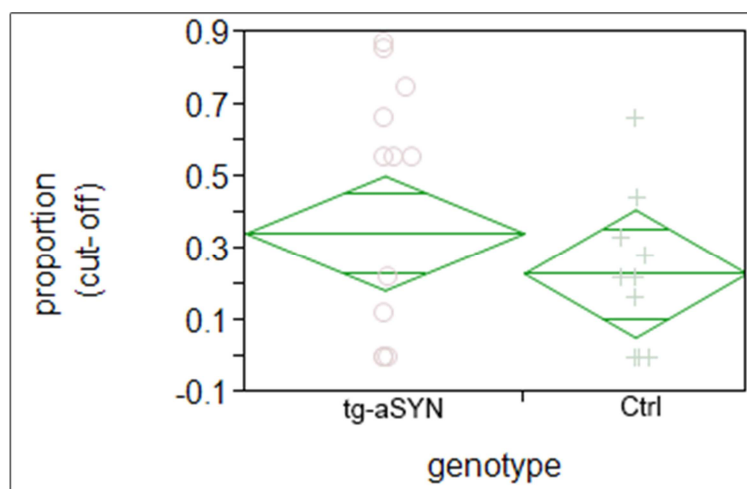


Figure 9: Proportion of censored data in the rotarod data set.

No differences between tg-aSYN and Ctrl mice were found between 25 and 33 weeks of age. Data is presented as mean diamonds and x-axis proportional ($n \geq 15$, male) (one-way ANOVA followed by Bonferroni's multiple comparison test).

Further statistical analyses required a better fitted model (confer 3.2.9) to solve the main questions (I to III) arising from the data:

- I) Is there a difference between both groups?
- II) Has age a significant influence on the performance of the groups?
- III) How distinct are the differences between both groups in mid-age time points?

The comparisons, calculated for the maximal time latency the mice were able to stay on the rod as well as for the time until the first passive rotation, revealed no significant differences between tg-aSYN and control mice (see Figure 10). A linear influence of age was calculated to control for age-related effects. Notable, age was found to have a strong influence on the performances of tg-aSYN and control mice, as they improved their performance with advancing age in both parameter ($p=0.046$, $p=0.0018$).

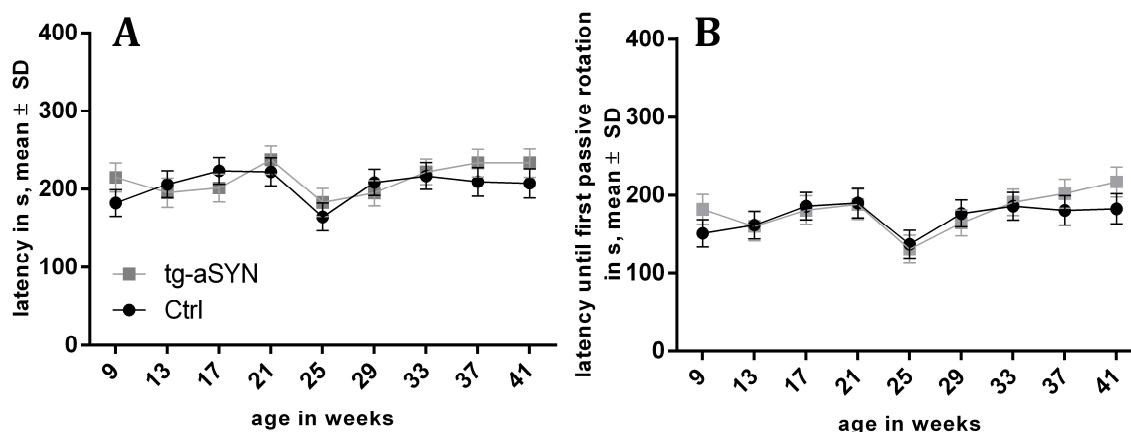


Figure 10: Age-dependent alteration in motor behavior of tg-aSYN and C57BL/6J mice.

Latency of rotarod performances (A) and time of first passive rotation (B) of tg-aSYN and Ctrl mice (C57BL/6J) showed no differences until the age of 300 d. However, age had a significant impact on both performances in both animal groups. Data is presented as means \pm SD ($n \geq 5$, male) (Linear Mixed-Effects Models with Censored Responses, LMEC).

4.1.3.2 Pole Test

To determine possible differences in the ability of orientation and to assess alterations in motor performance, the pole test was performed. For the accomplishment of this study, male heterozygous tg-aSYN and C57BL/6J (control) mice were used starting from the age of 50 d until the age of 300 d was reached.

While mice had to turn 180° on the top of the pole and had to climb down, first observations were made on their performance. Unsuccessful attempts (such as incomplete turn at the top and slipping) were not taken into account. Notably, these inadequate performances did not solely occur in the group of tg-aSYN mice, but scatter randomly in both groups. Therefore, no differences were seen in the accomplishment of turning respectively climbing down the pole. Surprisingly, no differences were observable in the time of the orientation performance of the pole test ($p=0.89$). Even more interestingly, control mice took significantly longer to climb down at late time points (37-41 weeks) in contrast to tg-aSYN mice ($p=0.001$) but not at mid-age time points from 25 to 33 weeks ($p=0.06$).

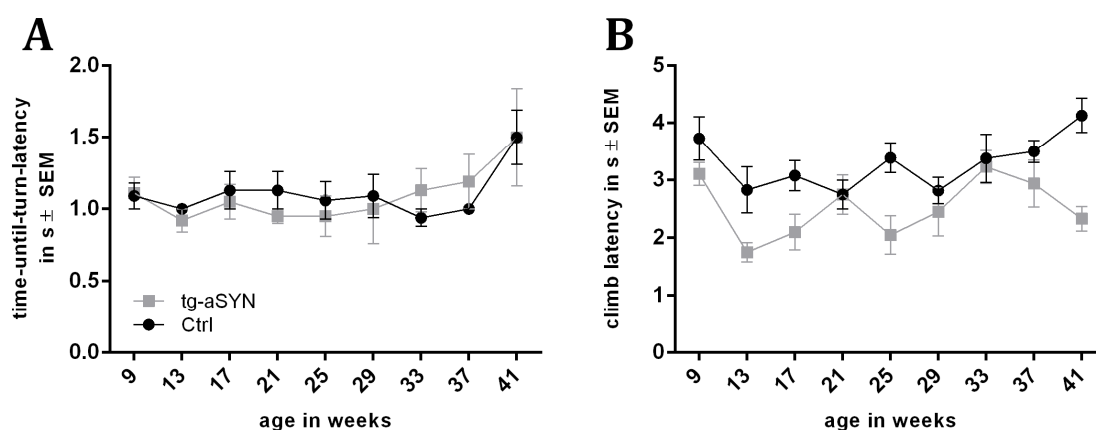


Figure 11: Changes in pole test performances of tg-aSYN and C57BL/6J mice.

No significant alterations were detected in time-until-turn-latency (A) until old age. The climb performance revealed surprisingly a worse performance of Ctrl mice when compared to tg-aSYN mice (B). Data is presented as means \pm SEM ($n \geq 5$, male). (restricted maximum likelihood (REML) approach and additional two-sided t-test with adjusted degrees of freedom).

4.2 Influence of specific mitochondrial polymorphism on aSYN pathology in tg-aSYN mice

To determine the influence of distinct mitochondrial polymorphism on the pathology of tg-aSYN mice, a novel mouse model was generated, the conplastic mouse – tg-aSYN-mtNOD. Different immunohistological, biochemical and behavioral analyses were performed in order to evaluate differences and similarities of both mouse models.

4.2.1 Immunohistological analyzes of tg-aSYN-mtNOD mice

Immunohistological analyzes of tg-aSYN-mtNOD mice, stained with anti-aSYN clone 5G4, revealed no obvious differences compared to tg-aSYN mice (see Figure 13 B-C). The stained structures were consistent with the formerly described immunoreactivity (confer 4.1.2).

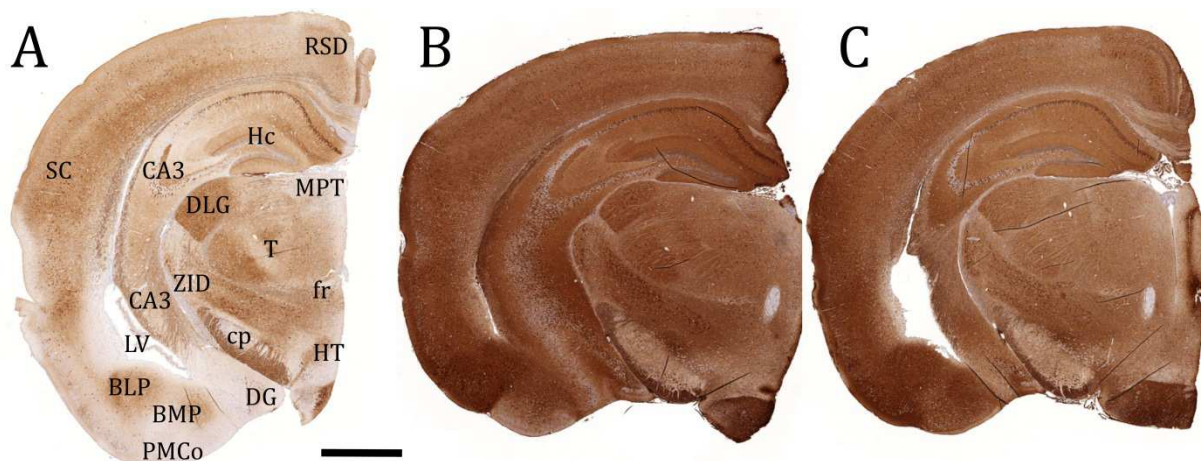


Figure 12: aSYN-immunoreactivity in 300 d old tg-aSYN and tg-aSYN-mtNOD mice.

Hemisphere sections were immunostained using an anti-human-aSYN antibody, clone 5G4, and were counterstained for nuclei with hematoxylin. Localization of anatomical structure is shown in (A). No vigorous differences are observable between tg-aSYN (B) and tg-aSYN-mtNOD mice (C). RSD, retrosplenial dysgranular cortex; Hc, hippocampus; MPT, medial prefrontal nucleus; SC, somatosensory cortex; CA, cornu ammonis; DLG, dorsal lateral geniculate nucleus; T, thalamus; ZID, zona incerta, dorsal part; fr, fasciculus retroflexus; cp, cerebral peduncle; LV, lateral ventricle; BLP, basolateral amygdaloid nucleus, posterior part; BMP, basomedial amygdaloid nucleus, posterior part; DG, dentate gyrus; HT, hypothalamus; PMCo, posteromedial cortical amygdaloid area; Scale bar = 1000 μ m.

However, a more intensive NeuN staining was observed in the cortex of 300 d old tg-aSYN-mtNOD mice compared to tg-aSYN mice (see Figure 13 A-B). Observable differences were not found in case of Iba1 and GFAP staining (see Figure 13 C-F).

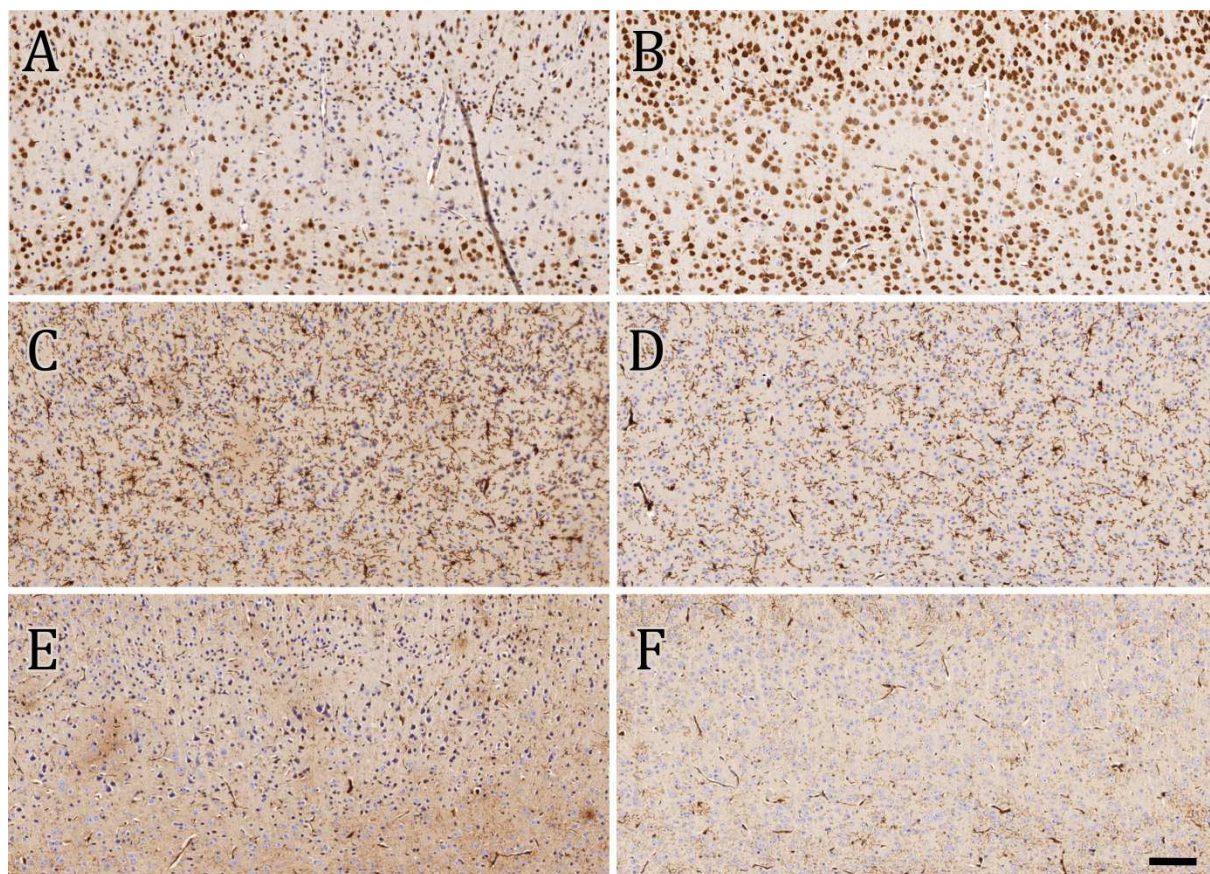


Figure 13: Immunohistochemical analyzes of 300 d old tg-aSYN and tg-aSYN-mtNOD mice.

The panel shows cortex sections of 300 d old tg-aSYN (left column) and tg-aSYN-mtNOD mice (right column). Stained with NeuN (A-B), the cortex of tg-aSYN-mtNOD mice (B) revealed a more intensive signal compared to tg-aSYN mice (A). No differences are visible upon Iba1 (C-D) and GFAP (E-F) staining between mouse models, tg-aSYN and tg-aSYN_mtNOD. Scale bar = 100 μ m.

As depicted in Figure 14A, the semi-quantitative analysis of the neuronal integrity showed a dramatic loss of neurons in 300 d old tg-aSYN-mtNOD mice compared to young ones, comparable to tg-aSYN and control mice. The above mentioned differences (confer 4.1.2) between tg-aSYN and control mice were not confirmed for tg-aSYN-mtNOD mice and the neuronal area was instead comparable to those of control mice (see Figure 14A). In contrast to the tg-aSYN mice which displayed only 65 % of the neurons that were found in the control group at the same age ($p=0.0435$), the tg-aSYN-mtNOD mice still had 95 % left.

Interestingly, old tg-aSYN-mtNOD mice exhibited a 50 % greater proportion of microglial area in the cortex compared to control mice (see Figure 14B), indicating a significantly greater microglial response in the brain of 300 d old tg-aSYN-mtNOD mice ($p=0.0301$). Tg-aSYN mice showed an about 40 % increased microglial area, significance was not reached.

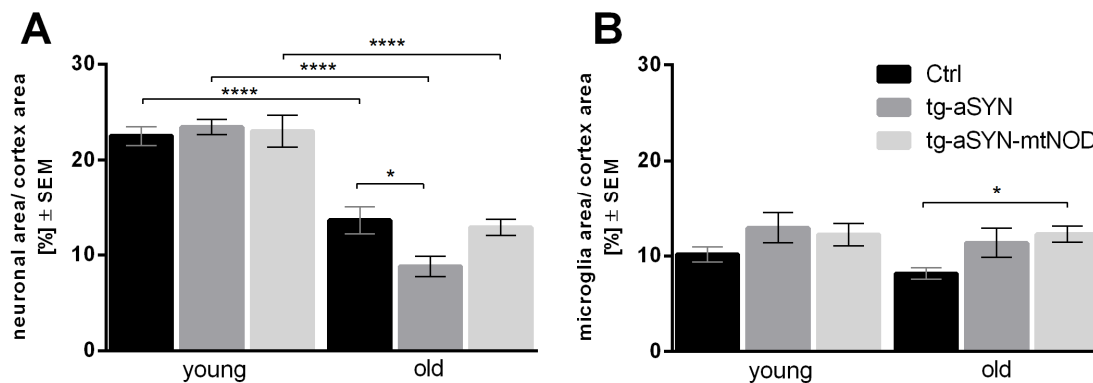


Figure 14: Semi-quantitative analysis of Immunohistochemistry in the cortex of tg-aSYN, tg-aSYN-mtNOD and C57BL/6J mice.

Analysis showed rescued neuron integrity in case of old tg-aSYN-mtNOD mice compared to tg-aSYN mice with no differences to Ctrl mice (A). A greater proportion of microglia was detected in the cortex of 300 d old tg-aSYN-mtNOD mice compared to Ctrl mice (B). Data is presented as means \pm SEM ($n \geq 5$), * $p \leq 0.05$; ** $p \leq 0.01$; *** $p \leq 0.001$ (one-way ANOVA followed by Sidak's multiple comparison test)

4.2.2 Determination of aSYN in tg-aSYN and tg-aSYN-mtNOD mice using ELISA

To verify aSYN burden in tg-aSYN and tg-aSYN-mtNOD mice, ELISA was performed. As a quantitative analysis of the immunohistochemical staining was impossible and gave only little insight into the distribution of the aggregated aSYN species labeled with anti-aSYN clone 5G4, the amount of aSYN in carbonate- and guanidine soluble fractions of the brain tissue of 50 d and 300 d old tg-aSYN and tg-aSYN-mtNOD mice was determined using this method.

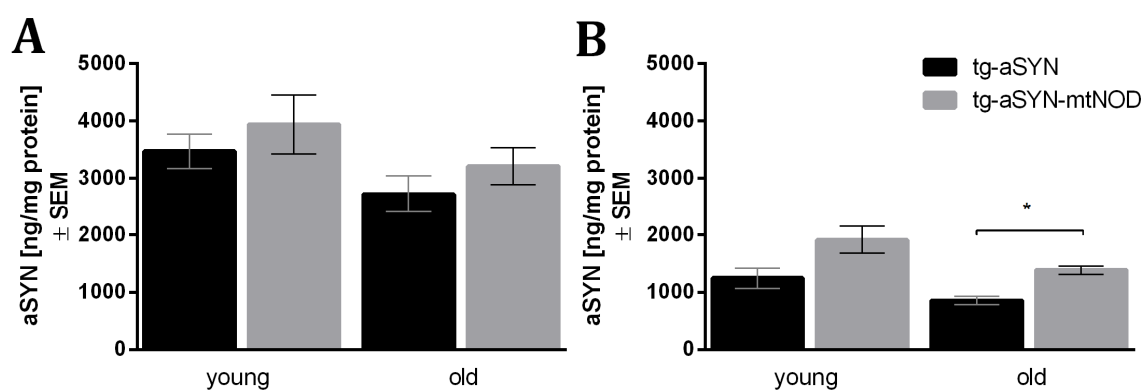


Figure 15: ELISA measurements of aSYN in the brain of tg-aSYN and tg-aSYN-mtNOD mice.

Mice with mitochondrial polymorphism showed a significantly greater amount of guanidine soluble aSYN in the late time point (B) compared to tg-aSYN mice, whereas the carbonate soluble aSYN revealed no differences (A). Notable was the unchanged amount of total aSYN between both time points. Data is presented as means \pm SEM ($n \geq 6$), * $p \leq 0.05$ (one-way ANOVA followed by Sidak's multiple comparison test)

The measurement of carbonate soluble aSYN, which includes monomeric and small oligomeric forms of aSYN, showed no significant differences between young and old tg-aSYN and tg-aSYN-mtNOD mice and between the time points (see Figure 15A).

Higher molecular species of aSYN were quantified using the guanidine soluble fraction of the brain tissue containing of the non-soluble, aggregated respectively fibrillar forms of the protein. No differences were visible at 50 d of age ($p=0.0635$), whereas the 1.6-fold amount of aSYN was detectable in 300 d old tg-aSYN-mtNOD mice compared to tg-aSYN, leading to a significantly greater aSYN burden in these mice ($p=0.036$; see Figure 15B).

4.2.3 Influence of mitochondrial polymorphisms on the behavior of tg-aSYN mice

The behavioral study of tg-aSYN-mtNOD mice was performed simultaneously with the above mentioned examination of tg-aSYN mice and results and statistics were evaluated equally. Tg-aSYN-mtNOD mice were compared to tg-aSYN and control mice that were already presented in section 4.2.3.

4.2.3.1 Rotarod

Observations made during the rotarod performances of the tg-aSYN-mtNOD mice revealed no obvious differences in the implementation of the task compared to tg-aSYN mice that are worth to be further described.

The first evaluation of data concentrated again on the proportion of censored data according to the cut-off time of 240 s in the rotarod method. A significantly greater proportion of data was censored in case of tg-aSYN-mtNOD mice in the mid-age time points 25-33 weeks compared to tg-aSYN mice ($p=0.0016$), indicating a better physiological fitness of these mice (see Figure 16). While 72 % of the gathered tg-aSYN-mtNOD data were censored, only 34 % of the tg-aSYN data fell into this category (as mentioned in section 4.1.3.1).

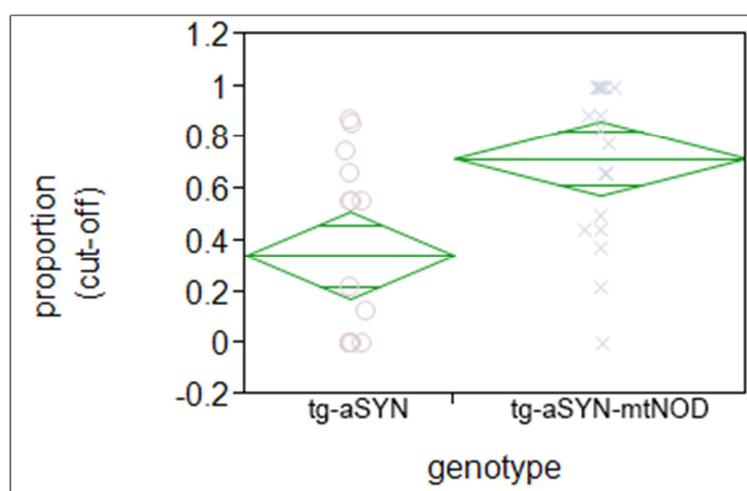


Figure 16: Proportion of censored data collected using rotarod.

Tg-aSYN-mtNOD mice displayed a significantly greater proportion of censored data (72 %) compared to tg-aSYN mice (34 %). Data is presented as mean diamonds and x-axis proportional ($n \geq 15$, male) (one-way ANOVA followed by Bonferroni's multiple comparison test).

The results of the latency time and the time until the first passive rotation showed again comparable results (see Figure 17A-B).

In order to answer the same questions as described in section 4.1.3.1, the results were compared to the data of tg-aSYN and control (see Figure 10). The tg-aSYN-mtNOD mice performed significantly better in both tasks ($p=0.016$, $p=0.032$) with the most distinct results again at mid-age time points between 25 and 33 weeks of age ($p=0.00008$, $p=0.00011$). Age has a significant influence on the performances of both tasks as mentioned before ($p=0.0062$, $p=0.000072$). Refer to Figure 17 for visualization.

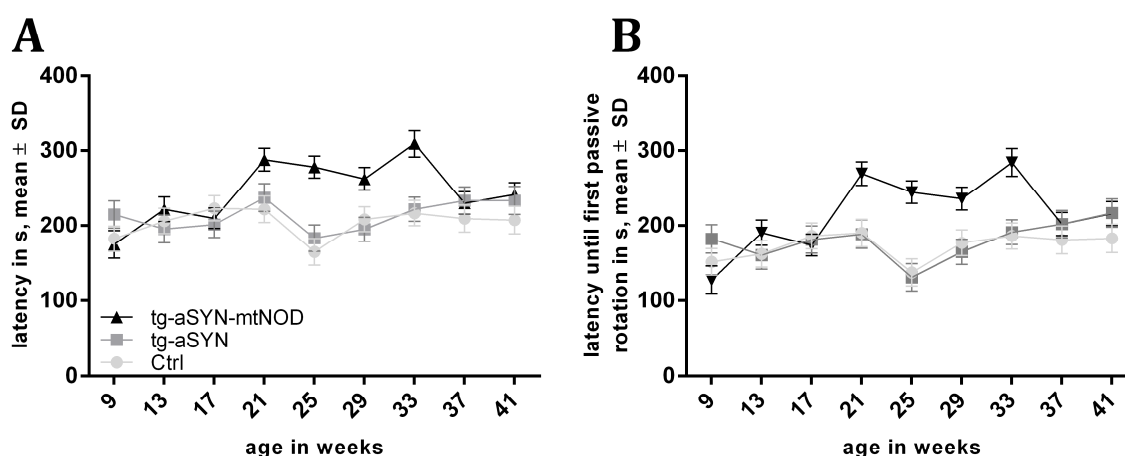


Figure 17: Motor performances of tg-aSYN, tg-aSYN-mtNOD and C57BL/6J mice.

Using rotarod, a tremendous difference between tg-aSYN-mtNOD, tg-aSYN and Ctrl mice, respectively, was determined in mid-age time points of 25 to 33 weeks. Tg-aSYN-mtNOD mice performed significantly better in both tasks. Age had a significant influence on both performances in all mouse models. Data is presented as means \pm SD ($n \geq 5$, male) (Linear Mixed-Effects Models with Censored Responses, LMEC).

4.2.3.2 Pole test

The determination of the influence of distinct mitochondrial polymorphisms on the motor skills of tg-aSYN-mtNOD mice was additionally performed by pole test. The procedure and analysis was the same as described before (4.1.3.2). Tg-aSYN-mtNOD mice displayed a better orientation performance (time-until-turn-latency) compared to tg-aSYN and control mice in old age ($p=0.0237$), i.e. 37-41 weeks but not at mid-age time points ($p \geq 0.06$). The climb performance however revealed neither in mid-age nor in old age any differences between tg-aSYN and tg-aSYN-mtNOD mice (see Figure 18).

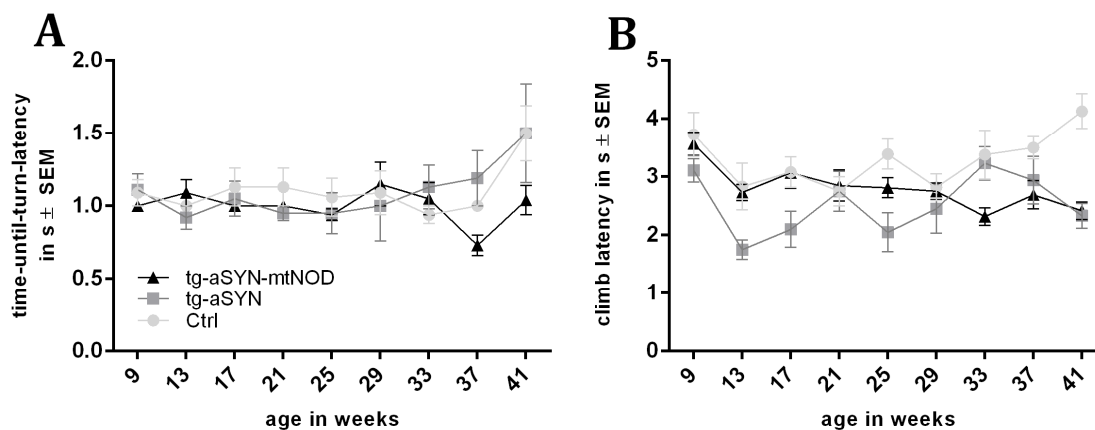


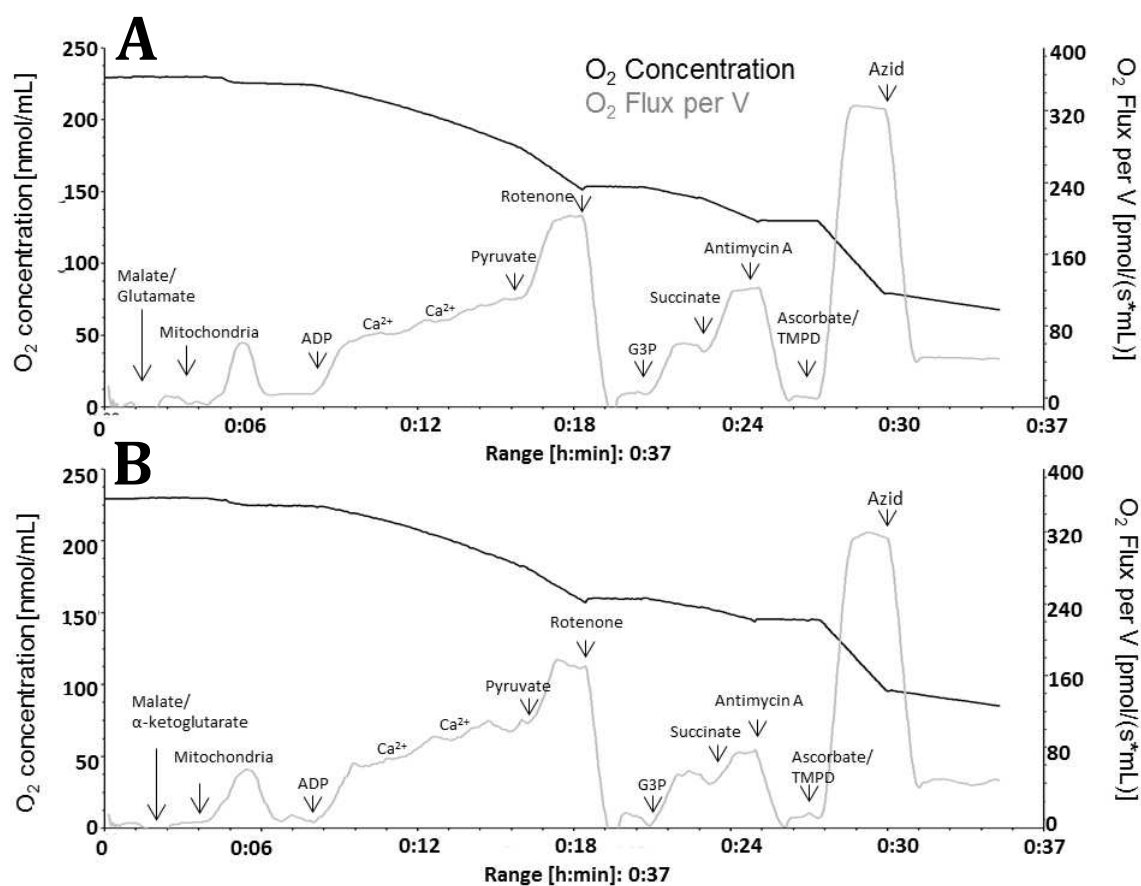
Figure 18: Influence of mitochondrial polymorphism on the pole test performance of tg-aSYN mice.

Tg-aSYN-mtNOD displayed significantly better time-until-turn-latencies compared to tg-aSYN mice (A) but no differences in climb performance were found (B). Data is presented as means \pm SEM ($n \geq 5$, male). (restricted maximum likelihood (REML) approach and additional two-sided t-test with adjusted degrees of freedom).

4.3 Respirometric measurements of isolated brain mitochondria

To analyze the functional effects of mitochondrial polymorphisms in tg-aSYN-mtNOD mice, respirometric measurements were performed using high resolution respirometry. In this method, the oxygen consumption of isolated brain mitochondria is used as a parameter for the function of single complexes and the entire mitochondrion.

In this study, mice of two different ages were used, 100 d and 200 d, which did not overexpress aSYN, i.e. mtNOD respectively C57BL/6J mice. As described in section 3.2.7, four different protocols (Table 14) served to assess parameters important for the understanding of the mitochondrial function. Substrates were added sequentially in order to measure complex-dependent respiration rates and to calculate control ratios. These protocols were performed consecutively and each measurement resulted in a specific curve as displayed exemplarily in Figure 19.



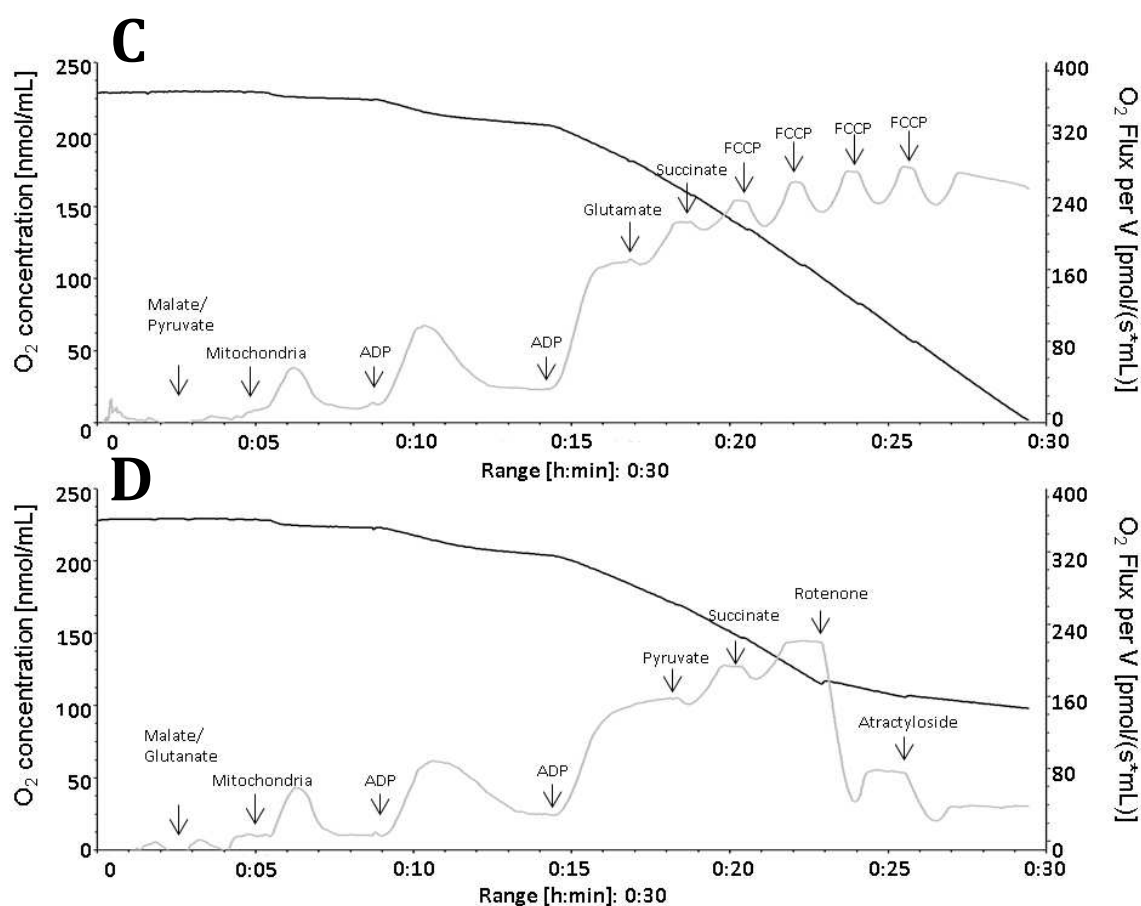


Figure 19: Representative respirograms of old C57BL/6J mice.

Shown is the sequential addition of substrate according to the four experimental approaches I-IV (A-D; see Table 14, page 37) and the resulting changes in O_2 concentration (black line) and O_2 flux (grey line), which were further evaluated. ADP, adenosine triphosphate; FCCP, Carbonyl cyanide-4-(trifluoromethoxy)phenylhydrazone; G3P, glycerol-3-phosphate; TMPD, N,N,N',N'-tetramethyl-p-phenylenediamine

4.3.1 Complex I- dependent respiration

The complex I-dependent respiration rates were measured using all four protocols with different substrate compositions. No changes occurred in maximal complex I-dependent respiration (state $3_{\text{compl.I}}$) in young and old animals of both mouse models, C57BL/6J and mtNOD when using the substrate composition of malate, glutamate and pyruvate as provided by protocol I, III and IV. Interestingly, the results of protocol II showed a significantly greater oxygen consumption in case of young mtNOD mice compared to control mice ($p=0.03$; see Figure 20A).

In protocol I as well as II the additional supply of Ca^{2+} led to a vigorous increase of the respiration rate, even though the Ca^{2+} dependent activation was higher when malate and glutamate were provided (protocol I; 163 % of the state 3 respiration rate without Ca^{2+} stimulation) than with malate and α -ketoglutarate provided (protocol II; ~134 % of the starting state 3 respiration rate) (see Figure 20B).

Comparing the respiratory rates after Ca^{2+} stimulation, they were only elevated by the polymorphisms in young mtNOD mice in case of α -ketoglutarate (protocol II). Here, mtNOD mice show significantly greater oxygen consumption in comparison to control mice ($p=0.04$, see Figure 20B).

It is important to note that the effect seen in the maximal complex I-dependent respiration rate (Figure 20A) is only a secondary effect of the stimulation caused by Ca^{2+} addition (Figure 20B).

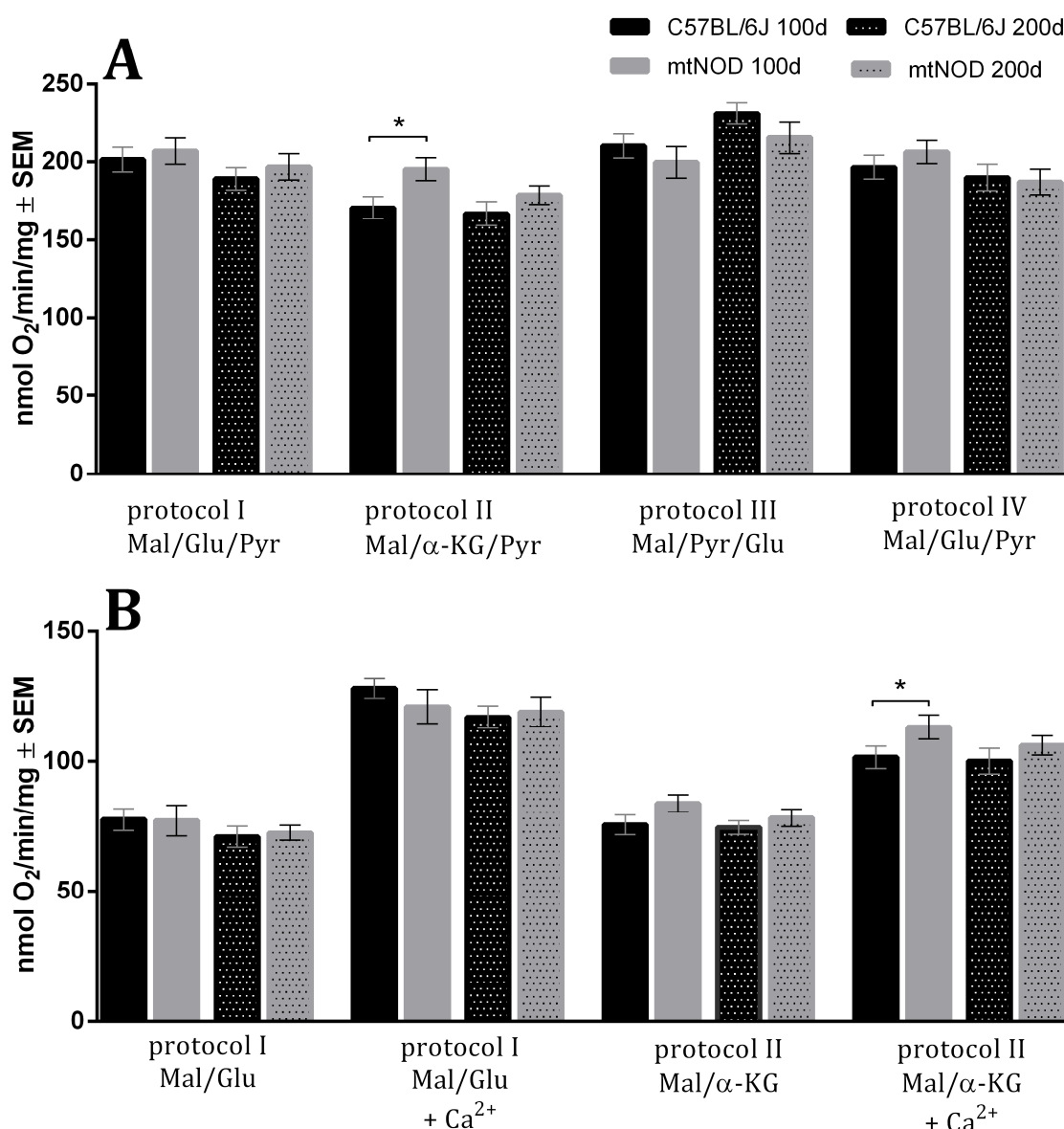


Figure 20: Complex I-dependent respiration of isolated brain mitochondria of mtNOD and C57BL/6J mice.

Maximal complex I respiration (A) showed no differences between age and strains. The significantly increased respiration rate measured with protocol II was considered to be secondary effect to the increased Ca^{2+} -dependent respiration illustrated in B. The stimulation of respiration using Ca^{2+} led to a vigorous increase in oxygen consumption with a larger extend in case of malate/glutamate as starting substrates (~163 %). However, the Ca^{2+} -dependent increase that followed the protocol II approach was significantly greater in young mtNOD mice compared to young Ctrl mice (B). Data is presented as means \pm SEM ($n \geq 14$), $*p < 0.05$ (one-way ANOVA followed by Sidak's multiple comparison test)

4.3.2 Complex II- dependent respiration

To assess the complex II-dependent respiration, complex I was inhibited using rotenone in protocol I, II and IV with different starting substrates. This inhibition was necessary, because both complexes simultaneously deliver their electrons to ubiquinone.

A further supply with glycerol-3-phosphate in protocol I and II led to an enhanced respiration (protocol I, 59 %; protocol II, 53 %) caused by an increased availability of reduction equivalents (FADH₂) and adjusted the respiration to the maximal complex II-dependent respiration (state 3_{Comp.II}) (see Figure 21A).

Interestingly, the complex II-dependent oxygen consumption measured in the presence of α -ketoglutarate (protocol II) was generally smaller compared to glutamate (protocol I) as illustrated in Figure 21A. The state 3_{Succ} rates (without glycerol-3-phosphate) based on protocol I revealed a decrease in 200 d old control mice compared to 100 d old ones ($p=0.049$), leading to a significantly smaller oxygen consumption in comparison with 200 d old mtNOD mice, too ($p=0.0001$; see Figure 21A). The tendency of this notion was also visible in the rates of protocol IV ($p<0.1$), but not in protocol II. However, in both approaches (I and II) young mtNOD mice showed a greater increase in oxygen consumption following the supply of glycerol-3-phosphate as compared to young control mice leading to a marked difference between old mtNOD and control mice ($p=0.0016$ for protocol I and $p=0.0412$ for protocol II; see Figure 21A). In conclusion, the most prominent difference between old mtNOD and control mice was seen in the maximal complex II-dependent respiration rate (with glycerol-3-phosphate) of protocol I and II.

Furthermore, after preventing the transport of ADP by adding atractyloside and comparing the non-phosphorylating respiration (state 4_{Succ/Atr}), similar results, as in Figure 21A, were obtained. Again, old control mice showed diminished complex II-dependent respiration rates in comparison to young control mice ($p=0.0016$) and old mtNOD mice ($p=0.011$; see Figure 21B).

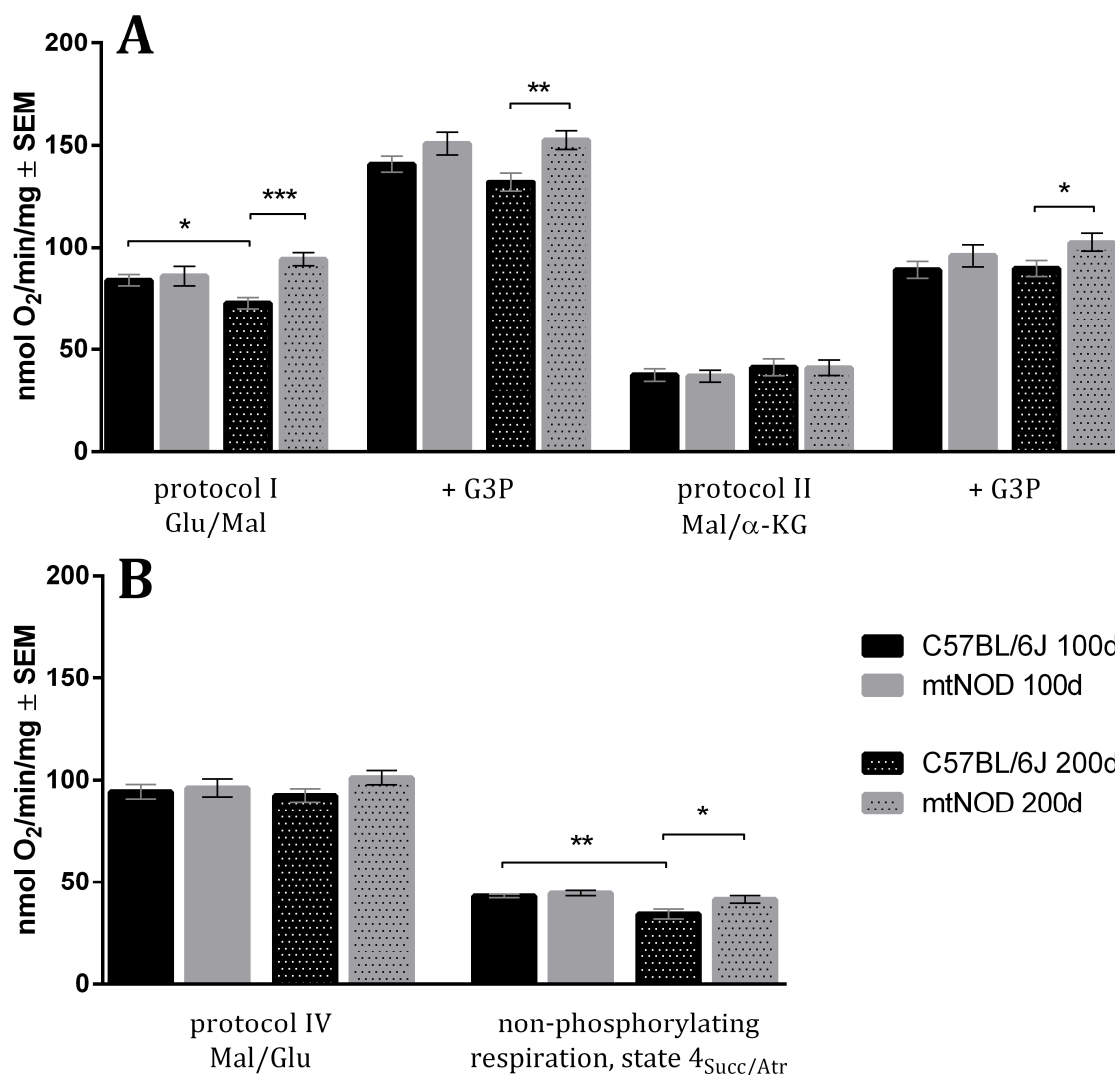


Figure 21: Complex II-dependent respiration rates of mtNOD and C57BL/6J mice.

The oxygen consumption measured in isolated brain mitochondria of 200 d old Ctrl mice was significantly lower compared to mtNOD mice when measurement was performed using protocol I (A, left) and tendentially lower when conducted with protocol IV (B, left). When supplied with glycerol-3-phosphate (G3P), old Ctrl mice displayed a significantly diminished respiration rate in comparison to mtNOD mice in both protocols (A). Even the non-phosphorylating respiration revealed confirming results (B, right). Succ, Succinate; Atr, Atractyloside. Data is presented as means \pm SEM ($n \geq 14$), * $p \leq 0.05$; ** $p \leq 0.01$; *** $p \leq 0.001$ (one-way ANOVA followed by Sidak's multiple comparison test respectively Kruskal-Wallis test followed by Dunn's multiple comparison test)

Subsequently, the quotients of maximal complex I- and complex II-dependent respiration (in the following referred to as CI/CII ratio) were calculated for rates measured upon previous described protocols I, II and IV. This ratio is often used as indicator of complex I impairments and was changed by polymorphism. A significantly diminished CI/CII ratio for old mtNOD mice was found compared to old control mice ($p=0.0074$; protocol I) but no changes can be observed for protocol II and IV (see Figure 22).

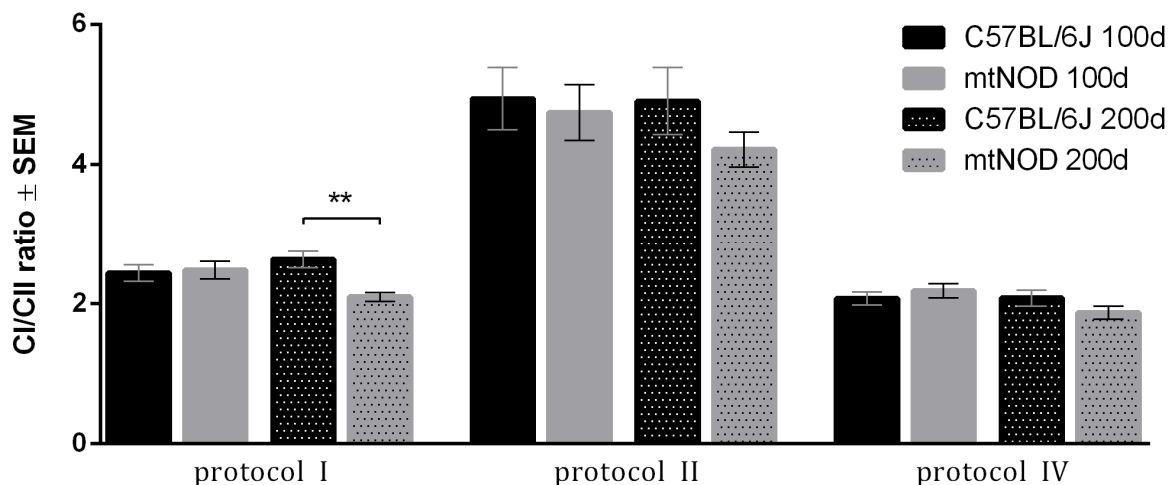


Figure 22: Complex I/Complex II ratio calculated from measurements based on protocol I, II and IV of mtNOD and C57BL/6J mice.

Significant changes occurred in old mtNOD mice compared to Ctrl based on the results achieved by protocol I. No changes were found in the same groups in protocol II and IV- dependent results. Data is presented as means \pm SEM ($n \geq 14$), * $p < 0.05$ (Kruskall-Wallis test followed by Dunn's multiple comparison test)

4.3.3 Complex III- dependent respiration

The maximal complex III-dependent respiration (state $3_{\text{compl.III}}$) was achieved by the addition of substrates to reach maximal complex I respiration followed by the administration of succinate to obtain complex II respiration as realized by measurements upon protocol III and IV. No changes due to age or genotype occurred as illustrated in Figure 23.

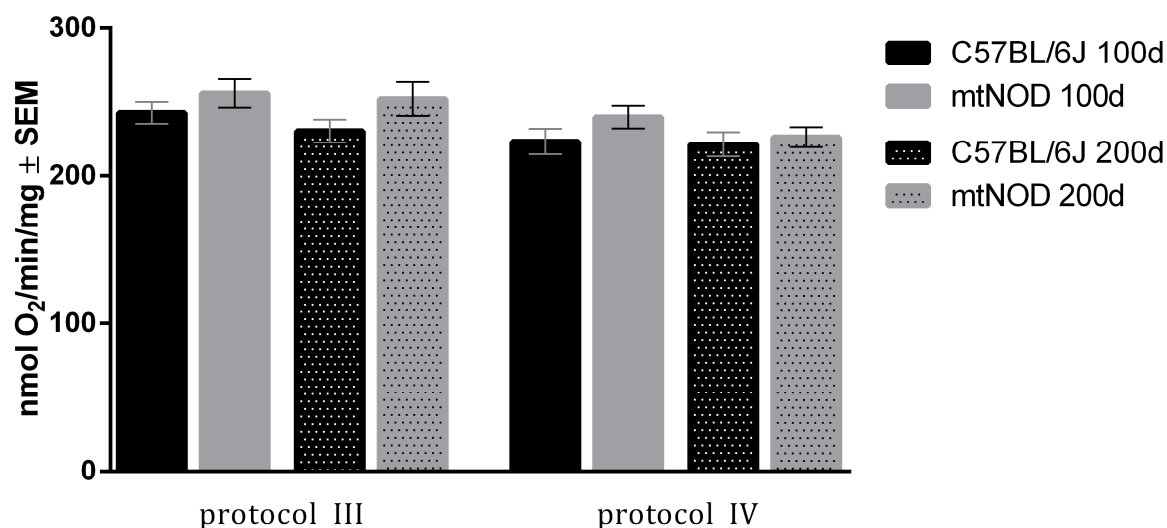


Figure 23: Complex III-dependent respiration rates of mtNOD and C57BL/6J mice.

These rates were measured from isolated mitochondria of 100 d and 200 d old mtNOD respectively C57BL/6J (Ctrl) mice. No changes occurred between ages and strains. Data is presented as means \pm SEM ($n \geq 12$).

4.3.4 Complex IV- dependent respiration

The next complex determined for respiration was complex IV, also referred to as cytochrome c-oxidase (COX). To ensure that only complex IV-dependent respiration was measured, complex I, II and III were fully inhibited by the addition of antimycin A. Complex IV-dependent respiration was then stimulated via the administration of TMPD, a powerful reduction equivalent that leads to the oxidation of cytochrome c by COX. Ascorbate regenerated TMPD with its antioxidant capacity. These steps were realized in protocol I and II. The respiration rate increased immediately and COX was afterwards inhibited by azide. The subsequently measured oxygen consumption was considered an artefact resulting from the auto-oxidation capacity of TMPD and was therefore subtracted from the complex IV-dependent respiration rates.

As illustrated in Figure 24, a significant difference was found between young and old mtNOD mice when measured using protocol II ($p=0.0093$). Here, the oxygen consumption dropped about nearly 20 % with age. The results measured upon protocol I only displayed a reduction in respiration of 10 % in mtNOD and control mice. No changes occurred when comparing both mouse models.

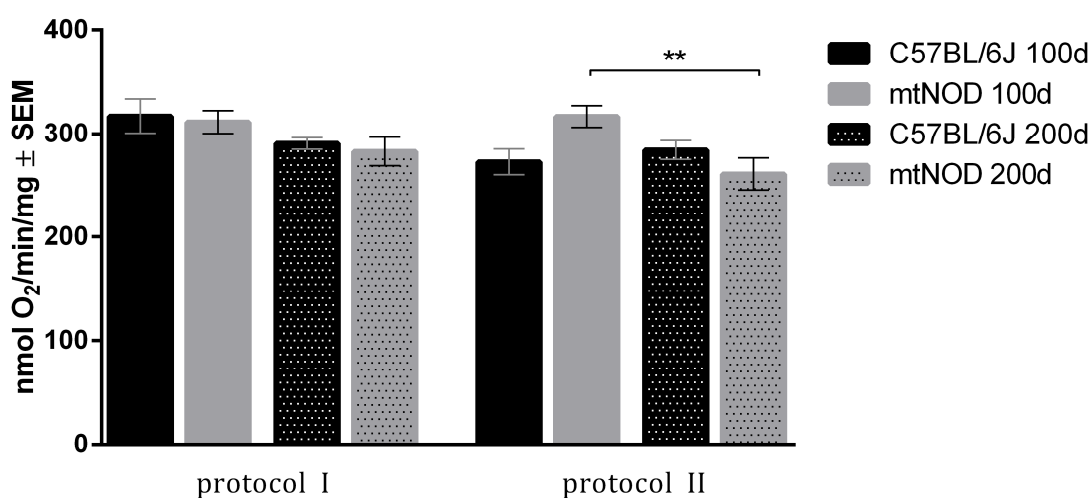


Figure 24: Complex IV-dependent respiration of mtNOD and C57BL/6J mice.

Complex IV-dependent respiration was determined from isolated brain mitochondria of 100 d and 200 d old mtNOD and Ctrl (C57BL/6J) mice. The oxygen consumption in old mtNOD mice dropped about ~20 % compared to young ones when measured using protocol II. No changes were found between both strains. Data is presented as means \pm SEM ($n \geq 14$), $*p < 0.05$ (one-way ANOVA followed by Sidak's multiple comparison test).

COX is known to provide an excessive capacity which is higher compared to the maximal uncoupled respiration that can be determined by the addition of FCCP (see 4.3.5) (Gnaiger *et al.*, 1998). To examine possible differences between mtNOD and control mice, the excessive capacity of COX was calculated by forming the quotient of the complex IV-dependent respiration (protocol I and II) and the maximal ETC capacity (protocol III, see 4.3.5).

The excess capacity of COX was found to range between 1- and 1.3-fold of the maximal ETC capacity. No significant changes were observed between age and strains (Figure 25).

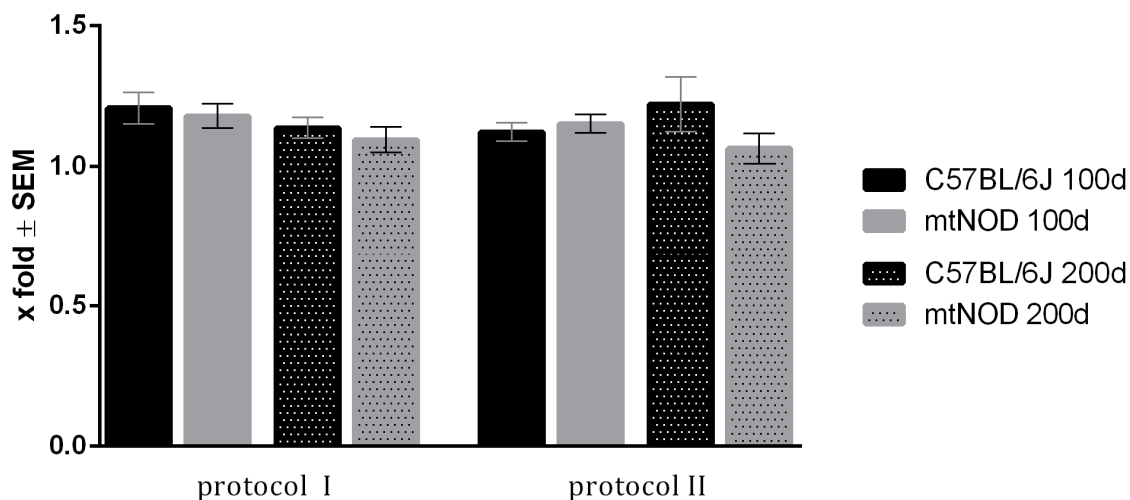


Figure 25: The excess capacity of complex IV (COX).

The excess capacity of COX related to the maximal respiration upon uncoupling with FCCP (4.3.5) revealed no changes between young and old Ctrl and mtNOD mice, respectively, nor between both strains. Data is presented as means \pm SEM ($n \geq 9$).

4.3.5 Maximal respiration rate upon uncoupling with FCCP

To examine the maximal capacity of the ETC and determine possible differences between mtNOD and control mice, it was necessary to uncouple the oxidative phosphorylation. This was achieved by the addition of FCCP. As a consequence, the proton flux is maximally increased. The addition of FCCP was performed step wise (protocol III) to prevent an inhibition of the ETC at certain concentrations and led to a peak that is displayed in Figure 26. The results revealed no differences between age and strains.

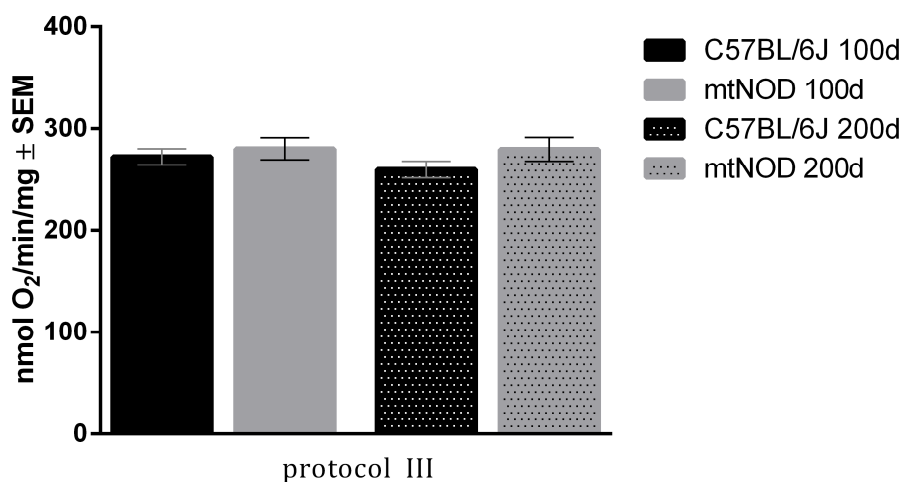


Figure 26: Maximal capacity of ETC measured after uncoupling of the oxidative phosphorylation with FCCP.

No changes between Ctrl and mtNOD and between ages were detectable. Data is presented as means \pm SEM ($n \geq 11$).

4.3.6 Resting states

Non-phosphorylating respiration rates were calculated for complex I- and II-dependent oxygen consumption. In fact, the complex II-dependent non-phosphorylating respiration following protocol IV was already displayed in Figure 21B in 4.3.2. For the sake of completeness, it is illustrated in this section once more (Figure 27A, left columns). As already described before, the non-phosphorylating respiration revealed striking differences between young and old control mice ($p=0.0016$) and control and mtNOD mice at the age of 200 d ($p=0.011$). In contrast to that no changes in age or strain were observable when comparing the non-phosphorylating respiration of complex I that was measured due to limited respectively lack of adenine nucleotide concentration neither based on protocol III (Figure 27B) nor IV (Figure 27A).

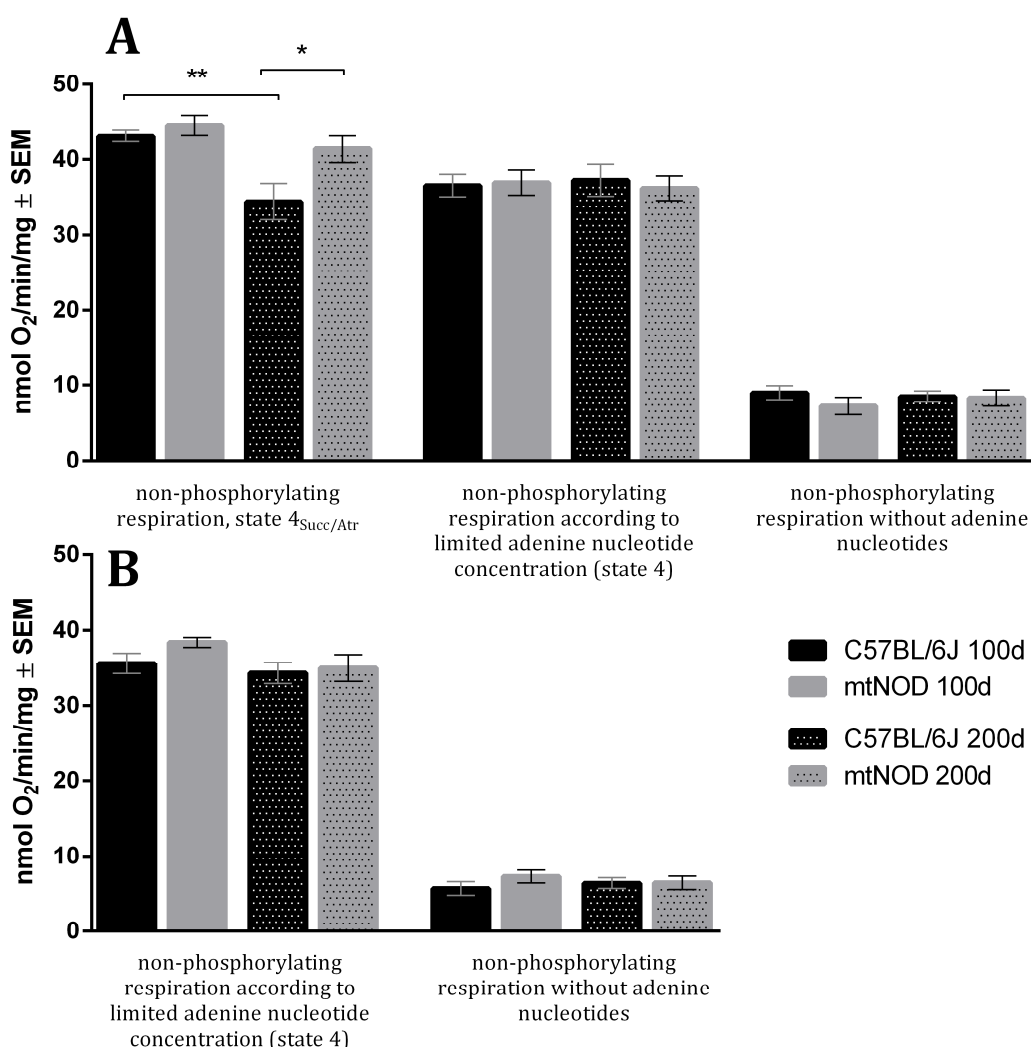


Figure 27: Different states of non-phosphorylating respiration for complex I- and complex II-dependent substrates.

After inhibition of the adenine nucleotide-carrier with atractyloside, the non-phosphorylating respiration with succinate as substrate was larger in old mtNOD mice compared to Ctrl and between young and old Ctrl mice, too (described before in 4.3.2) (Figure 25A, left). State 4 respirations in the presence of 75 nM adenine-nucleotides (mainly ADP) showed no changes caused by age and polymorphism. Non-phosphorylating respiration without added adenine nucleotides revealed also no changes (Figure 25A for protocol IV, Figure 25B for protocol III). Data is presented as means \pm SEM ($n \geq 11$), $*p \leq 0.05$; $**p \leq 0.01$ (one-way ANOVA followed by Sidak's multiple comparison test).

4.3.7 Respiratory Control Ratio

The respiratory control ratio (RCR) was used to determine the relation of maximal respiration capacity in the presence of ADP (state 3) and respiration without ATP-synthesis (state 4). The RCR was calculated for the respective states of complex I (protocol III, Figure 28, left set of columns) and II (protocol IV, Figure 28, right set of columns). Based on this ratio it is possible to make statements concerning the importance and control of the oxidative phosphorylation over the ETC and how tight both are coupled. The RCR displayed by complex I-dependent respiration rates was not changed by age or polymorphism, whereas RCR based on complex II-dependent respiration rates showed a significant increase in 200 d old control mice compared to young ones ($p=0.0028$). Here again, no difference between both mouse models was visible (Figure 28).

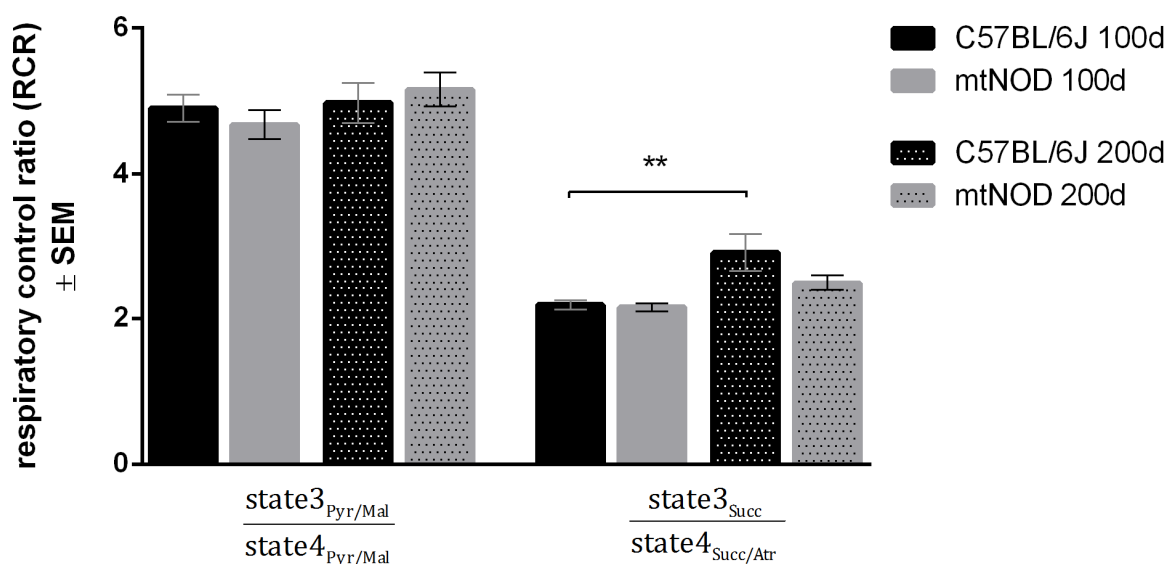


Figure 28: Respiratory control ratios (RCR) of mtNOD and C57BL/6J mice.

RCR calculated for complex I-dependent respiration (Malate/ Pyruvate; protocol III) and complex II-dependent respiration (Succinate/Attractyloside; protocol IV). No changes were observable in complex I, whereas 200 d control Ctrl mice showed significantly greater RCR (Succ/Atr) values compared to young ones. Data is presented as means \pm SEM ($n \geq 14$), * $p \leq 0.05$; ** $p \leq 0.01$ (one-way ANOVA followed by Sidak's multiple comparison test).

4.4 Relevance of ABC transporter -ABCC1- activity on the aSYN pathology of tg-aSYN mice

The increased complex II-dependent respiration found in mtNOD mice and the enhanced physiological performance of tg-aSYN-mtNOD mice led to the assumption that energy-dependent mechanism might be impaired in mice overexpressing human mutated aSYN leading to the pathological phenotype of this PD mouse model. The aforementioned results suggest a decreased ATP supply which is very likely to influence several metabolic processes. Consequential, the present work aimed to verify whether aSYN is transported via the ABC transporter -ABCC1-, a prominent energy-dependent clearance mechanism approved for A β in AD mice (Krohn *et al.*, 2011).

A novel mouse model was created for this study, the ABCC1 knock-out mouse denoted tg-aSYN-ABCC1^{-/-}.

4.4.1 Consequences of the ABCC1 knock-out on the histology of the tg-aSYN mice

Semi-quantitatively analyzed cortex section of 100 d old tg-aSYN and tg-aSYN-ABCC1^{-/-} mice revealed no difference in neuronal- and microglial area (see Figure 29).

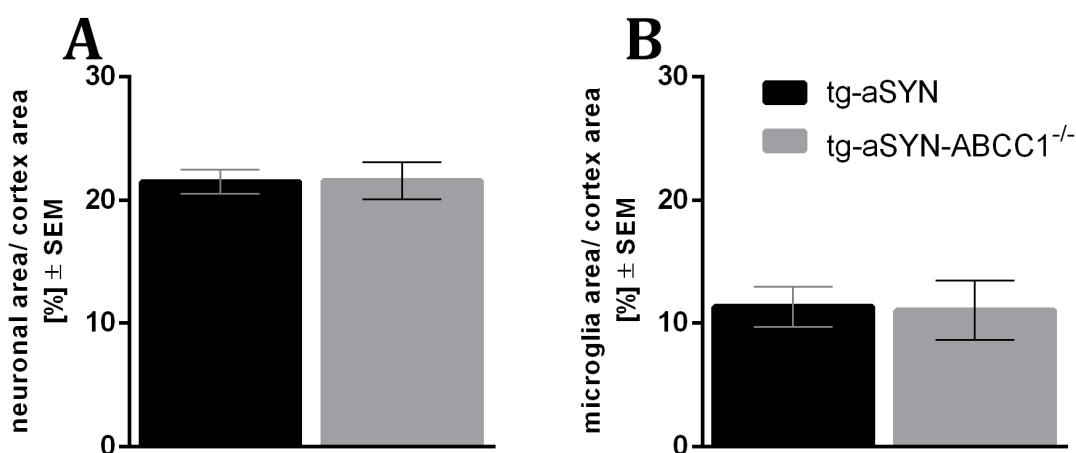


Figure 29: Determination of neuronal- and microglial area in the cortex of 100 d old tg-aSYN and tg-aSYN-ABCC1^{-/-} mice.

Semi-quantitative analyzes revealed no differences in neuronal area (A) and microglial area (B) in the cortex of 100 d old tg-aSYN compared to tg-aSYN-ABCC1^{-/-} mice. Data is presented as means \pm SEM (n = 6).

4.4.2 Quantification of aSYN upon ABCC1 knock-out using ELISA

To quantify the aSYN level in the brain of 100 d old tg-aSYN-ABCC1^{-/-} mice compared to 100 d old tg-aSYN mice, ELISA was performed with the carbonate fraction containing monomeric and small oligomeric aSYN and with the guanidine fraction containing non-soluble aSYN. Surprisingly, no significant differences were detected in either fraction comparing tg-aSYN-ABCC1^{-/-} and tg-aSYN (ABCC1^{+/+}) mice (see Figure 30).

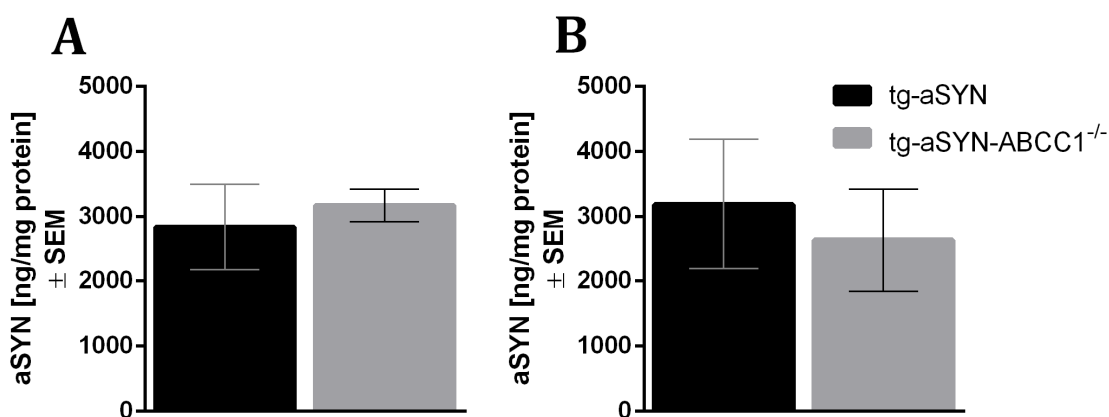


Figure 30: ELISA measurement of g-aSYN and tg-aSYN-ABCC1^{-/-} mice.

The carbonate fraction (A) revealed similar results compared with the guanidine fraction (B) in both examined mouse models. No significant changes were found. Data is presented as means ± SEM (n = 5).

4.4.3 Influence of ABCC1 activation using thiethylperazine on neuron integrity and the immune response

To validate a possible beneficial effect of ABCC1 activation on the pathology of tg-aSYN mice, thiethylperazine was administered. Tg-aSYN and tg-aSYN-ABCC1^{-/-} mice were treated daily with thiethylperazine while untreated as well as water-treated mice served as control.

Immunohistological analyzes were performed but unexpectedly, no visible changes were observed for thiethylperazine-treated compared to water-treated (control) mice (see Figure 31). The neuronal and the microglial area were quantified relative to the cortical area in a semi-quantitative approach. Surprisingly, an increased neuronal area (~23 %) was found in water-treated (control) mice when compared to untreated ones (p=0.0081). Thiethylperazine-treated tg-aSYN mice and tg-aSYN-ABCC1^{-/-} mice displayed no changes compared to untreated mice (see Figure 32A). Similarly, the examination of microglial area revealed no significant difference upon treatment (see Figure 32B).

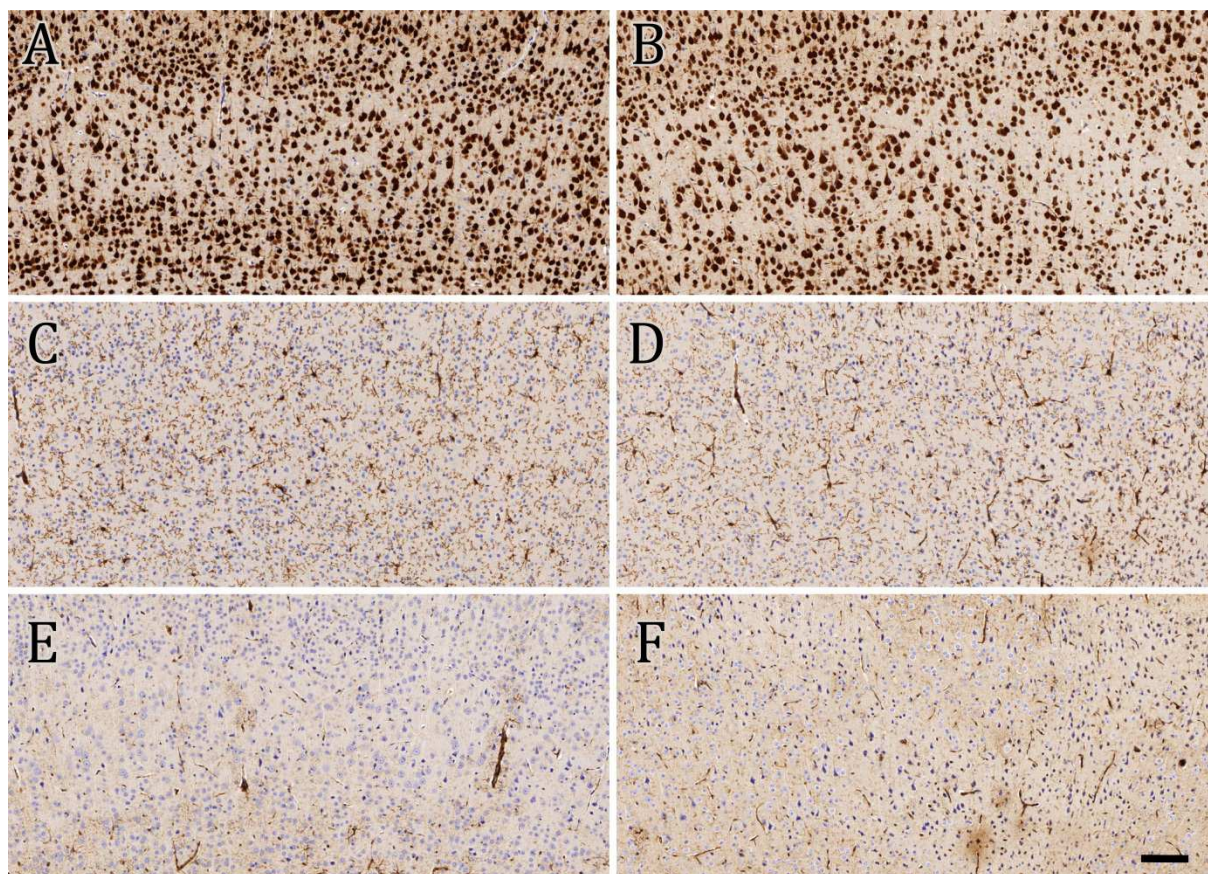


Figure 31: Immunohistochemical analyzes of thietylperazine- and water-treated tg-aSYN mice.

The panel shows a comparison between tg-aSYN mice either treated with thietylperazine (left column; A,C,E) or water (right column; B,D,F). A differences was not visible when stained with NeuN (A,B) nor in case of Iba1 staining (C,D) or GFAP staining (E,F). Scale bar = 100 μ m.

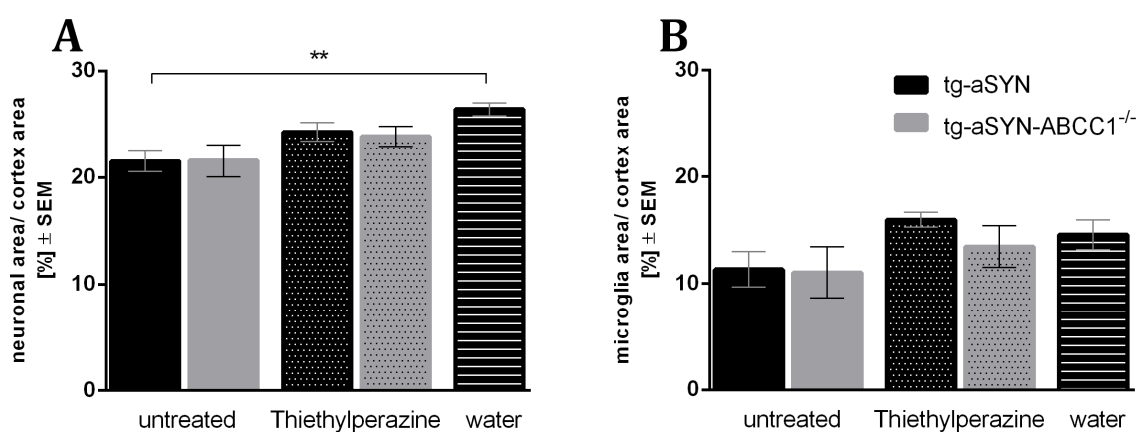


Figure 32: Semi-quantitative analyzes of neuronal and microglial area in the cortex of tg-aSYN and tg-aSYN-ABCC1^{-/-} mice upon treatment with thietylperazine.

The neuronal area per cortex area was unchanged in thietylperazine-treated mice of both mouse models compared to untreated mice (A). Interestingly, neuronal area of water-treated (control) mice showed a significant increase of ~23 % compared to untreated mice (A). The microglia area revealed no differences upon treatment (B). Data is presented as means \pm SEM ($n \geq 5$). (one-way ANOVA followed by Sidak's multiple comparison test).

4.4.4 ABCC1 activation – quantification of aSYN by ELISA

ELISA measurements were performed to investigate the influence of ABCC1 activity on the concentration of aSYN in the brain of tg-aSYN mice. A decrease in aSYN burden was excluded by the present results. Monomeric (carbonate-soluble) aSYN increased significantly upon thiethylperazine-treatment in tg-aSYN mice (42 %; $p=0.0406$; Figure 33A). By trend, also an increase in water-treated (control) mice was found ($p=0.0782$; see Figure 33A). As no significant difference was detected between thiethylperazine-treated tg-aSYN and tg-aSYN-ABCC1^{-/-} mice, a causal ABCC1-dependent mechanism could be excluded. The decrease of aggregated aSYN in the guanidine-soluble fraction upon thiethylperazine- and water-treatment was not significant (see Figure 33B).

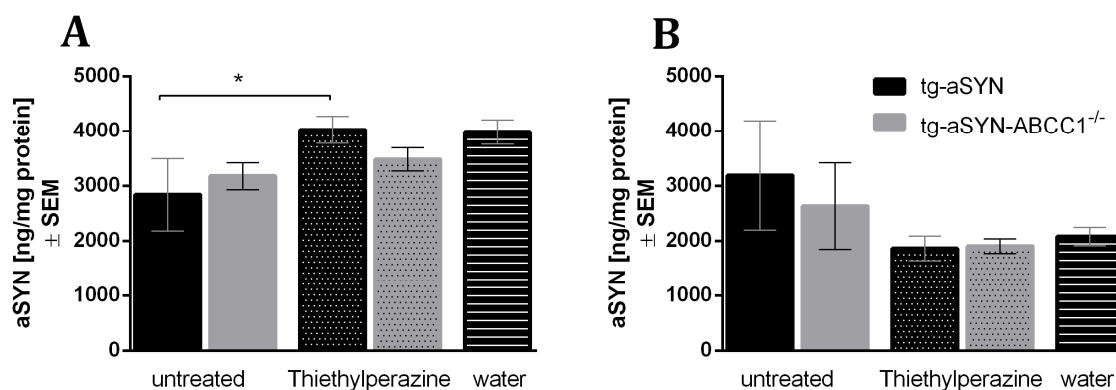


Figure 33: ELISA measurement of tg-aSYN and tg-aSYN-ABCC1^{-/-} mice upon treatment with thiethylperazine in contrast to untreated and water-treated mice.

Pharmacological activation of ABCC1 had no impact on the concentration of monomeric (carbonate-soluble) aSYN (A) or aggregated (guanidine-soluble) aSYN (B) in the brain of 100 d old tg-aSYN mice when compared to water-treated (control) mice. Interestingly, thiethylperazine increased the proportion of monomeric aSYN significantly in thiethylperazine-treated tg-aSYN compared to untreated mice (A), whereas guanidine-soluble aSYN showed no difference (B). Data is presented as means \pm SEM ($n \geq 5$). (one-way ANOVA followed by Sidak's multiple comparison test).

5. Discussion

Until today, the underlying cellular mechanisms leading to the abnormal aSYN expression and the resulting cell fate culminating in the characteristic symptoms of synucleopathies are still not fully understood. It is well accepted that the overexpression and deposition of aSYN causes the onset of PD. Starting with the accumulation of soluble monomers, aSYN accumulates into oligomers and further on into fibrils and deposits into the characteristic Lewy bodies and Lewy neurites. Besides age, genetic predisposition is a known risk factor for PD, but most often disease onset occurs sporadically without known cause. In the past, research has been focused on finding triggers of PD. Here, especially the recognition of pesticides like MPTP and rotenone led to new insights into PD pathogenesis (Moore *et al.*, 2005). With the comprehension of the mitochondrial damage caused by these pesticides, a new field of research emerged and promoted a different view on PD.

The present study aimed to characterize the well-known and widely used tg-aSYN mouse model with 'A30P' mutation, of which several contradictory results exist, and to investigate whether it is a proper model to mimic PD. Furthermore, the influence of mitochondrial polymorphism on the pathology in the tg-aSYN mouse model was of interest. Scheffler *et al.* determined certain mitochondrial polymorphisms in the context of Alzheimer's disease and found an increased production of ATP (Scheffler *et al.*, 2012). Inspired by this study, the respirometric analysis of isolated brain mitochondria in the present work extended these previous findings. It was additionally possible to find a conceivable explanation for the increased ATP production that was accompanied by improved motor performances and neuronal integrity found in this inbred mouse strain when compared to the common tg-aSYN mouse. The altered mitochondrial respiration in the aSYN overexpressing PD mouse model and the results found determining the tg-aSYN mouse model with mitochondrial polymorphisms led to the investigation whether the ATP-dependent ABC transporter activity/ function might be crucial to PD pathology and would be found beneficial to be improved pharmacologically.

5.1 The tg-aSYN mice is a convenient model for synucleopathies

Mouse models are widely used to model PD in research because of their human-like neurochemistry. Depending on the promoter and overexpressed protein, the known transgenic PD mouse models display different features of the disease. Mostly they are created on the basis of familial PD, using the overexpression of mutated aSYN to mimic the disease. Many models were generated in the past decade and described detailed; however, their relevance for PD research has been extensively discussed (Chesselet, 2008).

The, in the present study used, tg-aSYN mice overexpresses the 'A30P' mutated aSYN under the Thy1 promoter and were described different by diverse groups concerning phenotypic alteration, behavior and histology. In order to further investigate these mice in the context of PD and synucleopathies, their characteristics were re-evaluated focusing on parameters that were of interest for the further experiments.

The Thy1 promoter ensures a broad expression in neurons throughout the brain, cortical as well as subcortical and, still discussed, in the SNpc (Masliah *et al.*, 2000).

While some groups were not able to find aSYN expression in the SNpc (Neumann *et al.*, 2002; van der Putten *et al.*, 2000), Rockenstein and coworkers observed aSYN accumulation in this structure of the brain (Rockenstein *et al.*, 2002). Interestingly, using this promoter, no pathological glial, spinal or neuromuscular alterations were found (Rockenstein *et al.*, 2002). Furthermore, aSYN was found to accumulate in basal ganglia and thalamus but not in the spinal cord or neuromuscular junctions leading to the assumption that this mouse models properly mimics characteristics of PD (Rockenstein *et al.*, 2002). However, Van der Putten *et al.* acknowledged the presence of aSYN depositions in neuromuscular junctions and also found motor neuron degeneration and concluded additional DLB (dementia with Lewy bodies) aspects (van der Putten *et al.*, 2000). An aSYN expression in cell bodies of pyramidal neurons in cortex and limbic system was described in agreement (Rockenstein *et al.*, 2002; van der Putten *et al.*, 2000).

In the present work, a broad aSYN expression throughout various brain structures was approved histologically, including cortex, thalamus, hippocampus, basolateral amygdala, geniculate nucleus, zona incerta and the pyramidal neurons, which were stained most intensively. Other parts of the brain only displayed mild aSYN expression, like hypothalamus, medial amygdala and dentate gyrus. However, no aSYN expression was found in SNpc and olfactory bulb, two structures with prominent expression in post mortem brain tissue of PD patients. This gap between human disease and current mouse models has been described previously (Freichel *et al.*, 2007).

In contrast to Kovacs *et al.*, who developed and used the IgG1 κ isotype monoclonal antibody (5G4) to stain brain sections of human PD patients (Kovacs *et al.*, 2012), it was possible to find the synapses and somata in the cerebral neurons of mice to be strongly labelled, reflecting the overexpression of aSYN in the mouse model, similar to previous reports (Rockenstein *et al.*, 2002; van der Putten *et al.*, 2000). Kovacs and colleagues described a weak and diffuse reactivity of the antibody with monomeric aSYN when determined by Western Blot but a much higher binding affinity to aggregates (Kovacs *et al.*, 2012). However, the absence of these aggregates (Lewy body or Lewy neurite pathology) in the mouse brain (Meredith *et al.*, 2008) favored the widespread binding to small oligomers, which are enriched in synapses and somata due to the

artificial overexpression of human aSYN. This possibly explains the diffuse staining pattern seen in histology with a strong background signal in various structures of the brain.

Intense aSYN expression was observed in the cortical layer V as well as layer II/III. Here, the small and large pyramidal neurons originate which innervate for example the basal ganglia. In the hippocampus, the CA1 and CA3 region were stained most intensively by the anti-aSYN antibody whereas the CA2 region lacked reactivity. Interestingly, both stained regions are pyramidal cell fields, innervated by the entorhinal cortex and highly involved in learning and memory. Both brain structures are highly important in the pathology of PD, as they are involved in movement and cognition (Witter *et al.*, 2014). The finding that, contrary to the human situation, the SNpc is not involved in the pathology of the transgenic mouse models challenged the current view. A model that does not display one of the most prominent hallmarks of PD, the SNpc pathology, has to be regarded with caution.

Additionally, there are other promoters with different features that are widely used to mimic PD in animal models. For example, the tyrosine hydroxylase promoter is restricted to catecholaminergic neurons and leads to a nigrostriatal pathology. However, different studies revealed that either at least double mutated or truncated aSYN is essential to induce damage (Thiruchelvam *et al.*, 2004; Tofaris *et al.*, 2006). Additionally, neuronal loss occurs early in these mice but does not progress properly and do not include other brain structures. A broad expression in neurons of different structures such as neocortex, limbic system and olfactory regions is enabled by the PDGF-beta (platelet-derived growth factor) promoter (Chesselet, 2008). aSYN expression in glial cells triggered a pathology similar to features of multiple system atrophy rather than PD (Rockenstein *et al.*, 2002). Masliah *et al.* found that these mice develop motor deficits by the age of 12 month, display dopaminergic cell loss and build up inclusion bodies (Masliah *et al.*, 2000). Nonetheless, the expression of aSYN under the Thy1 promoter is several folds higher than under the PDGF promoter (Rockenstein *et al.*, 2002).

The neuronal expression of aSYN in the brain of tg-aSYN mice was fully developed as early as from 50 d of age and was histologically indistinguishable from of the expression at 300 d. The postnatal expression of aSYN under the Thy1 promoter increases exponentially in the first weeks of age (Moechars *et al.*, 1999). At the age of 50 d, fewer aSYN positive and degenerated neurons in the enlarged cortex sections were found than at the age of 300 d, suggesting a less progressed pathology. Relative quantification of the cortical neuronal area revealed significant differences between tg-aSYN mice and C57BL/6J control mice. Despite the missing LB pathology, tg-aSYN mice had an about 35 % reduced neuronal area in the cortex compared to control mice.

A possible explanation for this phenomenon is the probably ongoing removal of aSYN from the brain, which leads to an equilibrium between production and removal and thus, to the observed steady state of aSYN burden (in form of oligomers) in the brain of young and old tg-aSYN mice. However, the prominent neuronal cell loss indicates that small monomers and oligomeric forms

of aSYN are more toxic than the aggregated form (Lewy bodies in human brains). These findings confirm the role of aSYN in the pathology of PD. Although it is possible to correlate the number of LBs in a certain structure (e.g. SNpc) with the severity of local pathology in PD patients (Braak *et al.*, 2003), dying neurons do not necessarily contain LBs and especially dopaminergic neurons containing LBs do not undergo apoptosis to a greater extent than other cells (Schulz-Schaeffer, 2010). In conclusion, the overall disease progress does not correlate well with the formation of LBs and thus, they might be only an epiphenomenon to other still unknown mechanisms (Bellucci *et al.*, 2012). Interestingly, it was found that aSYN is able to spread like prions in an infective way and it was demonstrated that extracellular aSYN oligomers can introduce intracellular aSYN aggregation (Kovacs *et al.*, 2014; Danzer *et al.*, 2009). The previously described “dying back” hypothesis further supports these observations. aSYN, located mainly in presynaptic terminals, leads to synaptic dysfunction by oligomerization, when the normal binding of aSYN to synaptic vesicles as part of the SNARE-complex is disturbed (Burre *et al.*, 2010). Recently, Burré *et al.* showed that the ‘A30P’ mutation is unique among the aSYN point mutations in impairing SNARE-complex formation (Burre *et al.*, 2012). As a consequence the disturbed synaptic maintenance leads to disrupted neuronal activity culminating in its death. This phenomenon was already observed in DLB with the notion that 90 % of all aSYN aggregates were found in the presynapses (Schulz-Schaeffer, 2010). Thus, the question arises whether LBs are, in fact, not the crucial part of PD pathology, which would also explain the PD phenotype in mice without LB formation. Once more, these findings support the concept that monomeric and small oligomeric aSYN are the toxic species in PD and DLB.

Two behavioral tests, the rotarod and the pole test, were performed in order to assess possible motor alterations in tg-aSYN mice, similar to the progressive motor disease PD. Previous descriptions of age-dependent movement abnormalities in homozygous tg-aSYN mice included an unsteady gait, a weakening in the limbs and an abnormal tail posture within the first year of life (Neumann *et al.*, 2002). The in the present work used heterozygous mice displayed motor abnormalities starting at 300 d of age and interestingly a large proportion of old mice additionally featured severe eye defects in form of blindness in one eye (Gröger, 2012, Master thesis). Before reaching old age, their physiological appearance did not differ except for a tendency to lower weight in the first few months as determined in this work. Furthermore, Freichel and colleagues found old tg-aSYN mice to perform significantly worse in fear conditioning and active avoidance test, both requiring the involvement of amygdala and hippocampus. They also described a worsening in the rotarod performance but starting not earlier than 12 month of age (Freichel *et al.*, 2007). A preliminary study previously performed in our lab revealed no significant differences in the rotarod performance until 450 days of age, but with a rapid decline after reaching this old age. A difference between young and old tg-aSYN

mice was visible from 300 d of age, similar to findings made by Freichel et al. (Gröger, 2012, Master thesis; Freichel *et al.*, 2007).

In this study, the main interest lay on earlier time points in order to make out early differences and rotarod was performed starting at 9 weeks of age and was finished by the age of 41 weeks. No differences were found between tg-aSYN and control mice concerning the time mice were able to stay on the rotating rod and for the time they firstly accomplished a passive rotation, without actively walking on the rod. An exceptional slipping of the rod as described by Tabuse et al. did not occur (Tabuse *et al.*, 2010). These results confirmed the above mentioned findings made by Freichel and colleagues. Interestingly, statistical analyzes of the performances revealed a positive increase of performance with advancing age in both parameters. Mid-age tg-aSYN mice were found to tend to hyperactivity and concomitant with that to show increased swim speed in the morris water maze test (Freichel *et al.*, 2007), that phenomenon might explain the missing differences in motor performance tests and underline the results described in the present work.

A second test, the pole test, described as suitable for basal-ganglia related movement disorders (Fleming *et al.*, 2004) was performed again from 9 to 41 weeks of age. Although no difference was found concerning the orientation task, unexpectedly the climbing performance was performed significantly worse in case of control mice when compared to tg-aSYN mice, matching the described observations made by Freichel et al. (Freichel *et al.*, 2007).

The rotarod and pole test are methods to examine coordinated motor skills and are widely used to detect nigrostriatal damage and dopaminergic denervation (Fernagut *et al.*, 2003; Matsuura *et al.*, 1997; Fleming *et al.*, 2004). The missing difference between tg-aSYN mice and the C57BL/6J (control) mice is likely founded in the lack of SNpc pathology due to the expression pattern of the Thy1 promoter, described before (Neumann *et al.*, 2002; van der Putten *et al.*, 2000).

In sum, an impairment of motor coordination and performance was found in heterozygous tg-aSYN mice compared to non-transgenic control mice at the age of 9 to 41 weeks. Furthermore it was not possible to determine phenotypical changes regarding tg-aSYN mice in the respect age. With these findings, the present work fits well into already published results regarding the used tg-aSYN mouse model (Freichel *et al.*, 2007). With respect to our question whether this mouse model is suitable to study PD, the answer is ambiguous. While it is not suitable to model PD as motor disease, the robust expression of mutated aSYN throughout the brain allows investigation of dementia (concomitant with PD) and extranigral aspects of the disease as well as degeneration of neurons. It furthermore was found to feature different characteristics of DLB or a pre-manifested form of PD (Schell *et al.*, 2009; Freichel *et al.*, 2007; Meredith *et al.*, 2008) and can be generally denoted as model for α -synucleopathies.

5.2 Beneficial effects of mitochondrial polymorphisms on aSYN pathology in tg-aSYN mice

Mitochondrial dysfunction is one of the major hypotheses described today to be causative for PD. It is widely acknowledged that during age, mutations in the mitochondrial genome (mtDNA) accumulate followed by an excessive production of reactive oxygen species (ROS). A knock-in mouse model with a mutated mtDNA-polymerase A brought first evidence for the assumption of mitochondrial dysfunction being implicated in aging (Larsson, 2010). Here a deficiency in the proof-reading function of the protein was described leading to a decreased lifespan and early onset of age-related phenotypes (Trifunovic *et al.*, 2004). In addition, complex I-deficiency was discovered in the SNpc of PD patients, adding evidence to the hypothesis (Martin, 2012; Schapira, 2006).

For the investigation of mitochondrial influences on the aSYN pathology of tg-aSYN mice, a novel conplastic mouse strain was generated, the tg-aSYN-mtNOD mice. The mitochondrial genome for the novel mouse model was provided by the well-known none-obese diabetic (NOD/LtJ) mouse, a model used for autoimmune diabetes (Leiter, 2001). This model was sequenced previously and distinct differences were found in the mitochondrial genome (Yu *et al.*, 2009). Table 19 resumes the important polymorphisms.

Table 19: Mitochondria gene differences between NOD/LtJ and C57BL/6J mice. (adopted from (Yu *et al.*, 2009))

gene	mtDNA position	C57BL/6J	NOD/LtJ	amino acids
Cox3	9348 bp	G	A	Val > Ile
ND3	9461 bp	C	T	Met > Met
tRNA ^{Arg}	9821 bp	8A repeats	10A repeats	

In the present report, these two tg-aSYN mouse strains with mitochondrial genome differences expressing human aSYN with 'A30P' mutation were analyzed regarding aSYN load, immune response, neuron integrity, and behavioral changes with the focus on differences due to the mitochondrial polymorphisms.

Starting with the immunohistochemical analyzes of tg-aSYN-mtNOD mice, only small differences were found compared to tg-aSYN mice. However, the differences were not as distinct as to make definite statements. It obviously can be ruled out that the mtNOD genome has influence on the production of aSYN under the Thy1 promoter. To be sure, ELISA was performed. Differences were only found examining aggregated/ fibrillar forms, as here an increase in 300 d old tg-aSYN-mtNOD mice was visible compared to tg-aSYN mice. These findings emphasize the supposition of the higher molecular forms of aSYN to be less toxic than the smaller soluble monomeric moieties, and the aggregation to be a mechanism protecting neurons from further damage, as already described above (5.1). These observations fit into this theory and also get

well along with proposals made by several other research groups in the context of different neurodegenerative diseases (Zhang *et al.*, 2014; Conway *et al.*, 2000; Assayag *et al.*, 2007). Recently, Zhang and colleagues found a transgenic AD-mouse model to show AD progression without the development of a single plaque but with A β oligomer accumulation in the neurons (Zhang *et al.*, 2014). This notion in the context of AD was already described before (Walsh *et al.*, 2007); similarly, in PD research Conway *et al.* suggested that the aSYN oligomer formation is critical for pathogenesis rather than fibrillization (Conway *et al.*, 2000). Additional evidence is brought by the findings of *post mortem* brains of non-PD cases containing LBs (Gibb *et al.*, 1988). However, the aggregation as mechanism of protection to neurons seemed to be enhanced in tg-aSYN-mtNOD mice. Still, possible reasons are unknown.

Concomitant with these findings, the neuronal integrity in old age was highly disturbed in transgenic mice and also in old control mice as compared to young ones, indicating that the degeneration process is part of the normal aging. For tg-aSYN mice these observations were already described in 5.1. Intriguingly, determining the proportion of neuronal area in the cortex of tg-aSYN-mtNOD mice revealed that the neuronal integrity is completely rescued in 300 d old mice when compared to tg-aSYN mice. One possible explanation is that an impairment of the aSYN functionality as modulator of synaptic activity is missing due to the absence of the pathological aggregation behavior of aSYN leading to less dying neurons.

It was furthermore possible to detect a significantly increased immune response by microglia in 300 d old tg-aSYN-mtNOD mice when compared to control mice. An increased microglial response is one of the histological characteristics of PD in humans and known to correlate with aSYN burden in the brain (Russo *et al.*, 2014). Microglia are immune cells of the central nervous system, capable of phagocytosis and the secretion of proinflammatory cytokines. Their contribution to disease development is discussed controversially (McGeer *et al.*, 2008). It was described that microglia undergo a phenotypical change when activated chronically. Additionally, they change their secretion of proteins, which they use to increase adhesion and migration, phagocytosis and to stimulate neighboring cells (Olah *et al.*, 2011). Chronic inflammation is a pathological hallmark of different neurodegenerative diseases and increased microglia activity might be detrimental for neurons due to a chronic expression of neurotoxic factors. Chronic microglial activation leads to enhanced A β production in AD (Rojo *et al.*, 2008; Azizi *et al.*, 2012). The SNpc was found to host particularly high amounts of microglia (Lawson *et al.*, 1990). Notably, aSYN has a regulatory influence on the phenotypic alterations of microglia, as an increased reactive phenotype was found in aSYN knock-out mice compared to control. Furthermore, these microglia secreted elevated level of proinflammatory cytokines TNF α and IL-6, and displayed an impaired ability for phagocytosis compared to microglia from non-transgenic control mice (Austin *et al.*, 2006). A preferred theory today is that microglia have a variety of different activation states and corresponding phenotypes (Gordon, 2003). The

microglia found in the brains of aSYN knock-out mice revealed a ramified, vacuolar morphology (Austin *et al.*, 2006). The activation state of the microglia in this work is unknown. However, as neuronal integrity was completely intact in old tg-aSYN-mtNOD mice, the found increased microglial response in old tg-aSYN-mtNOD mice is in contrast with the discussed detrimental effect of microglial activity. These findings support the controversially debated hypothesis of a neuroprotective effect emanating from microglia (Hellwig *et al.*, 2013). An enhanced microglial presence was also found by Scheffler *et al.* in the vicinity of A β plaques in an mtNOD-mouse model of AD accompanied by a decreased level of cerebral A β load and higher uptake levels in microglia when compared to C57BL/6J controls. Moreover, a higher ATP level was described for the respective mouse model, which is according to the authors the reason for the increased microglial activity and important for the brain homeostasis (Scheffler *et al.*, 2012).

To verify that the described changes found in tg-aSYN-mtNOD mice were not only histological phenomena but had indeed a beneficial impact on motor skills, behavioral tests were performed and evaluated as described before. The rotarod test proved a great advantage of the tg-aSYN-mtNOD in mid-age time points (25-33 weeks) elicited by their mitochondrial polymorphisms and confirmed thereby formerly described results. The on the one hand strong difference between tg-aSYN and tg-aSYN-mtNOD mice in the rotarod performance but missing variance in the climb performance of the pole test could be explained by the less phenotypic alteration in the transgenic mice. The very sensitive pole test (Fernagut *et al.*, 2003) was most likely not suitable for extranigral aspect determination and stronger incentives for the mice were needed for future analyses. However, the ability of spatial orientation, a non-motor task, as part of the pole test was disturbed in old tg-aSYN and control mice and increased in tg-aSYN-mtNOD mice. Thus, a strong positive effect on the motor performance and spatial orientation task was found in tg-aSYN-mtNOD mice, confirming the results of the rotarod test.

In conclusion, the newly created tg-aSYN-mtNOD mice was found to feature great benefits with respect to neuronal integrity, microglial response, motor performance and spatial orientation compared to tg-aSYN mice without mitochondrial polymorphisms, especially in old age. These results add new evidence to the hypothesis that mitochondria have a great impact on the pathophysiological coherences in the PD brain.

5.3 Respirometric measurements revealed mtDNA specific differences in oxygen consumption of isolated brain mitochondria

In order to find an explanation for the beneficial effects found in tg-aSYN-mtNOD mice compared to tg-aSYN mice, the function was investigated in isolated brain mitochondria and evaluated by means of high-resolution respirometry with substrate inhibitor titrations (Kuznetsov *et al.*, 2008; Kupsch *et al.*, 2014). A set of four protocols (Trumbeckaite *et al.*, 2001; Gellerich *et al.*, 2002; Gellerich *et al.*, 2008; Gellerich *et al.*, 2012; Krebiehl *et al.*, 2010) allowed obtaining a

maximum of information based on the determination of the maximal substrate specific state 3-respiration, also upon Ca^{2+} stimulation, maximal rates limited by the capacity of the respiratory chain complexes, respiratory control ratios and non-phosphorylating states of respiration (state 4).

Starting with the evaluation of complex I-dependent respiration rates, a difference was solely found in state 3-respiration in young mtNOD mice when α -ketoglutarate/malate as starting substrate was used and only after maximal stimulation with Ca^{2+} . The ability of intramitochondrial Ca^{2+} to regulate oxidative phosphorylation via the activation of the pyruvate-, isocitrate- and α -ketoglutarat dehydrogenase leading to pyruvate formation through the tricarboxylic acid cycle, is known and widely accepted knowledge (McCormack *et al.*, 1979; McCormack *et al.*, 1993). However, this was considered not sufficient to explain increased oxidative phosphorylation by Ca^{2+} *in vivo* since these mechanisms only enhance the oxidation of the substrates (Gellerich *et al.*, 2010). Recently, it was described that extramitochondrial/cytosolic Ca^{2+} increases the activity of aralar (mitochondrial aspartate/glutamate carrier, AGC) as part of the malate/aspartate shuttle (MAS) leading to increased regeneration of NAD^+ to $\text{NADH}+\text{H}^+$ and an increased substrate transport into the mitochondria. The required Ca^{2+} concentration is small and do not lead to Ca^{2+} uptake into the mitochondria (Pardo *et al.*, 2006). Recently, Gellerich *et al.* described that extramitochondrial/cytosolic Ca^{2+} increases state 3-respiration most when glutamate/malate is provided as substrate, followed by α -ketoglutarate/malate while the presence of pyruvate/malate only display low stimulatory effect upon Ca^{2+} supply. Together, both mechanisms, intramitochondrial dehydrogenases and MAS activation, are believed to lead to an increase in substrate supply into the mitochondria and an enhanced formation of pyruvate (Gellerich *et al.*, 2012). The addition of pyruvate after Ca^{2+} stimulation led to a further increase in respiration in the present work (Figure 20A), explainable by the up-regulating effect of cytosolic Ca^{2+} on pyruvate formation rather than an influence on the capacity to oxidize pyruvate. Gellerich *et al.* furthermore describe that the increased state 3-respiration in the presence of α -ketoglutarate/malate depend on the activation of intramitochondrial α -ketoglutarate dehydrogenase and not on the activation of MAS. However, due to inconsistent findings upon inhibition of Ca^{2+} uptake into the mitochondria, further investigation is required. They conclude that Ca^{2+} controlled activation is realized by aralar using extramitochondrial/cytosolic Ca^{2+} and the intramitochondrial dehydrogenases utilizing intramitochondrial Ca^{2+} . Nonetheless, high extramitochondrial/ cytosolic Ca^{2+} concentration led to an intake of Ca^{2+} into the mitochondria and was found to activate intramitochondrial dehydrogenases (Gellerich *et al.*, 2012).

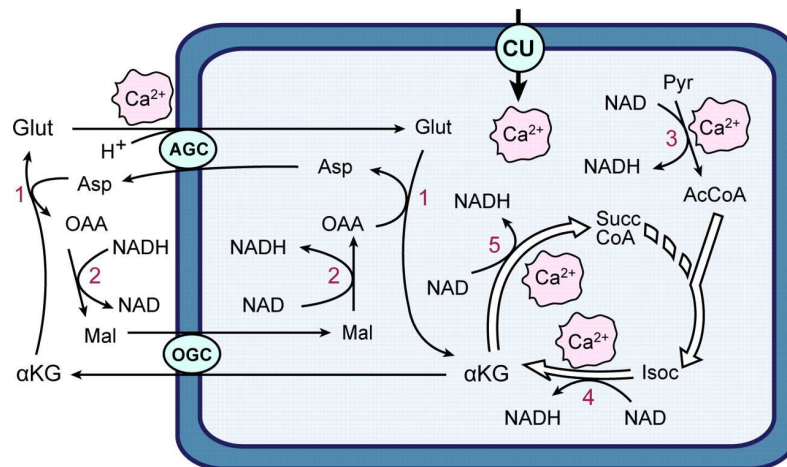


Figure 34: Cytosolic Ca^{2+} -regulation of Malate-aspartate NADH shuttle (MAS) and intramitochondrial Ca^{2+} stimulation of dehydrogenases control mitochondrial pyruvate supply (Satrustegui *et al.*, 2007).

MAS consists of four enzymes: (1) mitochondrial and cytosolic aspartate aminotransferase (AAT), (2) malate dehydrogenases, the α -ketoglutarate/malate carrier (OGC) and the aspartate/glutamate carrier (aralar, AGC), which is activated by cytosolic Ca^{2+} . Ca^{2+} transported into the mitochondria via the Ca^{2+} uniporter (CU) activates (3) pyruvate dehydrogenase, (4) isocitrate dehydrogenase (IDH) and (5) α -ketoglutarate dehydrogenase (α -KGDH). AcCoA, acetyl CoA; Asp, aspartate; Glut, glutamate; Isoc, isocitrate; α -KG, α -ketoglutarate; Mal, malate; OAA, oxalacetic acid; Pyr, pyruvate; SuccCoA, succinyl CoA (Satrustegui *et al.*, 2007).

In the present work, an additional supply of Ca^{2+} led to a greater increase in state 3-respiration measured with glutamate/malate as compared to α -ketoglutarate/malate, confirming the hypothesis described by Gellerich *et al.* (2012). The observed difference between young C57BL/6J and mtNOD mice might thus depend on alterations in the activation of the α -ketoglutarate dehydrogenase activity by intramitochondrial Ca^{2+} but other coherences might play an important role and should be further investigated.

It was possible to find the greatest differences in complex II-dependent parameter of mitochondrial function. The succinate-dependent state 3-respiration was diminished about 20 % in 200 d old C57BL/6J (Control) mice compared to mtNOD mice of the same age. As a consequence the complex I/complex II-ratio was also increased by 15 % in old Control mice. These differences were obtained by using glutamate/malate as starting substrate, α -ketoglutarate/malate did not led to differences unless further stimulation by glycerol-3-phosphate and was generally smaller compared to glutamate/malate. Furthermore, the non-phosphorylating respiration (state 4) revealed also significantly lower complex II-dependent respiration rates in brain mitochondria from 200 d old C57BL/6J mice compared to mtNOD mice. In contrast, complex I-limited rates of state 4-respiration were not changed (4.3.6, Figure 27). The basal oxygen consumption without or with low ADP (state 4), leading to a high ADP/ATP ratio, indicates, if increased, a proton leak across the membrane probably induced in isolation procedure (Horton *et al.*, 1981). Even if the state 4-respiration of 200 d old mtNOD seems increased in contrast to 200 d old C57BL/6J mice, it is more likely a

diminished state 4-respiration in case of C57BL/6J mice versus 100 d ones while the 200 d old mtNOD mice display unchanged state 4-respiration rates.

The, from the respective state 3 and state 4 calculated, respiratory control ratio (RCR) confirmed the findings. The complex I-dependent RCR displayed no differences while complex II-dependent RCR was increased in 200 d old C57BL/6J mice compared to 100 d old ones. The RCR is a dimension for coupling of ETC and oxidative phosphorylation and quantifies a possible leak in the inner mitochondrial membrane (Horton *et al.*, 1981). Here, the increased RCR in case of complex II-dependent respiration for 200 d old C57BL/6J mice is caused by the simultaneously diminished state 4-respiration. Membrane integrity is intact as proofed by the unchanged RCR for complex I-dependent respiration.

Explanation for these repeated findings of diminished succinate respiration in C57BL/6J mice might be a metabolic condition. The activity of succinate dehydrogenase (SDH) is known to depend on the concentration of oxaloacetate and malate, both inhibitors of SDH. The mitochondrial aspartate amino-transaminase (ASAT) catalyzes the reaction of glutamate and oxaloacetate to α -ketoglutarate and aspartate; either decreasing the oxaloacetate concentration if reacting with glutamate or *vice versa* if reacting with α -ketoglutarate (Panov *et al.*, 2009). However, this explains the finding of a lower succinate respiration measured with α -ketoglutarate compared to glutamate (4.3.2, Figure 21). The presence of α -ketoglutarate leads to an increasing oxaloacetate concentration partially inhibiting the SDH, while using glutamate as substrate leads to lowest oxaloacetate concentration not inhibiting the SDH. But the finding of reduced succinate respiration rate upon glutamate in old C57BL/6J mice cannot be explained by this principle (4.3.2, Figure 21), as it cannot be caused by an increased oxaloacetate concentration. Thus, a diminished activity of SDH or the electron-transferring flavoprotein-ubichinone oxidoreductase (ETF), possibly caused by increased oxidative stress could be a possible reason.

Although succinate is not an important substrate for feeding the brain's mitochondria, complex II is a crucial enzyme for mitochondrial respiration and has a pivotal role in the citrate cycle by limiting the supply of reducing equivalents to the respiratory chain. This complex differs from the others as it comprises of four subunits and its genes are all nuclear-encoded (Quinlan *et al.*, 2012). Mitochondrial diseases which are associated with deficiency in complex II lead to severe neurological phenotypes, such as encephalopathy, mostly together with a very short life span. These rare deficiencies in SDH were described by Alston *et al.* to lead to motor manifestations in two children with novel variants in *SDH* genes and probably to altered binding and procession of electrons in the respiratory chain (Alston *et al.*, 2012). A connection between SDH defects and tumorigenesis, i.e. angiogenesis, was also made before when succinate, among other citrate cycle intermediates, was found to influence the availability of hypoxia-inducible transcriptions factors (HIFs) and act as tumour suppressor (Koivunen *et al.*, 2007). The HIFs

play also an important role in other physiological and pathological issues, for example in cell proliferation, apoptosis and glucose utilization (Koivunen *et al.*, 2007). A decrease in complex II-dependent respiration as found in old C57BL/6J mice might not lead to the severe phenotypic alterations as described in patients with *SDH* gene mutations, but a noxious impact on metabolism is likely to occur with increasing age. However, this unknown metabolical impact emerging with ongoing age and triggered by a decreased complex II-dependent respiration, either affecting SDH or ETF, is apparently bypassed in mice with NOD polymorphisms.

After missing differences in complex III-dependent respiration, complex IV-dependent respiration revealed interesting results. While the respiration rate in both mouse strains, C57BL/6J and mtNOD mice, drops in the same extend with advancing age when measured with glutamate/malate as starting substrate, is this drop greater in mtNOD mice upon measurement with malate/ α -ketoglutarate. This finding depends on the increased respiration rate in 100 d old mtNOD mice, which cannot be found when measured with glutamate/malate. A decreased complex IV activity was described before for mtNOD mice depending on the polymorphism in *Cox3* (5.2, Table 19) (Scheffler *et al.*, 2012). However, a significant difference between C57BL/6J and mtNOD mice is missing. Furthermore, COX activity does not reach limit when supplied with saturating ADP and substrate but can be further stimulated to a maximum, also referred to as 'excess capacity' of COX (Gnaiger *et al.*, 1998). Thus, changes in complex IV-activity do not lead to effects on electron flux through the respiratory chain probably providing a safe range in case of mtDNA mutations as was found in different tissues and species (Letellier *et al.*, 1994; Gnaiger *et al.*, 1998). The minor results of the complex IV-dependent respiration in the present work have therefore certainly no impact on energy metabolism of brain mitochondria. Additionally, Gnaiger *et al.* proposed an economic ideal behind the excess capacity of COX by up-regulating the oxygen affinity, ensuring a "thermodynamic and kinetic optimum" upon maximal flux through the respiratory chain (Gnaiger *et al.*, 1998). The excess capacity was calculated as quotient of the complex IV-dependent respiration and the maximal ETC capacity upon uncoupling with FCCP. FCCP destroys the proton gradient across the inner membrane by forming a pore and serving as proton carrier integrated into the inner mitochondrial membrane. As a consequence, electron flux becomes maximally increased trying to compensate for the leak and to ensure maintenance of a proton gradient. The control of the ATP-synthase has no longer influence on the flux (Pesta *et al.*, 2012). The maximal ETC capacity after FCCP addition revealed no differences between age and strain. The, normalized to these results calculated, COX excess capacity revealed no differences, too and ranged between 1-1.3-fold (Figure 25). Thus, the mtNOD polymorphisms had no effect on maximal electron flux through the respiratory chain and did not change the activity of complex IV and the corresponding excess capacity.

Taken together, the in the present work examined mitochondrial polymorphisms reveal most vigorous differences in the respiration capacity of complex II of the respiratory chain.

It would be of utmost interest to perform respirometry also with transgenic mice to determine the additional influence of the overexpressed aSYN on the oxygen consumption of various complexes. The in the present work by respirometry achieved results are limited in the outright transferability on the findings made with the transgenic aSYN-mice. Nonetheless, it is possible to see connections between the described improved results in tg-aSYN-mtNOD mice compared to tg-aSYN mice and the found enhanced complex II-dependent respiration in the mtNOD background strain.

Thinkable is that the enhanced complex II-activity might compensate for the complex I-deficiency associated with PD leading to an equation in energy metabolism in tg-aSYN-mtNOD mice, which would explain the found improvements in neuron integrity, motor performance and spatial orientation. Evidence for this assumption was found in mice with MPTP induced parkinsonism, as it was shown that the complex I deficiency was bypassed by a complex II-dependend mechanism induced by an infusion of the ketone body d-beta-hydroxybutyrate, leading to improved mitochondrial respiration and ATP production (Tieu *et al.*, 2003).

An enhanced complex II-activity could also result in diminished ROS production, as it was shown that complex II can generate ROS in rates which exceed those of complex I and III, under certain circumstances (Quinlan *et al.*, 2012). Recently it was described that complex II also influences the ROS production in human skin mitochondria and that aging leads to a decreased enzyme activity (Anderson *et al.*, 2014).

Scheffler *et al.* found transgenic AD mice with mtNOD polymorphisms to have a significantly greater cellular ATP level and microglia activity concomitant with decreased A β burden in the brain (Scheffler *et al.*, 2012). ATP-dependent mechanisms that support the cell in the clearance of toxic peptides such as UPS might be increasingly activated in this mouse model. Consequences of a dysfunctional UPS were shown in parkin knock-out mice, resulting in a loss of function in dopaminergic neurons and in a decrease in mitochondrial respiration leading to a further decreased ATP level (Martin, 2012). Additionally, the insulin-degrading enzyme and neprilysin, proteases, are affected by inconsistent ATP level. Their contribution to PD, however, lacks still confirmation (Song *et al.*, 2004). An important mechanism for peptide removal is furthermore the active transport across the BBB by ABC transporters, as these are highly energy-dependent. This interesting phenomenon cannot be explained in fully detail today but unquestionable these results confirm the importance of the mitochondria-neurodegeneration network.

5.4 ABCC1 activity is not crucial for aSYN transport in the brain of tg-aSYN mice

The BBB (blood brain barrier) and the BCB (blood cerebrospinal fluid barrier) are important for the protection of the brain against harmful and toxic compounds from the blood. Exchange

across these barriers is tightly regulated. The active bi-directional transport is carried out by specific transport molecules located within the endothelial cell layer. Together with the surrounding pericytes and astrocytes' endfeet, these endothelial cells form the BBB. In contrast to the BCB, the BBB provides a specialized diffusion barrier build by tight junctions ensuring a certain homeostasis in the brain (Pahnke *et al.*, 2009; Zlokovic, 2008; Loscher *et al.*, 2005).

ABC transporters represent a large family of transport molecules present at the BBB, which recently gained great interest for their involvement in neurodegeneration. The ABC transporter ABCB1 (P-gp, P-glycoprotein 1; MDR1, multidrug resistance protein 1) was already intensively investigated for its implication in PD. Its activity was diminished in brain regions that are prominent in disease development, for example frontal regions with frontostriatal neuronal projections (Bartels *et al.*, 2009; Bartels *et al.*, 2008b; Kortekaas *et al.*, 2005). The role of another important ABC transporter ABCC1 (MRP, multidrug resistance-associated protein 1; refer to Figure 35 for topology) has only been studied in the context of AD. Previous investigations revealed that decreased ABCC1 activity in ABCC1 knock-out AD mice lead to an increased A β accumulation compared to controls (Krohn *et al.*, 2011). On the other hand, pharmacologically enhanced ABCC1 activity was found to reduce AD pathology by decreasing the A β burden in an AD mouse model (Krohn *et al.*, 2011; Hofrichter *et al.*, 2013). These results motivated the study of ABCC1 knock-out and activation on aSYN related pathology in the brain of tg-aSYN mice, in the present work.

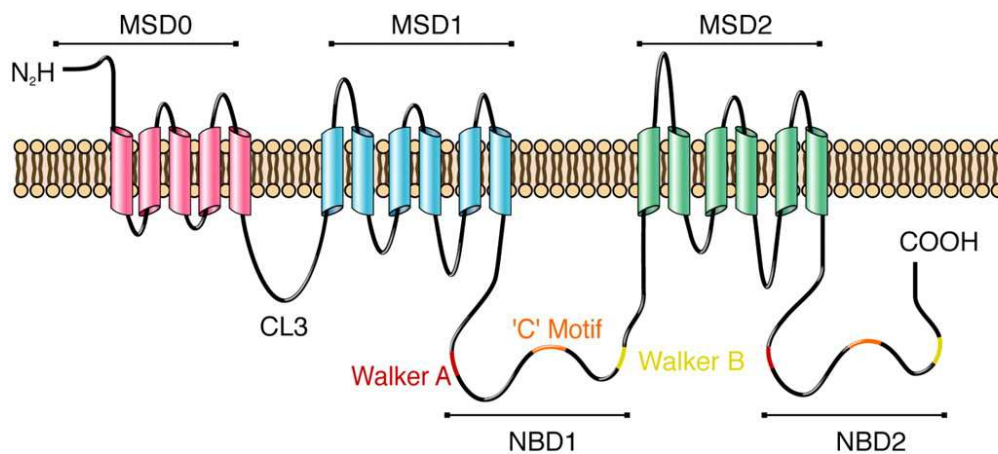


Figure 35: ABCC1 topology.

The topology of ABCC1 is characterized by three membrane spanning domains (MSD) containing of ranging numbers but typically six transmembrane helices, and two nucleotide binding domains (NBD). The N-terminus is located extracellular, while the C-terminus lies intracellular (adapted from (Deeley *et al.*, 2006)).

Starting from the premise that ABCC1 excretes aSYN across the BBB in an ATP-dependent manner, a decreased ATP availability and thus, a diminished ABCC1 activity causes an increase of intracellular aSYN.

According to the study of Krohn *et al.* (2011), mice at an age of 100 d were chosen. Histological analyzes revealed no differences upon ABCC1 knock-out. Surprisingly, the effect of ABCC1

knock-out on neuronal integrity and microglial immune response could be neglected. Even the level of monomeric, oligomeric and fibrillar aSYN in the brain of tg-aSYN and tg-aSYN-ABCC1^{-/-} mice was not altered by ABCC1 knock-out at 100 d of age. The validation of an effect upon ABCC1 activation on the pathology was performed by pharmacologically activation using thiethylperazine (Torecan®, Novartis). Thiethylperazine, a derivate of phenothiazine belonging to the class of neuroleptics is widely used as antiemetic. Phenothiazines are known to interact with both, ABCB1 and ABCC1 differentially. While the drug enhances the activity of ABCC1 vastly, as was shown in human erythrocyte culture, ABCB1 activity decreases upon treatment (Wesolowska *et al.*, 2005; Wesolowska, 2011).

In the present work, no difference was found between treated tg-aSYN and tg-aSYN-ABCC1^{-/-} (control) mice with respect to neuronal integrity, microglial response and aSYN concentration. Thus, a missing transport of aSYN via ABCC1 can be concluded. Additionally, also a missing transport by ABCB1 can be stated as the decreased ABCB1 activity as well had no influence on any of these parameters. These findings are consistent with the report of Sui and coworkers who found that ABCB1 is not involved in the transport of aSYN and furthermore showed a bi-directional transport of aSYN across the BBB via LRP-1 (Low density lipoprotein receptor-related protein 1)(Sui *et al.*, 2014).

Possible reason for the differences between aSYN and A β concerning the transport across the BBB by ABC transporters are most likely the structural differences between the peptides. While A β has only an atomic mass of 4 kDa and forms β -sheet structure, aSYN is substantially heavier (14 kDa) and natively unfolded (Bartels *et al.*, 2011).

One very interesting effect observed in the present study was the increase of the neuronal area in water- and thiethylperazine-treated mice compared to untreated mice, which was independent of ABCC1 knock-out. It was furthermore detected that also the aSYN level in the carbonate-soluble fraction that includes monomeric and small oligomeric aSYN, increases upon treatment with thiethylperazine and water, respectively. This effect could possibly be triggered by stress and anxiety due to handling of the mice (Lapin, 1995)

5.5 Conclusion

Taken together, the results of the present work contribute to the understanding of mitochondrial deficiency in PD. Even if the tg-aSYN mice with the 'A30P' mutation display mainly extranigral aspects of PD and should rather be denoted as general model for synucleopathies, the expression of human aSYN in the brain was robust.

The increased complex II activity due to the polymorphisms in the mtDNA of NOD/J mice was found to bypass the diminished respiration in the diseased mouse brain, leading to improved neuronal and behavioral physiology in the novel tg-aSYN-mtNOD mouse model.

A proposed increased ATP production causing an enhancement of various energy-dependent clearance mechanisms of the brain led to the follow-up study of an aSYN transport by the specific ABC transporter ABCC1. The hypothesized transport of aSYN by ABCC1, verified by a study determining the effect of a knock-out and the pharmacologically activation of ABCC1 on the pathology of tg-aSYN mice, was not confirmed.

In sum, the work acknowledges beneficial and protective effects of specific mitochondrial polymorphisms in α -synucleinopathies that should be further investigated and utilized for future pharmaceutical applications.

References

- 2008 Alzheimer's disease facts and figures. *Alzheimers Dement*, 4 (2):110-133.
- Abeliovich A, Schmitz Y, Farinas I, Choi-Lundberg D, Ho WH, Castillo PE, Shinsky N, Verdugo JM, Armanini M, Ryan A, Hynes M, Phillips H, Sulzer D, Rosenthal A. 2000. Mice lacking alpha-synuclein display functional deficits in the nigrostriatal dopamine system. *Neuron*, 25 (1):239-252.
- Alberts B. JA, Lewis J., et al. . 2002. *The Mitochondrion* <http://www.ncbi.nlm.nih.gov/books/NBK26894/>: New York: Garland Science.
- Alston CL, Davison JE, Meloni F, van der Westhuizen FH, He L, Hornig-Do HT, Peet AC, Gissen P, Goffrini P, Ferrero I, Wassmer E, McFarland R, Taylor RW. 2012. Recessive germline SDHA and SDHB mutations causing leukodystrophy and isolated mitochondrial complex II deficiency. *J Med Genet*, 49 (9):569-577.
- Anderson A, Bowman A, Boulton SJ, Manning P, Birch-Machin MA. 2014. A role for human mitochondrial complex II in the production of reactive oxygen species in human skin. *Redox Biol*, 2C:1016-1022.
- Andres-Mateos E, Perier C, Zhang L, Blanchard-Fillion B, Greco TM, Thomas B, Ko HS, Sasaki M, Ischiropoulos H, Przedborski S, Dawson TM, Dawson VL. 2007. DJ-1 gene deletion reveals that DJ-1 is an atypical peroxiredoxin-like peroxidase. *Proc Natl Acad Sci U S A*, 104 (37):14807-14812.
- Assayag K, Yakunin E, Loeb V, Selkoe DJ, Sharon R. 2007. Polyunsaturated fatty acids induce alpha-synuclein-related pathogenic changes in neuronal cells. *Am J Pathol*, 171 (6):2000-2011.
- Austin SA, Floden AM, Murphy EJ, Combs CK. 2006. Alpha-synuclein expression modulates microglial activation phenotype. *J Neurosci*, 26 (41):10558-10563.
- Azizi G, Mirshafiey A. 2012. The potential role of proinflammatory and antiinflammatory cytokines in Alzheimer disease pathogenesis. *Immunopharmacol Immunotoxicol*, 34 (6):881-895.
- Balesh DR, Z and Floriano, W. 2011. Unfolded annealing molecular dynamics conformers for wild-type and disease-associated variants of alpha-synuclein show no propensity for beta-sheet formation. *Journal of Biophysical Chemistry*, 2:124-134.
- Baltazar MT, Dinis-Oliveira RJ, de Lourdes Bastos M, Tsatsakis AM, Duarte JA, Carvalho F. 2014. Pesticides exposure as etiological factors of Parkinson's disease and other neurodegenerative diseases--a mechanistic approach. *Toxicol Lett*, 230 (2):85-103.
- Barcelo-Coblijn G, Golovko MY, Weinhofer I, Berger J, Murphy EJ. 2007. Brain neutral lipids mass is increased in alpha-synuclein gene-ablated mice. *J Neurochem*, 101 (1):132-141.
- Bartels AL, van Berckel BN, Lubberink M, Luurtsema G, Lammertsma AA, Leenders KL. 2008a. Blood-brain barrier P-glycoprotein function is not impaired in early Parkinson's disease. *Parkinsonism Relat Disord*, 14 (6):505-508.
- Bartels AL, Kortekaas R, Bart J, Willemsen AT, de Klerk OL, de Vries JJ, van Oostrom JC, Leenders KL. 2009. Blood-brain barrier P-glycoprotein function decreases in specific brain regions with aging: a possible role in progressive neurodegeneration. *Neurobiol Aging*, 30 (11):1818-1824.
- Bartels AL, Willemsen AT, Kortekaas R, de Jong BM, de Vries R, de Klerk O, van Oostrom JC, Portman A, Leenders KL. 2008b. Decreased blood-brain barrier P-glycoprotein function in the progression of Parkinson's disease, PSP and MSA. *J Neural Transm*, 115 (7):1001-1009.
- Bartels T, Choi JG, Selkoe DJ. 2011. alpha-Synuclein occurs physiologically as a helically folded tetramer that resists aggregation. *Nature*, 477 (7362):107-110.
- Begley DJ. 2004. ABC transporters and the blood-brain barrier. *Curr Pharm Des*, 10 (12):1295-1312.

- Bellucci A, Navarria L, Zaltieri M, Missale C, Spano P. 2012. alpha-Synuclein synaptic pathology and its implications in the development of novel therapeutic approaches to cure Parkinson's disease. *Brain Res*, 1432:95-113.
- Benabid AL, Chabardes S, Mitrofanis J, Pollak P. 2009. Deep brain stimulation of the subthalamic nucleus for the treatment of Parkinson's disease. *Lancet Neurol*, 8 (1):67-81.
- Bernheimer H, Birkmayer W, Hornykiewicz O, Jellinger K, Seitelberger F. 1973. Brain dopamine and the syndromes of Parkinson and Huntington. Clinical, morphological and neurochemical correlations. *J Neurol Sci*, 20 (4):415-455.
- Bertram L, Tanzi RE. 2005. The genetic epidemiology of neurodegenerative disease. *J Clin Invest*, 115 (6):1449-1457.
- Betarbet R, Sherer TB, MacKenzie G, Garcia-Osuna M, Panov AV, Greenamyre JT. 2000. Chronic systemic pesticide exposure reproduces features of Parkinson's disease. *Nat Neurosci*, 3 (12):1301-1306.
- Beyer K, Domingo-Sabat M, Ariza A. 2009. Molecular pathology of Lewy body diseases. *Int J Mol Sci*, 10 (3):724-745.
- Bisaglia M, Trolia A, Bellanda M, Bergantino E, Bubacco L, Mammi S. 2006. Structure and topology of the non-amyloid-beta component fragment of human alpha-synuclein bound to micelles: implications for the aggregation process. *Protein Sci*, 15 (6):1408-1416.
- Bjorklund T, Cederfjall EA, Kirik D. 2010. Gene therapy for dopamine replacement. *Prog Brain Res*, 184:221-235.
- Blachly-Dyson E, Zambronicz EB, Yu WH, Adams V, McCabe ER, Adelman J, Colombini M, Forte M. 1993. Cloning and functional expression in yeast of two human isoforms of the outer mitochondrial membrane channel, the voltage-dependent anion channel. *J Biol Chem*, 268 (3):1835-1841.
- Blandini F, Nappi G, Tassorelli C, Martignoni E. 2000. Functional changes of the basal ganglia circuitry in Parkinson's disease. *Prog Neurobiol*, 62 (1):63-88.
- Bleasel JM, Hsiao JH, Halliday GM, Kim WS. 2013. Increased expression of ABCA8 in multiple system atrophy brain is associated with changes in pathogenic proteins. *J Parkinsons Dis*, 3 (3):331-339.
- Bohnert M, Wenz LS, Zerbes RM, Horvath SE, Stroud DA, von der Malsburg K, Muller JM, Oeljeklaus S, Perschil I, Warscheid B, Chacinska A, Veenhuis M, van der Klei IJ, Daum G, Wiedemann N, Becker T, Pfanner N, van der Laan M. 2012. Role of mitochondrial inner membrane organizing system in protein biogenesis of the mitochondrial outer membrane. *Mol Biol Cell*, 23 (20):3948-3956.
- Bonda DJ, Wang X, Perry G, Smith MA, Zhu X. 2010. Mitochondrial dynamics in Alzheimer's disease: opportunities for future treatment strategies. *Drugs Aging*, 27 (3):181-192.
- Bonifati V. 2014. Genetics of Parkinson's disease--state of the art, 2013. *Parkinsonism Relat Disord*, 20 Suppl 1:S23-28.
- Borghi R, Marchese R, Negro A, Marinelli L, Forloni G, Zaccheo D, Abbruzzese G, Tabaton M. 2000. Full length alpha-synuclein is present in cerebrospinal fluid from Parkinson's disease and normal subjects. *Neurosci Lett*, 287 (1):65-67.
- Braak H, Del Tredici K, Rub U, de Vos RA, Jansen Steur EN, Braak E. 2003. Staging of brain pathology related to sporadic Parkinson's disease. *Neurobiol Aging*, 24 (2):197-211.
- Brucale M, Sandal M, Di Maio S, Rampioni A, Tessari I, Tosatto L, Bisaglia M, Bubacco L, Samori B. 2009. Pathogenic mutations shift the equilibria of alpha-synuclein single molecules towards structured conformers. *Chembiochem*, 10 (1):176-183.

- Burns RS, Chiueh CC, Markey SP, Ebert MH, Jacobowitz DM, Kopin IJ. 1983. A primate model of parkinsonism: selective destruction of dopaminergic neurons in the pars compacta of the substantia nigra by N-methyl-4-phenyl-1,2,3,6-tetrahydropyridine. *Proc Natl Acad Sci U S A*, 80 (14):4546-4550.
- Burre J, Sharma M, Sudhof TC. 2012. Systematic mutagenesis of alpha-synuclein reveals distinct sequence requirements for physiological and pathological activities. *J Neurosci*, 32 (43):15227-15242.
- Burre J, Sharma M, Tsetsenis T, Buchman V, Etherton MR, Sudhof TC. 2010. Alpha-synuclein promotes SNARE-complex assembly in vivo and in vitro. *Science*, 329 (5999):1663-1667.
- Burre J, Vivona S, Diao J, Sharma M, Brunger AT, Sudhof TC. 2013. Properties of native brain alpha-synuclein. *Nature*, 498 (7453):E4-6; discussion E6-7.
- Cabin DE, Shimazu K, Murphy D, Cole NB, Gottschalk W, McIlwain KL, Orrison B, Chen A, Ellis CE, Paylor R, Lu B, Nussbaum RL. 2002. Synaptic vesicle depletion correlates with attenuated synaptic responses to prolonged repetitive stimulation in mice lacking alpha-synuclein. *J Neurosci*, 22 (20):8797-8807.
- Cecchini G. 2003. Function and structure of complex II of the respiratory chain. *Annu Rev Biochem*, 72:77-109.
- Chance B, Williams GR. 1955. Respiratory enzymes in oxidative phosphorylation. III. The steady state. *J Biol Chem*, 217 (1):409-427.
- Chandra S, Gallardo G, Fernandez-Chacon R, Schluter OM, Sudhof TC. 2005. Alpha-synuclein cooperates with CSPalpha in preventing neurodegeneration. *Cell*, 123 (3):383-396.
- Chandra S, Fornai F, Kwon HB, Yazdani U, Atasoy D, Liu X, Hammer RE, Battaglia G, German DC, Castillo PE, Sudhof TC. 2004. Double-knockout mice for alpha- and beta-synucleins: effect on synaptic functions. *Proc Natl Acad Sci U S A*, 101 (41):14966-14971.
- Chesselet MF. 2008. In vivo alpha-synuclein overexpression in rodents: a useful model of Parkinson's disease? *Exp Neurol*, 209 (1):22-27.
- Choi W, Zibae S, Jakes R, Serpell LC, Davletov B, Crowther RA, Goedert M. 2004. Mutation E46K increases phospholipid binding and assembly into filaments of human alpha-synuclein. *FEBS Lett*, 576 (3):363-368.
- Cimen MY. 2008. Free radical metabolism in human erythrocytes. *Clin Chim Acta*, 390 (1-2):1-11.
- Cirrito JR, Deane R, Fagan AM, Spinner ML, Parsadanian M, Finn MB, Jiang H, Prior JL, Sagare A, Bales KR, Paul SM, Zlokovic BV, Piwnicka-Worms D, Holtzman DM. 2005. P-glycoprotein deficiency at the blood-brain barrier increases amyloid-beta deposition in an Alzheimer disease mouse model. *J Clin Invest*, 115 (11):3285-3290.
- Clark JB, Nicklas WJ. 1970. The metabolism of rat brain mitochondria. Preparation and characterization. *J Biol Chem*, 245 (18):4724-4731.
- Connor B, Kozlowski DA, Unnerstall JR, Elsworth JD, Tillerson JL, Schallert T, Bohn MC. 2001. Glial cell line-derived neurotrophic factor (GDNF) gene delivery protects dopaminergic terminals from degeneration. *Exp Neurol*, 169 (1):83-95.
- Conway KA, Lee SJ, Rochet JC, Ding TT, Williamson RE, Lansbury PT, Jr. 2000. Acceleration of oligomerization, not fibrillization, is a shared property of both alpha-synuclein mutations linked to early-onset Parkinson's disease: implications for pathogenesis and therapy. *Proc Natl Acad Sci U S A*, 97 (2):571-576.
- Cook C, Stetler C, Petrucelli L. 2012. Disruption of protein quality control in Parkinson's disease. *Cold Spring Harb Perspect Med*, 2 (5):a009423.

- Cotzias GC, Papavasiliou PS, Gellene R. 1969. Modification of Parkinsonism--chronic treatment with L-dopa. *N Engl J Med*, 280 (7):337-345.
- Coune PG, Schneider BL, Aebischer P. 2012. Parkinson's disease: gene therapies. *Cold Spring Harb Perspect Med*, 2 (4):a009431.
- Cuperus R, Leen R, Tytgat GA, Caron HN, van Kuilenburg AB. 2010. Fenretinide induces mitochondrial ROS and inhibits the mitochondrial respiratory chain in neuroblastoma. *Cell Mol Life Sci*, 67 (5):807-816.
- Danzer KM, Krebs SK, Wolff M, Birk G, Hengeler B. 2009. Seeding induced by alpha-synuclein oligomers provides evidence for spreading of alpha-synuclein pathology. *J Neurochem*, 111 (1):192-203.
- Dauer W, Przedborski S. 2003. Parkinson's disease: mechanisms and models. *Neuron*, 39 (6):889-909.
- de Araujo NB, Moraes HS, Silveira H, Arcoverde C, Vasques PE, Barca ML, Knapskog AB, Engedal K, Coutinho ES, Deslandes AC, Laks J. 2014. Impaired cognition in depression and Alzheimer (AD): a gradient from depression to depression in AD. *Arq Neuropsiquiatr*, 72 (9):671-679.
- Deeley RG, Westlake C, Cole SP. 2006. Transmembrane transport of endo- and xenobiotics by mammalian ATP-binding cassette multidrug resistance proteins. *Physiol Rev*, 86 (3):849-899.
- Deetjen S, Hescheler. 2004. *Physiologie*. 4 Aufl.: Urban & Fischer Verlag/Elsevier GmbH.
- Del Tredici KB, H. 2000. Idiopathic Parkinson's Disease: Staging an α -Synucleinopathy with a Predictable Pathoanatomy. <http://www.ncbi.nlm.nih.gov/books/NBK6077/>: Madame Curie Bioscience Database; Austin (TX): Landes Bioscience.
- Dementia <http://www.who.int/mediacentre/factsheets/fs362/en/>
- Diagnostic and Statistical Manual of Mental Disorders. 2013. 5 Aufl.: American Psychiatric Association.
- Dias V, Junn E, Mouradian MM. 2013. The role of oxidative stress in Parkinson's disease. *J Parkinsons Dis*, 3 (4):461-491.
- Dickson DW, Fujishiro H, Orr C, DelleDonne A, Josephs KA, Frigerio R, Burnett M, Parisi JE, Klos KJ, Ahlskog JE. 2009a. Neuropathology of non-motor features of Parkinson disease. *Parkinsonism Relat Disord*, 15 Suppl 3:S1-5.
- Dickson DW, Braak H, Duda JE, Duyckaerts C, Gasser T, Halliday GM, Hardy J, Leverenz JB, Del Tredici K, Wszolek ZK, Litvan I. 2009b. Neuropathological assessment of Parkinson's disease: refining the diagnostic criteria. *Lancet Neurol*, 8 (12):1150-1157.
- El-Agnaf OM, Salem SA, Paleologou KE, Cooper LJ, Fullwood NJ, Gibson MJ, Curran MD, Court JA, Mann DM, Ikeda S, Cookson MR, Hardy J, Allsop D. 2003. Alpha-synuclein implicated in Parkinson's disease is present in extracellular biological fluids, including human plasma. *FASEB J*, 17 (13):1945-1947.
- Emmanouilidou E, Stefanis L, Vekrellis K. 2010. Cell-produced alpha-synuclein oligomers are targeted to, and impair, the 26S proteasome. *Neurobiol Aging*, 31 (6):953-968.
- Espay AJ, LeWitt PA, Kaufmann H. 2014. Norepinephrine deficiency in Parkinson's disease: the case for noradrenergic enhancement. *Mov Disord*, 29 (14):1710-1719.
- Fearnley JM, Lees AJ. 1991. Ageing and Parkinson's disease: substantia nigra regional selectivity. *Brain*, 114 (Pt 5):2283-2301.
- Fernagut PO, Chalon S, Diguët E, Guilloteau D, Tison F, Jaber M. 2003. Motor behaviour deficits and their histopathological and functional correlates in the nigrostriatal system of dopamine transporter knockout mice. *Neuroscience*, 116 (4):1123-1130.

- Fleming SM, Salcedo J, Fernagut PO, Rockenstein E, Masliah E, Levine MS, Chesselet MF. 2004. Early and progressive sensorimotor anomalies in mice overexpressing wild-type human alpha-synuclein. *J Neurosci*, 24 (42):9434-9440.
- Fredenburg RA, Rospigliosi C, Meray RK, Kessler JC, Lashuel HA, Eliezer D, Lansbury PT, Jr. 2007. The impact of the E46K mutation on the properties of alpha-synuclein in its monomeric and oligomeric states. *Biochemistry*, 46 (24):7107-7118.
- Freichel C, Neumann M, Ballard T, Muller V, Woolley M, Ozmen L, Borroni E, Kretzschmar HA, Haass C, Spooren W, Kahle PJ. 2007. Age-dependent cognitive decline and amygdala pathology in alpha-synuclein transgenic mice. *Neurobiol Aging*, 28 (9):1421-1435.
- Freitag S, Schachner M, Morellini F. 2003. Behavioral alterations in mice deficient for the extracellular matrix glycoprotein tenascin-R. *Behav Brain Res*, 145 (1-2):189-207.
- Fujiwara H, Hasegawa M, Dohmae N, Kawashima A, Masliah E, Goldberg MS, Shen J, Takio K, Iwatsubo T. 2002. alpha-Synuclein is phosphorylated in synucleinopathy lesions. *Nat Cell Biol*, 4 (2):160-164.
- Gellerich FN, Deschauer M, Chen Y, Muller T, Neudecker S, Zierz S. 2002. Mitochondrial respiratory rates and activities of respiratory chain complexes correlate linearly with heteroplasmy of deleted mtDNA without threshold and independently of deletion size. *Biochim Biophys Acta*, 1556 (1):41-52.
- Gellerich FN, Kapischke M, Kunz W, Neumann W, Kuznetsov A, Brdiczka D, Nicolay K. 1994. The influence of the cytosolic oncotic pressure on the permeability of the mitochondrial outer membrane for ADP: implications for the kinetic properties of mitochondrial creatine kinase and for ADP channelling into the intermembrane space. *Mol Cell Biochem*, 133-134:85-104.
- Gellerich FN, Trumbeckaite S, Opalka JR, Seppet E, Rasmussen HN, Neuhoff C, Zierz S. 2000. Function of the mitochondrial outer membrane as a diffusion barrier in health and diseases. *Biochem Soc Trans*, 28 (2):164-169.
- Gellerich FN, Gizatullina Z, Trumbeckaite S, Nguyen HP, Pallas T, Arandarcikaite O, Vielhaber S, Seppet E, Striggow F. 2010. The regulation of OXPHOS by extramitochondrial calcium. *Biochim Biophys Acta*, 1797 (6-7):1018-1027.
- Gellerich FN, Gizatullina Z, Trumbekaite S, Korzeniewski B, Gaynutdinov T, Seppet E, Vielhaber S, Heinze HJ, Striggow F. 2012. Cytosolic Ca²⁺ regulates the energization of isolated brain mitochondria by formation of pyruvate through the malate-aspartate shuttle. *Biochem J*, 443 (3):747-755.
- Gellerich FN, Gizatullina Z, Nguyen HP, Trumbeckaite S, Vielhaber S, Seppet E, Zierz S, Landwehrmeyer B, Riess O, von Horsten S, Striggow F. 2008. Impaired regulation of brain mitochondria by extramitochondrial Ca²⁺ in transgenic Huntington disease rats. *J Biol Chem*, 283 (45):30715-30724.
- Giasson BI, Duda JE, Murray IV, Chen Q, Souza JM, Hurtig HI, Ischiropoulos H, Trojanowski JQ, Lee VM. 2000. Oxidative damage linked to neurodegeneration by selective alpha-synuclein nitration in synucleinopathy lesions. *Science*, 290 (5493):985-989.
- Gibb WR, Lees AJ. 1988. The relevance of the Lewy body to the pathogenesis of idiopathic Parkinson's disease. *J Neurol Neurosurg Psychiatry*, 51 (6):745-752.
- Gnaiger E, Lassnig B, Kuznetsov A, Rieger G, Margreiter R. 1998. Mitochondrial oxygen affinity, respiratory flux control and excess capacity of cytochrome c oxidase. *J Exp Biol*, 201 (Pt 8):1129-1139.
- Goetz CG. 2011. The history of Parkinson's disease: early clinical descriptions and neurological therapies. *Cold Spring Harb Perspect Med*, 1 (1):a008862.
- Gordon S. 2003. Alternative activation of macrophages. *Nat Rev Immunol*, 3 (1):23-35.

- Gröger V. 2012. Characterization of alpha-synuclein overexpressing mice as a model of Parkinson's disease and Dementia with Lewy Bodies [Master thesis]. Otto-von-Guericke-University Magdeburg, Department of Neurology.
- Gu M, Owen AD, Toffa SE, Cooper JM, Dexter DT, Jenner P, Marsden CD, Schapira AH. 1998. Mitochondrial function, GSH and iron in neurodegeneration and Lewy body diseases. *J Neurol Sci*, 158 (1):24-29.
- Hellwig S, Heinrich A, Biber K. 2013. The brain's best friend: microglial neurotoxicity revisited. *Front Cell Neurosci*, 7:71.
- Hodara R, Norris EH, Giasson BI, Mishizen-Eberz AJ, Lynch DR, Lee VM, Ischiropoulos H. 2004. Functional consequences of alpha-synuclein tyrosine nitration: diminished binding to lipid vesicles and increased fibril formation. *J Biol Chem*, 279 (46):47746-47753.
- Hofrichter J, Krohn M, Schumacher T, Lange C, Feistel B, Walbroel B, Heinze HJ, Crockett S, Sharbel TF, Pahnke J. 2013. Reduced Alzheimer's disease pathology by St. John's Wort treatment is independent of hyperforin and facilitated by ABCC1 and microglia activation in mice. *Curr Alzheimer Res*, 10 (10):1057-1069.
- Hong S, Hwang J, Kim JY, Shin KS, Kang SJ. 2014. Heptachlor induced nigral dopaminergic neuronal loss and Parkinsonism-like movement deficits in mice. *Exp Mol Med*, 46:e80.
- Horton AA, Spencer JA. 1981. Decline in respiratory control ratio of rat liver mitochondria in old age. *Mech Ageing Dev*, 17 (3):253-259.
- The ICD-10 Classification of Mental and Behavioural Disorders. 1992.
<http://www.who.int/classifications/icd/en/bluebook.pdf>
- Irrcher I, Aleyasin H, Seifert EL, Hewitt SJ, Chhabra S, Phillips M, Lutz AK, Rousseaux MW, Bevilacqua L, Jahani-Asl A, Callaghan S, MacLaurin JG, Winklhofer KF, Rizzu P, Rippstein P, Kim RH, Chen CX, Fon EA, Slack RS, Harper ME, McBride HM, Mak TW, Park DS. 2010. Loss of the Parkinson's disease-linked gene DJ-1 perturbs mitochondrial dynamics. *Hum Mol Genet*, 19 (19):3734-3746.
- Iwai A, Masliah E, Yoshimoto M, Ge N, Flanagan L, de Silva HA, Kittel A, Saitoh T. 1995. The precursor protein of non-A beta component of Alzheimer's disease amyloid is a presynaptic protein of the central nervous system. *Neuron*, 14 (2):467-475.
- Jenner P. 2003. Oxidative stress in Parkinson's disease. *Ann Neurol*, 53 Suppl 3:S26-36; discussion S36-28.
- Jo E, Fuller N, Rand RP, St George-Hyslop P, Fraser PE. 2002. Defective membrane interactions of familial Parkinson's disease mutant A30P alpha-synuclein. *J Mol Biol*, 315 (4):799-807.
- Kahle PJ, Neumann M, Ozmen L, Muller V, Odoy S, Okamoto N, Jacobsen H, Iwatsubo T, Trojanowski JQ, Takahashi H, Wakabayashi K, Bogdanovic N, Riederer P, Kretschmar HA, Haass C. 2001. Selective insolubility of alpha-synuclein in human Lewy body diseases is recapitulated in a transgenic mouse model. *Am J Pathol*, 159 (6):2215-2225.
- Kamp F, Beyer K. 2006. Binding of alpha-synuclein affects the lipid packing in bilayers of small vesicles. *J Biol Chem*, 281 (14):9251-9259.
- Kamp F, Exner N, Lutz AK, Wender N, Hegermann J, Brunner B, Nuscher B, Bartels T, Giese A, Beyer K, Eimer S, Winklhofer KF, Haass C. 2010. Inhibition of mitochondrial fusion by alpha-synuclein is rescued by PINK1, Parkin and DJ-1. *EMBO J*, 29 (20):3571-3589.
- Kaplitt MG, Leone P, Samulski RJ, Xiao X, Pfaff DW, O'Malley KL, During MJ. 1994. Long-term gene expression and phenotypic correction using adeno-associated virus vectors in the mammalian brain. *Nat Genet*, 8 (2):148-154.

- Keeney PM, Xie J, Capaldi RA, Bennett JP, Jr. 2006. Parkinson's disease brain mitochondrial complex I has oxidatively damaged subunits and is functionally impaired and misassembled. *J Neurosci*, 26 (19):5256-5264.
- Kennedy PK, Ormerod MG, Singh S, Pande G. 2004. Variation of mitochondrial size during the cell cycle: A multiparameter flow cytometric and microscopic study. *Cytometry A*, 62 (2):97-108.
- Kim WS, Halliday GM. 2012. Changes in sphingomyelin level affect alpha-synuclein and ABCA5 expression. *J Parkinsons Dis*, 2 (1):41-46.
- Klein C, Westenberger A. 2012. Genetics of Parkinson's disease. *Cold Spring Harb Perspect Med*, 2 (1):a008888.
- Koivunen P, Hirsila M, Remes AM, Hassinen IE, Kivirikko KI, Myllyharju J. 2007. Inhibition of hypoxia-inducible factor (HIF) hydroxylases by citric acid cycle intermediates: possible links between cell metabolism and stabilization of HIF. *J Biol Chem*, 282 (7):4524-4532.
- Kopito RR. 2000. Aggresomes, inclusion bodies and protein aggregation. *Trends Cell Biol*, 10 (12):524-530.
- Kordower JH, Emborg ME, Bloch J, Ma SY, Chu Y, Leventhal L, McBride J, Chen EY, Palfi S, Roitberg BZ, Brown WD, Holden JE, Pyzalski R, Taylor MD, Carvey P, Ling Z, Trono D, Hantraye P, Deglon N, Aebischer P. 2000. Neurodegeneration prevented by lentiviral vector delivery of GDNF in primate models of Parkinson's disease. *Science*, 290 (5492):767-773.
- Kortekaas R, Leenders KL, van Oostrom JC, Vaalburg W, Bart J, Willemsen AT, Hendrikse NH. 2005. Blood-brain barrier dysfunction in parkinsonian midbrain in vivo. *Ann Neurol*, 57 (2):176-179.
- Kovacs GG, Wagner U, Dumont B, Pikkarainen M, Osman AA, Streichenberger N, Leisser I, Verchere J, Baron T, Alafuzoff I, Budka H, Perret-Liaudet A, Lachmann I. 2012. An antibody with high reactivity for disease-associated alpha-synuclein reveals extensive brain pathology. *Acta Neuropathol*, 124 (1):37-50.
- Kovacs GG, Breydo L, Green R, Kis V, Puska G, Lorincz P, Perju-Dumbrava L, Giera R, Pirker W, Lutz M, Lachmann I, Budka H, Uversky VN, Molnar K, Laszlo L. 2014. Intracellular processing of disease-associated alpha-synuclein in the human brain suggests prion-like cell-to-cell spread. *Neurobiol Dis*, 69:76-92.
- Krasnoslobodtsev AV, Volkov IL, Asiago JM, Hindupur J, Rochet JC, Lyubchenko YL. 2013. alpha-Synuclein misfolding assessed with single molecule AFM force spectroscopy: effect of pathogenic mutations. *Biochemistry*, 52 (42):7377-7386.
- Krebiehl G, Ruckerbauer S, Burbulla LF, Kieper N, Maurer B, Waak J, Wolburg H, Gizatullina Z, Gellerich FN, Voitalla D, Riess O, Kahle PJ, Proikas-Cezanne T, Kruger R. 2010. Reduced basal autophagy and impaired mitochondrial dynamics due to loss of Parkinson's disease-associated protein DJ-1. *PLoS One*, 5 (2):e9367.
- Krohn M, Lange C, Hofrichter J, Scheffler K, Stenzel J, Steffen J, Schumacher T, Bruning T, Plath AS, Alfen F, Schmidt A, Winter F, Rateitschak K, Wree A, Gsponer J, Walker LC, Pahnke J. 2011. Cerebral amyloid-beta proteostasis is regulated by the membrane transport protein ABCC1 in mice. *J Clin Invest*, 121 (10):3924-3931.
- Kruger R, Kuhn W, Muller T, Voitalla D, Graeber M, Kosel S, Przuntek H, Eppelen JT, Schols L, Riess O. 1998. Ala30Pro mutation in the gene encoding alpha-synuclein in Parkinson's disease. *Nat Genet*, 18 (2):106-108.
- Kupsch A, Schmidt W, Gizatullina Z, Debska-Vielhaber G, Voges J, Striggow F, Panther P, Schwegler H, Heinze HJ, Vielhaber S, Gellerich FN. 2014. 6-Hydroxydopamine impairs mitochondrial function in the rat model of Parkinson's disease: respirometric, histological, and behavioral analyses. *J Neural Transm*, 121 (10):1245-1257.

- Kuznetsov AV, Veksler V, Gellerich FN, Saks V, Margreiter R, Kunz WS. 2008. Analysis of mitochondrial function in situ in permeabilized muscle fibers, tissues and cells. *Nat Protoc*, 3 (6):965-976.
- Lam FC, Liu R, Lu P, Shapiro AB, Renoir JM, Sharom FJ, Reiner PB. 2001. beta-Amyloid efflux mediated by p-glycoprotein. *J Neurochem*, 76 (4):1121-1128.
- Landrigan PJ, Sonawane B, Butler RN, Trasande L, Callan R, Droller D. 2005. Early environmental origins of neurodegenerative disease in later life. *Environ Health Perspect*, 113 (9):1230-1233.
- Langston JW, Ballard PA, Jr. 1983. Parkinson's disease in a chemist working with 1-methyl-4-phenyl-1,2,5,6-tetrahydropyridine. *N Engl J Med*, 309 (5):310.
- Lapin IP. 1995. Only controls: effect of handling, sham injection, and intraperitoneal injection of saline on behavior of mice in an elevated plus-maze. *J Pharmacol Toxicol Methods*, 34 (2):73-77.
- Larsson NG. 2010. Somatic mitochondrial DNA mutations in mammalian aging. *Annu Rev Biochem*, 79:683-706.
- Lawson LJ, Perry VH, Dri P, Gordon S. 1990. Heterogeneity in the distribution and morphology of microglia in the normal adult mouse brain. *Neuroscience*, 39 (1):151-170.
- Lazaro DF, Rodrigues EF, Langohr R, Shahpasandzadeh H, Ribeiro T, Guerreiro P, Gerhardt E, Krohnert K, Klucken J, Pereira MD, Popova B, Kruse N, Mollenhauer B, Rizzoli SO, Braus GH, Danzer KM, Outeiro TF. 2014. Systematic comparison of the effects of alpha-synuclein mutations on its oligomerization and aggregation. *PLoS Genet*, 10 (11):e1004741.
- Lee EN, Lee SY, Lee D, Kim J, Paik SR. 2003. Lipid interaction of alpha-synuclein during the metal-catalyzed oxidation in the presence of Cu²⁺ and H₂O₂. *J Neurochem*, 84 (5):1128-1142.
- Lee VM, Trojanowski JQ. 2006. Mechanisms of Parkinson's disease linked to pathological alpha-synuclein: new targets for drug discovery. *Neuron*, 52 (1):33-38.
- Leiter EH. 2001. The NOD mouse: a model for insulin-dependent diabetes mellitus. *Curr Protoc Immunol*, Chapter 15:Unit 15 19.
- Leonard JV, Schapira AH. 2000. Mitochondrial respiratory chain disorders I: mitochondrial DNA defects. *Lancet*, 355 (9200):299-304.
- Letellier T, Heinrich R, Malgat M, Mazat JP. 1994. The kinetic basis of threshold effects observed in mitochondrial diseases: a systemic approach. *Biochem J*, 302 (Pt 1):171-174.
- Li J, Uversky VN, Fink AL. 2001. Effect of familial Parkinson's disease point mutations A30P and A53T on the structural properties, aggregation, and fibrillation of human alpha-synuclein. *Biochemistry*, 40 (38):11604-11613.
- Li J, Uversky VN, Fink AL. 2002. Conformational behavior of human alpha-synuclein is modulated by familial Parkinson's disease point mutations A30P and A53T. *Neurotoxicology*, 23 (4-5):553-567.
- Lin MT, Beal MF. 2006. Mitochondrial dysfunction and oxidative stress in neurodegenerative diseases. *Nature*, 443 (7113):787-795.
- Loscher W, Potschka H. 2005. Blood-brain barrier active efflux transporters: ATP-binding cassette gene family. *NeuroRx*, 2 (1):86-98.
- Luengo-Fernandez RL, R; Gray, A. 2010. Dementia 2010. www.dementia2010.org: University of Oxford.
- Luoma P, Melberg A, Rinne JO, Kaukonen JA, Nupponen NN, Chalmers RM, Oldfors A, Rautakorpi I, Peltonen L, Majamaa K, Somer H, Suomalainen A. 2004. Parkinsonism, premature menopause, and mitochondrial DNA polymerase gamma mutations: clinical and molecular genetic study. *Lancet*, 364 (9437):875-882.

- Ma QL, Chan P, Yoshii M, Ueda K. 2003. Alpha-synuclein aggregation and neurodegenerative diseases. *J Alzheimers Dis*, 5 (2):139-148.
- Machiya Y, Hara S, Arawaka S, Fukushima S, Sato H, Sakamoto M, Koyama S, Kato T. 2010. Phosphorylated alpha-synuclein at Ser-129 is targeted to the proteasome pathway in a ubiquitin-independent manner. *J Biol Chem*, 285 (52):40732-40744.
- Madine J, Doig AJ, Middleton DA. 2006. A study of the regional effects of alpha-synuclein on the organization and stability of phospholipid bilayers. *Biochemistry*, 45 (18):5783-5792.
- Mahler ME, Cummings JL, Benson DF. 1987. Treatable dementias. *West J Med*, 146 (6):705-712.
- Mannella CA. 2006. The relevance of mitochondrial membrane topology to mitochondrial function. *Biochim Biophys Acta*, 1762 (2):140-147.
- Maroteaux L, Scheller RH. 1991. The rat brain synucleins; family of proteins transiently associated with neuronal membrane. *Brain Res Mol Brain Res*, 11 (3-4):335-343.
- Maroteaux L, Campanelli JT, Scheller RH. 1988. Synuclein: a neuron-specific protein localized to the nucleus and presynaptic nerve terminal. *J Neurosci*, 8 (8):2804-2815.
- Martin LJ. 2010. Mitochondrial and Cell Death Mechanisms in Neurodegenerative Diseases. *Pharmaceuticals (Basel)*, 3 (4):839-915.
- Martin LJ. 2012. Biology of mitochondria in neurodegenerative diseases. *Prog Mol Biol Transl Sci*, 107:355-415.
- Masliah E, Rockenstein E, Veinbergs I, Mallory M, Hashimoto M, Takeda A, Sagara Y, Sisk A, Mucke L. 2000. Dopaminergic loss and inclusion body formation in alpha-synuclein mice: implications for neurodegenerative disorders. *Science*, 287 (5456):1265-1269.
- Massano J, Bhatia KP. 2012. Clinical approach to Parkinson's disease: features, diagnosis, and principles of management. *Cold Spring Harb Perspect Med*, 2 (6):a008870.
- Matsuura K, Kabuto H, Makino H, Ogawa N. 1997. Pole test is a useful method for evaluating the mouse movement disorder caused by striatal dopamine depletion. *J Neurosci Methods*, 73 (1):45-48.
- Maturana MG, Pinheiro AS, Souza TL, Follmer C. 2014. Unveiling the role of the pesticides paraquat and rotenone on alpha-synuclein fibrillation in vitro. *Neurotoxicology*, 46C:35-43.
- McClendon S, Rospigliosi CC, Eliezer D. 2009. Charge neutralization and collapse of the C-terminal tail of alpha-synuclein at low pH. *Protein Sci*, 18 (7):1531-1540.
- McCormack JG, Denton RM. 1979. The effects of calcium ions and adenine nucleotides on the activity of pig heart 2-oxoglutarate dehydrogenase complex. *Biochem J*, 180 (3):533-544.
- McCormack JG, Denton RM. 1993. Mitochondrial Ca²⁺ transport and the role of intramitochondrial Ca²⁺ in the regulation of energy metabolism. *Dev Neurosci*, 15 (3-5):165-173.
- McGeer PL, McGeer EG. 2008. Glial reactions in Parkinson's disease. *Mov Disord*, 23 (4):474-483.
- McKenna MC, Waagepetersen HS, Schousboe A, Sonnewald U. 2006. Neuronal and astrocytic shuttle mechanisms for cytosolic-mitochondrial transfer of reducing equivalents: current evidence and pharmacological tools. *Biochem Pharmacol*, 71 (4):399-407.
- Meredith GE, Sonsalla PK, Chesselet MF. 2008. Animal models of Parkinson's disease progression. *Acta Neuropathol*, 115 (4):385-398.
- Miller DS. 2015. Regulation of ABC Transporters Blood-Brain Barrier: The Good, the Bad, and the Ugly. *Adv Cancer Res*, 125:43-70.

- Moechars D, Dewachter I, Lorent K, Reverse D, Baekelandt V, Naidu A, Tesseur I, Spittaels K, Haute CV, Checler F, Godaux E, Cordell B, Van Leuven F. 1999. Early phenotypic changes in transgenic mice that overexpress different mutants of amyloid precursor protein in brain. *J Biol Chem*, 274 (10):6483-6492.
- Mollenhauer BF, H; Deuschl, G; Storch, A; Oertl, W; Trenkwalder, c. 2010. Lewy Body and Parkinsonian Dementia: Common, but Often Misdiagnosed Conditions. *Dtsch Arztebl Int*, 107 (39):684-691.
- Montes S, Rivera-Mancia S, Diaz-Ruiz A, Tristan-Lopez L, Rios C. 2014. Copper and copper proteins in Parkinson's disease. *Oxid Med Cell Longev*, 2014:147251.
- Moore DJ, West AB, Dawson VL, Dawson TM. 2005. Molecular pathophysiology of Parkinson's disease. *Annu Rev Neurosci*, 28:57-87.
- Morris M, Koyama A, Masliah E, Mucke L. 2011. Tau reduction does not prevent motor deficits in two mouse models of Parkinson's disease. *PLoS One*, 6 (12):e29257.
- Mosley RL, Hutter-Saunders JA, Stone DK, Gendelman HE. 2012. Inflammation and adaptive immunity in Parkinson's disease. *Cold Spring Harb Perspect Med*, 2 (1):a009381.
- Müller-Esterl W. 2004. *Biochemie: Eine Einführung für Mediziner und Naturwissenschaftler*. Springer, Berlin.
- Mylene M, Sebastien M, Sophie CC, Jerome L, Jevita P, Pierre V, Nicolaie G, Herve V, Gerard B, Elisabeth S, Raymund S. 2013. Neurosurgery in Parkinson's disease: Social adjustment, quality of life and coping strategies. *Neural Regen Res*, 8 (30):2856-2867.
- Neumann M, Kahle PJ, Giasson BI, Ozmen L, Borroni E, Spooen W, Muller V, Odoy S, Fujiwara H, Hasegawa M, Iwatsubo T, Trojanowski JQ, Kretzschmar HA, Haass C. 2002. Misfolded proteinase K-resistant hyperphosphorylated alpha-synuclein in aged transgenic mice with locomotor deterioration and in human alpha-synucleinopathies. *J Clin Invest*, 110 (10):1429-1439.
- Nicklas WJ, Vyas I, Heikkila RE. 1985. Inhibition of NADH-linked oxidation in brain mitochondria by 1-methyl-4-phenyl-pyridine, a metabolite of the neurotoxin, 1-methyl-4-phenyl-1,2,5,6-tetrahydropyridine. *Life Sci*, 36 (26):2503-2508.
- Obeso JA, Marin C, Rodriguez-Oroz C, Blesa J, Benitez-Temino B, Mena-Segovia J, Rodriguez M, Olanow CW. 2008. The basal ganglia in Parkinson's disease: current concepts and unexplained observations. *Ann Neurol*, 64 Suppl 2:S30-46.
- Ogawa N, Hirose Y, Ohara S, Ono T, Watanabe Y. 1985. A simple quantitative bradykinesia test in MPTP-treated mice. *Res Commun Chem Pathol Pharmacol*, 50 (3):435-441.
- Okochi M, Walter J, Koyama A, Nakajo S, Baba M, Iwatsubo T, Meijer L, Kahle PJ, Haass C. 2000. Constitutive phosphorylation of the Parkinson's disease associated alpha-synuclein. *J Biol Chem*, 275 (1):390-397.
- Olah M, Biber K, Vinet J, Boddeke HW. 2011. Microglia phenotype diversity. *CNS Neurol Disord Drug Targets*, 10 (1):108-118.
- Olanow CW, Tatton WG. 1999. Etiology and pathogenesis of Parkinson's disease. *Annu Rev Neurosci*, 22:123-144.
- Pahnke J, Langer O, Krohn M. 2014. Alzheimer's and ABC transporters--new opportunities for diagnostics and treatment. *Neurobiol Dis*, 72 Pt A:54-60.
- Pahnke J, Walker LC, Scheffler K, Krohn M. 2009. Alzheimer's disease and blood-brain barrier function--Why have anti-beta-amyloid therapies failed to prevent dementia progression? *Neurosci Biobehav Rev*, 33 (7):1099-1108.

- Pahnke J, Frohlich C, Krohn M, Schumacher T, Paarmann K. 2013. Impaired mitochondrial energy production and ABC transporter function-A crucial interconnection in dementing proteopathies of the brain. *Mech Ageing Dev*, 134 (10):506-515.
- Panov A, Schonfeld P, Dikalov S, Hemendinger R, Bonkovsky HL, Brooks BR. 2009. The neuromediator glutamate, through specific substrate interactions, enhances mitochondrial ATP production and reactive oxygen species generation in nonsynaptic brain mitochondria. *J Biol Chem*, 284 (21):14448-14456.
- Pardo B, Contreras L, Serrano A, Ramos M, Kobayashi K, Iijima M, Saheki T, Satrustegui J. 2006. Essential role of aralar in the transduction of small Ca²⁺ signals to neuronal mitochondria. *J Biol Chem*, 281 (2):1039-1047.
- Perier C, Vila M. 2012. Mitochondrial biology and Parkinson's disease. *Cold Spring Harb Perspect Med*, 2 (2):a009332.
- Perrin RJ, Woods WS, Clayton DF, George JM. 2001. Exposure to long chain polyunsaturated fatty acids triggers rapid multimerization of synucleins. *J Biol Chem*, 276 (45):41958-41962.
- Pesta D, Gnaiger E. 2012. High-resolution respirometry: OXPHOS protocols for human cells and permeabilized fibers from small biopsies of human muscle. *Methods Mol Biol*, 810:25-58.
- Priyadarshi A, Khuder SA, Schaub EA, Priyadarshi SS. 2001. Environmental risk factors and Parkinson's disease: a metaanalysis. *Environ Res*, 86 (2):122-127.
- Pronin AN, Morris AJ, Surguchov A, Benovic JL. 2000. Synucleins are a novel class of substrates for G protein-coupled receptor kinases. *J Biol Chem*, 275 (34):26515-26522.
- Przedborski S, Vila M, Jackson-Lewis V. 2003. Neurodegeneration: what is it and where are we? *J Clin Invest*, 111 (1):3-10.
- Przedborski S, Jackson-Lewis V, Yokoyama R, Shibata T, Dawson VL, Dawson TM. 1996. Role of neuronal nitric oxide in 1-methyl-4-phenyl-1,2,3,6-tetrahydropyridine (MPTP)-induced dopaminergic neurotoxicity. *Proc Natl Acad Sci U S A*, 93 (10):4565-4571.
- Przedborski S, Kostic V, Jackson-Lewis V, Naini AB, Simonetti S, Fahn S, Carlson E, Epstein CJ, Cadet JL. 1992. Transgenic mice with increased Cu/Zn-superoxide dismutase activity are resistant to N-methyl-4-phenyl-1,2,3,6-tetrahydropyridine-induced neurotoxicity. *J Neurosci*, 12 (5):1658-1667.
- Quinlan CL, Orr AL, Perevoshchikova IV, Treberg JR, Ackrell BA, Brand MD. 2012. Mitochondrial complex II can generate reactive oxygen species at high rates in both the forward and reverse reactions. *J Biol Chem*, 287 (32):27255-27264.
- Ramsay RR, Kowal AT, Johnson MK, Salach JI, Singer TP. 1987. The inhibition site of MPP⁺, the neurotoxic bioactivation product of 1-methyl-4-phenyl-1,2,3,6-tetrahydropyridine is near the Q-binding site of NADH dehydrogenase. *Arch Biochem Biophys*, 259 (2):645-649.
- Rhinn H, Qiang L, Yamashita T, Rhee D, Zolin A, Vanti W, Abeliovich A. 2012. Alternative alpha-synuclein transcript usage as a convergent mechanism in Parkinson's disease pathology. *Nat Commun*, 3:1084.
- Richardson JR, Shalat SL, Buckley B, Winnik B, O'Suilleabhain P, Diaz-Arrastia R, Reisch J, German DC. 2009. Elevated serum pesticide levels and risk of Parkinson disease. *Arch Neurol*, 66 (7):870-875.
- Rockenstein E, Mallory M, Hashimoto M, Song D, Shults CW, Lang I, Masliah E. 2002. Differential neuropathological alterations in transgenic mice expressing alpha-synuclein from the platelet-derived growth factor and Thy-1 promoters. *J Neurosci Res*, 68 (5):568-578.
- Rojas LE, Fernandez JA, Maccioni AA, Jimenez JM, Maccioni RB. 2008. Neuroinflammation: implications for the pathogenesis and molecular diagnosis of Alzheimer's disease. *Arch Med Res*, 39 (1):1-16.

- Rosenblad C, Martinez-Serrano A, Bjorklund A. 1998. Intrastratial glial cell line-derived neurotrophic factor promotes sprouting of spared nigrostriatal dopaminergic afferents and induces recovery of function in a rat model of Parkinson's disease. *Neuroscience*, 82 (1):129-137.
- Russo I, Bubacco L, Greggio E. 2014. LRRK2 and neuroinflammation: partners in crime in Parkinson's disease? *J Neuroinflammation*, 11:52.
- Satrustegui J, Pardo B, Del Arco A. 2007. Mitochondrial transporters as novel targets for intracellular calcium signaling. *Physiol Rev*, 87 (1):29-67.
- Schapira AH. 2006. Etiology of Parkinson's disease. *Neurology*, 66 (10 Suppl 4):S10-23.
- Schapira AH, Jenner P. 2011. Etiology and pathogenesis of Parkinson's disease. *Mov Disord*, 26 (6):1049-1055.
- Schapira AH, Cooper JM, Dexter D, Clark JB, Jenner P, Marsden CD. 1990. Mitochondrial complex I deficiency in Parkinson's disease. *J Neurochem*, 54 (3):823-827.
- Scheffler K, Stenzel J, Krohn M, Lange C, Hofrichter J, Schumacher T, Bruning T, Plath AS, Walker L, Pahnke J. 2011. Determination of spatial and temporal distribution of microglia by 230nm-high-resolution, high-throughput automated analysis reveals different amyloid plaque populations in an APP/PS1 mouse model of Alzheimer's disease. *Curr Alzheimer Res*, 8 (7):781-788.
- Scheffler K, Krohn M, Dunkelmann T, Stenzel J, Miroux B, Ibrahim S, von Bohlen Und Halbach O, Heinze HJ, Walker LC, Gsponer JA, Pahnke J. 2012. Mitochondrial DNA polymorphisms specifically modify cerebral beta-amyloid proteostasis. *Acta Neuropathol*, 124 (2):199-208.
- Schell H, Hasegawa T, Neumann M, Kahle PJ. 2009. Nuclear and neuritic distribution of serine-129 phosphorylated alpha-synuclein in transgenic mice. *Neuroscience*, 160 (4):796-804.
- Schiess M. 2003. Nonsteroidal anti-inflammatory drugs protect against Parkinson neurodegeneration: can an NSAID a day keep Parkinson disease away? *Arch Neurol*, 60 (8):1043-1044.
- Schlossmacher MG, Frosch MP, Gai WP, Medina M, Sharma N, Forno L, Ochiishi T, Shimura H, Sharon R, Hattori N, Langston JW, Mizuno Y, Hyman BT, Selkoe DJ, Kosik KS. 2002. Parkin localizes to the Lewy bodies of Parkinson disease and dementia with Lewy bodies. *Am J Pathol*, 160 (5):1655-1667.
- Schon EA, DiMauro S, Hirano M. 2012. Human mitochondrial DNA: roles of inherited and somatic mutations. *Nat Rev Genet*, 13 (12):878-890.
- Schulz-Schaeffer WJ. 2010. The synaptic pathology of alpha-synuclein aggregation in dementia with Lewy bodies, Parkinson's disease and Parkinson's disease dementia. *Acta Neuropathol*, 120 (2):131-143.
- Sedelis M, Schwarting RK, Huston JP. 2001. Behavioral phenotyping of the MPTP mouse model of Parkinson's disease. *Behav Brain Res*, 125 (1-2):109-125.
- Sharon R, Bar-Joseph I, Frosch MP, Walsh DM, Hamilton JA, Selkoe DJ. 2003. The formation of highly soluble oligomers of alpha-synuclein is regulated by fatty acids and enhanced in Parkinson's disease. *Neuron*, 37 (4):583-595.
- Simon-Sanchez J, Schulte C, Bras JM, Sharma M, Gibbs JR, Berg D, Paisan-Ruiz C, Lichtner P, Scholz SW, Hernandez DG, Kruger R, Federoff M, Klein C, Goate A, Perlmutter J, Bonin M, Nalls MA, Illig T, Gieger C, Houlden H, Steffens M, Okun MS, Racette BA, Cookson MR, Foote KD, Fernandez HH, Traynor BJ, Schreiber S, Arepalli S, Zonozzi R, Gwinn K, van der Brug M, Lopez G, Chanock SJ, Schatzkin A, Park Y, Hollenbeck A, Gao J, Huang X, Wood NW, Lorenz D, Deuschl G, Chen H, Riess O, Hardy JA, Singleton AB, Gasser T. 2009. Genome-wide association study reveals genetic risk underlying Parkinson's disease. *Nat Genet*, 41 (12):1308-1312.

- Singer TP, Castagnoli N, Jr., Ramsay RR, Trevor AJ. 1987. Biochemical events in the development of parkinsonism induced by 1-methyl-4-phenyl-1,2,3,6-tetrahydropyridine. *J Neurochem*, 49 (1):1-8.
- Singleton AB, Farrer MJ, Bonifati V. 2013. The genetics of Parkinson's disease: progress and therapeutic implications. *Mov Disord*, 28 (1):14-23.
- Song ES, Juliano MA, Juliano L, Fried MG, Wagner SL, Hersh LB. 2004. ATP effects on insulin-degrading enzyme are mediated primarily through its triphosphate moiety. *J Biol Chem*, 279 (52):54216-54220.
- statistisches Bundesamt 2015.
<https://www.destatis.de/DE/ZahlenFakten/GesellschaftStaat/Gesundheit/Todesursachen/Todesursachen.html>
- Stefanis L. 2012. alpha-Synuclein in Parkinson's disease. *Cold Spring Harb Perspect Med*, 2 (2):a009399.
- Stockl M, Fischer P, Wanker E, Herrmann A. 2008. Alpha-synuclein selectively binds to anionic phospholipids embedded in liquid-disordered domains. *J Mol Biol*, 375 (5):1394-1404.
- Sui YT, Bullock KM, Erickson MA, Zhang J, Banks WA. 2014. Alpha synuclein is transported into and out of the brain by the blood-brain barrier. *Peptides*, 62:197-202.
- Swart C, Haylett W, Kinnear C, Johnson G, Bardien S, Loos B. 2014. Neurodegenerative disorders: dysregulation of a carefully maintained balance? *Exp Gerontol*, 58:279-291.
- Szeto HH. 2006. Mitochondria-targeted peptide antioxidants: novel neuroprotective agents. *AAPS J*, 8 (3):E521-531.
- Tabuse M, Yaguchi M, Ohta S, Kawase T, Toda M. 2010. A simple behavioral test for locomotor function after brain injury in mice. *J Clin Neurosci*, 17 (11):1412-1416.
- Tansey MG, Goldberg MS. 2010. Neuroinflammation in Parkinson's disease: its role in neuronal death and implications for therapeutic intervention. *Neurobiol Dis*, 37 (3):510-518.
- Thiruchelvam MJ, Powers JM, Cory-Slechta DA, Richfield EK. 2004. Risk factors for dopaminergic neuron loss in human alpha-synuclein transgenic mice. *Eur J Neurosci*, 19 (4):845-854.
- Tieu K, Perier C, Caspersen C, Teismann P, Wu DC, Yan SD, Naini A, Vila M, Jackson-Lewis V, Ramasamy R, Przedborski S. 2003. D-beta-hydroxybutyrate rescues mitochondrial respiration and mitigates features of Parkinson disease. *J Clin Invest*, 112 (6):892-901.
- Tobaben S, Thakur P, Fernandez-Chacon R, Sudhof TC, Rettig J, Stahl B. 2001. A trimeric protein complex functions as a synaptic chaperone machine. *Neuron*, 31 (6):987-999.
- Tofaris GK, Spillantini MG. 2005. Alpha-synuclein dysfunction in Lewy body diseases. *Mov Disord*, 20 Suppl 12:S37-44.
- Tofaris GK, Garcia Reitböck P, Humby T, Lambourne SL, O'Connell M, Ghetti B, Gossage H, Emson PC, Wilkinson LS, Goedert M, Spillantini MG. 2006. Pathological changes in dopaminergic nerve cells of the substantia nigra and olfactory bulb in mice transgenic for truncated human alpha-synuclein(1-120): implications for Lewy body disorders. *J Neurosci*, 26 (15):3942-3950.
- Trifunovic A, Wredenberg A, Falkenberg M, Spelbrink JN, Rovio AT, Bruder CE, Bohlooly YM, Gidlof S, Oldfors A, Wibom R, Tornell J, Jacobs HT, Larsson NG. 2004. Premature ageing in mice expressing defective mitochondrial DNA polymerase. *Nature*, 429 (6990):417-423.
- Trostchansky A, Lind S, Hodara R, Oe T, Blair IA, Ischiropoulos H, Rubbo H, Souza JM. 2006. Interaction with phospholipids modulates alpha-synuclein nitration and lipid-protein adduct formation. *Biochem J*, 393 (Pt 1):343-349.

- Trumbeckaite S, Opalka JR, Neuhof C, Zierz S, Gellerich FN. 2001. Different sensitivity of rabbit heart and skeletal muscle to endotoxin-induced impairment of mitochondrial function. *Eur J Biochem*, 268 (5):1422-1429.
- Ulusoy A, Febbraro F, Jensen PH, Kirik D, Romero-Ramos M. 2010. Co-expression of C-terminal truncated alpha-synuclein enhances full-length alpha-synuclein-induced pathology. *Eur J Neurosci*, 32 (3):409-422.
- van der Putten H, Wiederhold KH, Probst A, Barbieri S, Mistl C, Danner S, Kauffmann S, Hofele K, Spooren WP, Ruegg MA, Lin S, Caroni P, Sommer B, Tolnay M, Bilbe G. 2000. Neuropathology in mice expressing human alpha-synuclein. *J Neurosci*, 20 (16):6021-6029.
- Vogelgesang S, Warzok RW, Cascorbi I, Kunert-Keil C, Schroeder E, Kroemer HK, Siegmund W, Walker LC, Pahnke J. 2004. The role of P-glycoprotein in cerebral amyloid angiopathy; implications for the early pathogenesis of Alzheimer's disease. *Curr Alzheimer Res*, 1 (2):121-125.
- Walsh DM, Selkoe DJ. 2007. A beta oligomers - a decade of discovery. *J Neurochem*, 101 (5):1172-1184.
- Wang XF, Li S, Chou AP, Bronstein JM. 2006. Inhibitory effects of pesticides on proteasome activity: implication in Parkinson's disease. *Neurobiol Dis*, 23 (1):198-205.
- Weinreb PH, Zhen W, Poon AW, Conway KA, Lansbury PT, Jr. 1996. NACP, a protein implicated in Alzheimer's disease and learning, is natively unfolded. *Biochemistry*, 35 (43):13709-13715.
- Wen JJ, Dhiman M, Whorton EB, Garg NJ. 2008. Tissue-specific oxidative imbalance and mitochondrial dysfunction during *Trypanosoma cruzi* infection in mice. *Microbes Infect*, 10 (10-11):1201-1209.
- Wesolowska O. 2011. Interaction of phenothiazines, stilbenes and flavonoids with multidrug resistance-associated transporters, P-glycoprotein and MRP1. *Acta Biochim Pol*, 58 (4):433-448.
- Wesolowska O, Mosiadz D, Motohashi N, Kawase M, Michalak K. 2005. Phenothiazine maleates stimulate MRP1 transport activity in human erythrocytes. *Biochim Biophys Acta*, 1720 (1-2):52-58.
- Witter MP, Canto CB, Couey JJ, Koganezawa N, O'Reilly KC. 2014. Architecture of spatial circuits in the hippocampal region. *Philos Trans R Soc Lond B Biol Sci*, 369 (1635):20120515.
- World Alzheimer Report 2009. <http://www.alz.co.uk/>.
- World Alzheimer Report 2010. <http://www.alz.co.uk/>.
- World Population Prospects: *The 2012 Revision, Key Findings and Advance Tables*. 2013. http://esa.un.org/wpp/documentation/pdf/WPP2012_%20KEY%20FINDINGS.pdf.
- Wu DC, Teismann P, Tieu K, Vila M, Jackson-Lewis V, Ischiropoulos H, Przedborski S. 2003. NADPH oxidase mediates oxidative stress in the 1-methyl-4-phenyl-1,2,3,6-tetrahydropyridine model of Parkinson's disease. *Proc Natl Acad Sci U S A*, 100 (10):6145-6150.
- Yu X, Wester-Rosenlof L, Gimsa U, Holzhueter SA, Marques A, Jonas L, Hagenow K, Kunz M, Nizze H, Tiedge M, Holmdahl R, Ibrahim SM. 2009. The mtDNA nt7778 G/T polymorphism affects autoimmune diseases and reproductive performance in the mouse. *Hum Mol Genet*, 18 (24):4689-4698.
- Zalman LS, Nikaido H, Kagawa Y. 1980. Mitochondrial outer membrane contains a protein producing nonspecific diffusion channels. *J Biol Chem*, 255 (5):1771-1774.
- Zarranz JJ, Alegre J, Gomez-Esteban JC, Lezcano E, Ros R, Ampuero I, Vidal L, Hoenicka J, Rodriguez O, Atares B, Llorens V, Gomez Tortosa E, del Ser T, Munoz DG, de Yebenes JG. 2004. The new mutation, E46K, of alpha-synuclein causes Parkinson and Lewy body dementia. *Ann Neurol*, 55 (2):164-173.

- Zeng BY, Iravani MM, Lin ST, Irifune M, Kuoppamaki M, Al-Barghouthy G, Smith L, Jackson MJ, Rose S, Medhurst AD, Jenner P. 2006. MPTP treatment of common marmosets impairs proteasomal enzyme activity and decreases expression of structural and regulatory elements of the 26S proteasome. *Eur J Neurosci*, 23 (7):1766-1774.
- Zhang Y, Lu L, Jia J, Jia L, Geula C, Pei J, Xu Z, Qin W, Liu R, Li D, Pan N. 2014. A lifespan observation of a novel mouse model: in vivo evidence supports abeta oligomer hypothesis. *PLoS One*, 9 (1):e85885.
- Zhu M, Li J, Fink AL. 2003. The association of alpha-synuclein with membranes affects bilayer structure, stability, and fibril formation. *J Biol Chem*, 278 (41):40186-40197.
- Zlokovic BV. 2008. The blood-brain barrier in health and chronic neurodegenerative disorders. *Neuron*, 57 (2):178-201.
- Zschiebsch K. 2012. Functional effects of mitochondrial polymorphisms in mice [Master thesis]. Otto-von-Guericke University Magdeburg, Department of Neurology.

List of figures

Figure 1: Nigrostriatal pathology in the PD brain.....	12
Figure 2: α - synuclein transcript with mutations respectively phosphorylation and nitration sites	16
Figure 3: Schematic illustration of the ETC and additionally reactions catalyzed by complex I and II	23
Figure 4: Weight of tg-aSYN and C57BL/6J mice from 9 to 41 weeks of age.....	42
Figure 5: aSYN-immunoreactivity of 50 d old and 300 d old tg-aSYN mice.....	43
Figure 6: Load of human aSYN in cortex and hippocampus of young and old tg-aSYN mice.....	44
Figure 7: Immunohistochemical analyses of young and old tg-aSYN mice.....	45
Figure 8: Semi-quantitative analysis of immunohistochemistry.....	46
Figure 9: Proportion of censored data in the rotarod data set.....	47
Figure 10: Age-dependent alteration in motor behavior of tg-aSYN and C57BL/6J mice.....	47
Figure 11: Changes in pole test performances of tg-aSYN and C57BL/6J mice.....	48
Figure 12: aSYN-immunoreactivity in 300 d old tg-aSYN and tg-aSYN-mtNOD mice.....	49
Figure 13: Immunohistochemical analyzes of 300 d old tg-aSYN and tg-aSYN-mtNOD mice.....	50
Figure 14: Semi-quantitative analysis of Immunohistochemistry in the cortex of tg-aSYN, tg- aSYN-mtNOD and C57BL/6J mice.....	51
Figure 15: ELISA measurements of aSYN in the brain of tg-aSYN and tg-aSYN-mtNOD mice.....	51
Figure 16: Proportion of censored data collected using rotarod.....	52
Figure 17: Motor performances of tg-aSYN, tg-aSYN-mtNOD and C57BL/6J mice.....	53
Figure 18: Influence of mitochondrial polymorphism on the pole test performance of tg-aSYN mice.....	54
Figure 19: Representative respirograms of old C57BL/6J mice.....	56
Figure 20: Complex I-dependent respiration of isolated brain mitochondria of mtNOD and C57BL/6J mice.....	57
Figure 21: Complex II-dependent respiration rates of mtNOD and C57BL/6J mice.....	59
Figure 22: Complex I/Complex II ratio calculated from measurements based on protocol I, II and IV of mtNOD and C57BL/6J mice.....	60
Figure 23: Complex III-dependent respiration rates of mtNOD and C57BL/6J mice.....	60
Figure 24: Complex IV-dependent respiration of mtNOD and C57BL/6J mice.....	61
Figure 25: The excess capacity of complex IV (COX).....	62
Figure 26: Maximal capacity of ETC measured after uncoupling of the oxidative phosphorylation with FCCP.....	62
Figure 27: Different states of non-phosphorylating respiration for complex I- and complex II- dependent substrates.....	63

Figure 28: Respiratory control ratios (RCR) of mtNOD and C57BL/6J mice.....	64
Figure 29: Determination of neuronal- and microglial area in the cortex of 100 d old tg-aSYN and tg-aSYN-ABCC1 ^{-/-} mice.....	65
Figure 30: ELISA measurement of g-aSYN and tg-aSYN-ABCC1 ^{-/-} mice.....	66
Figure 31: Immunohistochemical analyzes of thiethylperazine- and water-treated tg-aSYN mice.	67
Figure 32: Semi-quantitative analyzes of neuronal and microglial area in the cortex of tg-aSYN and tg-aSYN-ABCC1 ^{-/-} mice upon treatment with thiethylperazine.....	67
Figure 33: ELISA measurement of tg-aSYN and tg-aSYN-ABCC1 ^{-/-} mice upon treatment with thiethylperazine in contrast to untreated and water-treated mice.....	68
Figure 34: Cytosolic Ca ²⁺ -regulation of Malate-aspartate NADH shuttle (MAS) and intramitochondrial Ca ²⁺ stimulation of dehydrogenases control mitochondrial pyruvate supply (Satrustegui <i>et al.</i> , 2007).....	78
Figure 35: ABCC1 topology.....	82

List of tables

Table 1: Stages and affected brain structures in PD pathology.....	13
Table 2: Classification of functional states of mitochondrial respiration.....	24
Table 3: Composition of Lysis buffer.....	31
Table 4: Pipette scheme PCR Master Mix for the detection of human aSYN.....	31
Table 5: Pipette scheme PCR Master Mix for the detection of ABCC1.....	31
Table 6: Cycler protocol for the amplification of human aSYN.....	32
Table 7: Cycler protocol for the amplification of ABCC1.....	32
Table 8: Composition of TAE (Tris-Acetate-EDTA) buffer.....	32
Table 9: Composition of PBS (pH 7.4).....	34
Table 10: Composition of Carbonate buffer (pH 11.5).....	35
Table 11: Composition of Guanidine buffer (pH 8).....	35
Table 12: Composition of MSE-A (pH 7.4).....	36
Table 13: Composition of MSE-B (pH 7.4).....	36
Table 14: Order of substrate addition according to the four experimental protocols.....	37
Table 15: Composition of BIM-1000 (pH 7.4).....	38
Table 16: Composition of BIM-0 (pH 7.4).....	38
Table 17: substrates and their solvents used for respirometry.....	39
Table 18: Dehydration protocol for paraformaldehyde-fixed brain hemispheres.....	39
Table 19: Mitochondria gene differences between NOD/LtJ and C57BL/6J mice.....	74

Acknowledgements/Danksagung

Zum Schluss bleibt es mir noch, mich bei den Menschen zu bedanken, die mich unterstützt haben und mir während der Entstehung dieser Arbeit zur Seite standen.

Vielen Dank Prof. Pahnke, dass Sie mir die Möglichkeit gegeben haben meine Arbeit anfertigen zu können und mich immer dabei unterstützt haben. Die schöne Zusammenarbeit mit Ihnen werde ich in bester Erinnerung behalten und auch die Gespräche die so manches Mal meine Zweifel vertrieben und meinen Enthusiasmus wieder geweckt haben.

Auch bei Ihnen Prof. Gellerich möchte ich mich bedanken, da Sie mir so oft mit Rat und Tat zu Seite standen. Prof. Schwabe und Martin Radloff danke ich ebenfalls für die immense Hilfe die sie beide mir haben zukommen lassen und für die tiefen Einblicke in die Welt der Statistik. Ebenso gebührt mein Dank Dr. Lachmann für die Bereitstellung der ELISA-Kits.

Liebe NRLer, habt vielen Dank für die schöne Zeit in Magdeburg. Markus, Tini, Ruth, Christoph, Johannes, Alex, Thomas und Steffi, Ihr habt mir den Alltag verschönert und so viele tolle Momente geschaffen, die mir in Erinnerung bleiben werden.

Liebe Luisa, neben den vielen tollen Mittagessen im Freien hast Du hast mich auch bei der kritischen Endphase der Arbeit großartig unterstützt. Dafür danke ich Dir ganz besonders.

Bedanken möchte ich mich auch bei Laura und Frank. Ihr seid die besten Freunde der Welt.

Ein ganz besonderes Dankeschön geht an meine liebe Familie, die mich durch alle guten und schweren Zeiten begleitet hat, immer für mich da ist und deren Tür immer offen steht.

Lars, ohne Deine liebevolle Fürsorge, Deine endlose Unterstützung und Deine unermüdliche Motivation wäre das nicht möglich gewesen. Ich danke Dir!

Declaration/Eidesstattliche Erklärung

Hiermit erkläre ich, dass ich die von mir eingereichte Dissertation zum dem Thema

“The influence of specific mitochondrial polymorphisms on the α -synuclein-induced pathology in a mouse model of Parkinson’s disease”

selbstständig verfasst, nicht schon als Dissertation verwendet habe und die von mir benutzten Hilfsmittel und Quellen vollständig angegeben wurden.

Weiterhin erkläre ich, dass ich weder diese noch andere Arbeiten zur Erlangung des akademischen Grades doctor rerum naturalium (Dr. rer. nat.) an anderen Einrichtungen eingereicht habe.

Magdeburg, 20.02.2015

Christina Schwitlick

List of publications

Krohn M, Bracke A, Avchalumov Y, Schumacher T, Hofrichter J, Paarmann K, **Fröhlich C**, Lange C, Brüning T, von Bohlen Und Halbach O, Pahnke J (2015) Accumulation of murine amyloid- β mimics early Alzheimer's disease. *Brain*. 2015 May 18. pii: awv137

Jens Pahnke, **Christina Fröhlich**, Kristin Paarmann, Markus Krohn, Nenad Bogdanovice, Dag Årslund, Bengt Winblad (2014) Cerebral ABC Transporter-common Mechanisms May Modulate Neurodegenerative Diseases and Depression in Elderly Subjects. *Arc Med Res*, 2014 Nov;45(8):738-43.

Pahnke J, **Fröhlich Ch**, Krohn M, Schumacher T, Paarmann K (2013) Impaired mitochondrial energy production and ABC transporter function – a crucial interconnection in dementing proteopathies of the brain. *Mech Ageing Dev*; 2013 Oct;134(10):506-15

Fröhlich C, Paarmann K, Steffen J, Stenzel J, Krohn M, Heinze HJ & Pahnke J (2013) Genomic background-related activation of microglia and reduced beta-amyloidosis in a mouse model of Alzheimer's disease. *Eur J Microbiol Immunol (Bp)*, 2013 Mar 1;3(1):21-27

Schumacher T, Krohn M, Hofrichter J, Lange C, Stenzel J, Steffen J, Dunkelmann T, Paarmann K, **Fröhlich C**, Uecker A, Plath AS, Sommer A, Brüning T, Heinze HJ, Pahnke J (2012) ABC transporters B1, C1 and G2 differentially regulate neuroregeneration in mice. *PloS one*, 2012;7(4):e35613